UNIVERSITÀ
DEGLI STUDI
DI PADOVA

UNIVERSITÀ DEGLI STUDI DI PADOVA

DIPARTIMENTO DI INGEGNERIA INDUSTRIALE

TESI DI LAUREA MAGISTRALE
IN INGEGNERIA DEI MATERIALI

DEPOSIZIONE ELETTROFORETICA DI FILM DI MXENE PER APPLICAZIONI FUNZIONALI

(Electrophoretic Deposition of MXene films for functional applications)

Relatore: Prof. Alessandro Martucci

Correlatore: Prof. Michel W. Barsoum

Laureando: PIERALBERTO COLLINI

ANNO ACCADEMICO 2016-2017

Abstract

The two-dimensional (2D) materials world is gaining increasing enthusiasm in the scientific community and after the discovery of the progenitor – graphene - many other members joined family owing to the interesting and novel properties brought by their peculiar morphology.

In 2011, an etching method was devised that allowed the synthesis of new two-dimensional early transition metal carbides, named MXenes after their MAX phase-precursor and similarity to graphene. Since then, a detailed characterization of different MXene compositions has been accomplished and in more than 300 refereed journal articles their impressive properties and technological potentialities have been discussed. With such a wide spectrum of potential applications comes the need to expand MXenes processability, especially with regard to their colloidal suspensions. To date many technique have been used, such as spin-coating, electrospraying and in a single, recent publication, electrophoretic deposition (EPD). Herein the fabrication of $Ti_3C_2T_x$ MXene films using EPD is reported. Two colloidal suspensions were used: aqueous- and propylene carbonate-, PC, based suspensions. The effects of the potential difference, deposition time and solvent on film morphologies, flake orientations, and functional properties were explored. The Sarkar theory was used to model the process. Distinct behavior for aqueous and non-aqueous deposition at constant voltage were modeled and provided consistent predictions even in a single case of a proof of concept experiment carried out under constant current conditions.

Surprisingly, the EPD-fabricated films showed electrical conductivities of 7400 S/cm, i.e. values comparable with the highest reported in the literature for $Ti_3C_2T_x$ made using more traditional approaches. Finally, as a further technological example, the EPD films were tested as electrodes for electrochemical capacitor in 1 M H_2SO_4 and the results were in agreement with previous literature values reported for vacuum filtered films.

In conclusion, EPD is a high throughput method to produce relatively thick MXene films of good quality, and is thus promising in terms of scalability for the production of MXene films for at least some technological applications.

Abstract in italiano

Il mondo dei materiali bidimensionali sta generando un crescente entusiasmo all'interno della comunità scientifica e successivamente alla scoperta del capostipite – il grafene – vari altri membri si sono aggiunti alla famiglia grazie alle eccezionali e innovative proprietà generate dalla loro particolare microstruttura. In quest'ottica è stato recentemente sviluppato un metodo di sintesi chimica che ha permesso l'identificazione di una nuova classe di carburi metallici bidimensionali, nominati *MXenes* prendendo spunto dai loro precursori - *MAX phases* -e dalla notevole somiglianza con il grafene stesso. Da allora, differenti composizioni di *MXene* sono state caratterizzate dettagliatamente e in più di 300 articoli sono state descritte le loro notevoli proprietà e potenzialità tecnologiche. Tuttavia da una tale gamma di possibili applicazioni, è sorto il bisogno di espandere la processabilità del materiale, in particolare con riferimento al trattamento di sue soluzioni colloidali. Attualmente già molte metodologie sono state proposte, spaziando dallo *spin-coating* all'*electrospraying*, ma solo un unico e recentissimo articolo è stato pubblicato sulla deposizione elettroforetica (EPD).

In questo lavoro viene presentata la fabbricazione di film in $Ti_3C_2T_x$ (*MXene*) mediante EPD, riportando uno studio sistematico condotto su sospensioni stabili a base di acqua e propilene carbonato: differenze di potenziale constanti sono state impiegate per indagare l'effetto dei parametri di processo – come ad esempio voltaggio applicato, tempo di trattamento e solvente – su morfologia dei film, orientazione dei foglietti di *MXene*, e proprietà funzionali. Ricorrendo alla ben nota teoria di Sarkar', inoltre, la cinetica del fenomeno è stata modellata, individuando comportamenti differenti a seconda della natura acquosa o meno del solvente e fornendo previsioni corrette anche nel caso di un esperimento realizzato in condizioni di corrente costante (anziché voltaggio).

In particolare, i film fabbricati mediante EPD hanno mostrato conducibilità elettriche fino a 7400 S/cm, collocandosi ai vertici delle prestazioni per quanto riguarda i valori ottenuti in precedenza da film fabbricati con approccio tradizionale. Infine, un ulteriore esempio tecnologico è stato sperimentato utilizzando porzioni di film come elettrodo di un condensatore elettrochimico in H_2SO_4 1M e, anche in questo caso, i risultati si sono attestati su valori confrontabili con la letteratura inerente film ottenuti da filtraggio sotto vuoto.

In conclusione, l'EPD si è dimostrata un metodo ad alta capacità produttiva per fabbricare film di *MXene* ed è promettente per la sua scalabilità industriale e le svariate applicazioni tecnologiche.

Acknowledgments

Among the many people who deserve my gratitude and acknowledgment for the productions of the present thesis I would like to start mentioning those I worked with at Drexel University. My advisors, Prof. Michel Barsoum, supported me from the very beginning, when I was setting up my travel to the U.S., to the last days and even after my departure. His scientific expertise and curiosity was very inspiring and his suggestions always very helpful throughout all my research experience. I would like to equally thank my co-advisor, Prof. Aaron Fafarman, for his encouragements, passion and confidence in me that constituted a continuous stimulus and a great opportunity to work serenely and live a fruitful experience. Also, I am extremely grateful to Sankalp Kota: he assisted me in the non-trivial task of harmonizing Drexel's and Padua University's responsibilities and provided me with great help, not only on the work side.

Thanks also to my Italian advisor, Prof. Alessandro Martucci, who helped me pursuing the desire to conduct my thesis research abroad and always provided me with help when needed, with outstanding alacrity and very helpful suggestions.

I am sincerely grateful to Maureen Prewitt, my host in Philadelphia, who made my staying comfortable and constantly supported me even during the course of a very annoying knee issue, making me feel home and helping my commuting from my place to the lab when my walking was difficult.

Last but not least, this experience and the derived accomplishments were possible only thanks to my family, that unconditionally supported me with their love and financial help. I really hope I will be able to reward them for all the efforts they exerted in growing me up and giving me the possibility to follow my dreams.

Table of contents

Chapter 1

Introduction

Since the discovery of graphene monolayers in 2004,[1] material science has added a new thriving branch to its core and many applications have bloomed wherever the outstanding properties of two-dimensional solids (defined as structures with high aspect ratios when considering thickness and surface) introduced groundbreaking advantages compared to the preexisting technologies. This discovery was followed by a host of studies regarding graphene's characterization and its impressive properties paved the way for a huge research endeavor devoted to find new classes of 2D materials with different chemistry and tunable features. Such efforts resulted in a host of publications about materials, ranging from insulators to semiconductors, from metals to even superconductors, among which hexagonal boron nitride, (hBN)[2], transition-metal dichacogenides (TDMs)[3] and transition metal oxides and hydroxides are worth mentioning. To cite some of the most remarkable examples, 2D materials have found space in many technological areas such as electronic devices (sensors, transistors, *etc*.)[4], electrochemical energy storage electrodes[5], and reinforcement in composites[6].

Among all the cited application, especially the energy storage field has garnered much attention in the last few decades since the need to overcome oil/coke industry, harmonize anthropic activities and create a healthy planet has become more urgent. The scientific community was hence prompted to research alternative sources of green and sustainable energy, but the birth of innovative ways to generate electricity in a renewable fashion, introduced a further issue. Unfortunately, despite their remarkable potential, most of the so-called eco-friendly energy sources, such as solar, hydroelectrical, wind and tide, have the major drawback of being discontinuous, challenging engineers and scientist to address such problem and supply energy reliably for 24 hours a day in spite of possible production peaks.

Furthermore, many consumer markets applications are currently flooding people's lives and everyone has experienced the striking spread of miniaturized electronics with a huge diffusion of mobile phones, computers, cameras and, in general, of any kind of portable

devices. The high mobility of these apparatuses and the growing demand of long lasting life in the time spanning consecutive recharges have tremendously triggered the research in order to pinpoint new technologies able to meet the market requirements.

Finally, the automotive sector, in its most general sense (transportation, mechanical tools, port-cranes *etc.*), is constantly targeting the development of non-fossil-fuel propelled engines and, accordingly, many efforts are expended to make into reality the scenario of a world where most of the mechanics is electrically driven.

Thus, it is self-evident that the success and progress of all the aforementioned technological fields are strictly correlated with the fabrication of new energy storage systems where performances in terms of power and energy densities, dimensions, lifetime, recharge rates, cyclability, reliability and safety standards are optimized.

Currently the devices available to play that role are divided in two main categories: traditional batteries, where chemical reactants supply energy with so-called "faradaic processes" when a redox reaction occurs at the interface between the electrode's surface and the electrolyte solution resulting a charge transfer; electrochemical capacitors (ECs), that, even though not very popular, are gaining approval owing to their complementarity with traditional batteries. In fact, ECs are based on a completely different mechanism in which the accumulation of ions against the electrodes' surfaces is much faster and more reversible than faradaic processes. Briefly, thanks to materials characterized by high values of specific surface areas (like porous carbon and 2D materials), the formation of a electrochemical double-layer is harnessed to store charge exactly as it happens in a conventional capacitor, but orders of magnitude greater capacitances are possible with ECs[7]. Such systems deliver outstanding cyclability, with almost constant properties during a life up to millions of charge-discharge cycles and charging times as small as milliseconds (i.e. high power). Notwithstanding the abovementioned qualities, electrochemical capacitors ate still on their way to meet market needs and more effort is expected in the upcoming years to overcome their disadvantages - such as low energy density and propensity for self-discharge - and get to the required efficiency. Hence, although engineering efforts have incrementally advanced ECs' performances breakthroughs that only fundamental research can provide are needed and in this context have to be seen the present work.

In 2011 the 2D materials family welcomed a new member when Naguib *et al.*[8] discovered a procedure to etch so-called MAX phases[9] in an exfoliated structure named MXenes after their precursor and the analogies with graphene. Speaking about the parent phases,

they are a confirmed class of ternary transition metal carbides or nitrides with a $M_{N+1}AX_N$, chemical formula: M is an early transition metal, A represents mostly elements from the III A or IV A groups such as Al, Ga, Si, or Ge, X is C and/or N and N = 1, 2, or 3. As said before, an etching process removes the A-atoms layer connecting single MX stacks and produces an exfoliated structure where multiple lamellas are piled close to each other but partially separated in an accordion-like structure. The most fascinating feature shown by MXenes is likely their ability to replace A atoms with surface terminating functional groups (typically -OH, -O and -F[10]) which adsorbs on the layers and interact forming weak bonds. Therefore, MXenes have a formula of $M_{N+1}X_NT_x$, where T stands for a generic surface termination group. Thanks to this peculiarity, mechanical action can delaminate the exfoliated structure and generate single- or few-layered flakes which can be easily dispersed both in aqueous and non-aqueous suspensions.

So far, more than 300 refereed journal articles have been written on MXenes: the more than 20 varying compositions synthesized to date[11–17] possess a unique combination of high electrical conductivities and hydrophilicity. They are thus being explored for a host of applications, such as electrodes for energy storage,[18–21] transparent conductive coatings,[22–24] water purification,[25–27] and electromagnetic interference shielding,[28,29] among others.[30]

Following the direction marked by all the published literature, this thesis was conceived with the purpose of optimizing the current practice adopted to produce colloidal MXene suspensions and explore the feasibility of a new processing of such solutions. At the beginning of the study, vacuum filtration,[31] spin-coating,[23,32] spray coating,[24] spray drying,[33] and electrospraying,[34] among others, were reported as possible MXene colloids manipulation techniques, but nothing was available as for electrophoretic deposition, acronym EPD (nonetheless during the course of the research, a paper of non-aqueous EPD of $Ti_3C_2T_x$ was published[35]).

EPD is a well-established processing technique known since more than a century ago[36], that allows to treat systems constituted by charged particles dispersed in a liquid solvent. Harnessing the drive provided by an electric field acting on charged entities, the method consists in two distinct processes observable when a stable colloid is placed in between two electrodes and a potential is switched on: first the particles move toward the oppositely charged electrode (electrophoresis) and then a semi-solid deposit starts forming as a result of coagulation caused by the destabilization impressed by the external force (deposition). The technique has found many applications in the last decades and was implemented for high-throughput production of dense ceramic structures ranging

from thin coatings to bulk layers several centimeters thick.[37] Its success are not only due to various advantages where flexibility and scalability of the deposition apparatus are likely the preeminent ones but also to fast deposition rate and possibility of controlling the microstructure. This resulted in an extensive employment of EPD for commercial-scale production of various engineering and traditional ceramics,[37–39] but it was only in the recent years that a renewed interest was attracted on the technique thanks to the improvements in colloids fabrication. Therefore, to date, reports have been published describing EPD as versatile technique for making films and nanocomposites of 2D materials such as graphene, transition metal dichalcogenides, and layered transition metal oxides. [40–45]

As noted above, however, the method hadn't been explored for MXene suspensions and, hence, in the present study such process was thoroughly examined and optimized until a viable route for high-throughput MXene film synthesis was found. The kinetics of the process were also explored to tune mass deposition and, in turn, film thickness, namely one the most sensitive parameter in many functional applications where 2D materials can find place. Furthermore, the films' structures, properties, and chemical composition were investigated as function of applied voltage and different dispersion media for the colloidal suspensions. With respect to the latter, different kind of dispersion media have been tried and many organic solvents found application owing to the occurrence of water electrolysis in EPD from aqueous suspensions and the resulting worsening in process control. Nevertheless water suspensions are still attractive because of low environmental impact, cost and a simplicity that support their application in large scale industrial production'0. Keeping this in mind, water and non-aqueous solvents (*viz.* propylene carbonate and dimethyl sulfoxide) were experimented herein and diverse properties where highlighted, paving the way for different kind of applications. EPD fabricated films where tested in terms of both the electrical conductivity and the charge storage capacity when working as EC electrodes, given that the latter is likely the most common way of assessing energy storage potentialities of a 2D material.

The present work has the two-fold goals of first describing how to etch MAX phases and delaminate the resulting MXene to maximize colloidal suspension concentrations and then to characterize the EPD films obtained from such suspensions. In addition to the introduction and a final section devoted to sum up and present further possible developments, the thesis consists of 5 chapters. Chapter 2 is devoted to a literature survey focused on three topics: MAX phases, their etching to fabricate MXenes and the final production of colloidal suspensions; electrophoretic deposition, with particular respect to technique fundamentals, modelling and applications; electrochemical double-layer

capacitors as an advanced solution to cooperate with traditional batteries in the energy storage field. Chapter 3 describes coherently the materials and methods used throughout this work. MAX phases sintering, etching and optimization of colloidal suspensions both in aqueous and non-aqueous media are discussed in Chapter 4. Systematic studies conducted on such solutions under several working conditions – effect of applied voltage, applied current and deposition time- are presented in Chapter 5.

Finally, Chapter 6 explores some features of the EPD technique providing a comparison between two different solvents in terms of process kinetics and analyzing properties of the as-synthesized material such as film conductivity and charge storage specific capacity when tested as supercapacitor electrode.

Chapter 2

Background and literature survey

This chapter provides insight into the main topics useful to approach and better understand the research results discussed in this thesis throughout the subsequent chapters. Literature was surveyed to build a background knowledge summary regarding both the electrophoretic deposition process and the production of MXene colloids. In detail, MAX phases general properties and applications are described, as well as the synthesis of their derived phases known as MXene. Afterwards, a comprehensive dissertation about the current EPD characteristics, kinetics and applications in the field of advanced materials is provided. Finally, an introductory presentation of electrochemical capacitors and especially electrochemical double-layer capacitors (EDLCs) is given.

2.1 MAX phases

The history of MAX phases lays its foundations in the seventies, when Nowotny released a review article[46] illustrating the main results of the work he and coworkers had conducted across the previous decade discovering and investigating a plethora (more than 100) of carbides and nitrides. Roughly a third of that remarkable number was constituted by compounds named H- or Hägg phases, i.e. ceramics with a M_2AX chemistry, where M is an early transition metal, A is an A-group element (mainly IIIA and IVA) and X is C and/or N. The crystalline structures of such materials are layered and hexagonal, where M_2X blocks are regularly intercalated by monoatomic sheets of pure A element. During the same extended experimental campaign, the researchers discovered also two slightly differently arranged compounds, Ti_3SiC_2 and Ti_3GeC_2, both identified by a structural relation to the H-phases, since in this case M_3X_2 were interleaved by A layers.

Although the considerable amount of work devoted to such materials, from the time of the H-phases discovery (identified as 211 phases) some decades passed before further studies were undertaken. This is not true, however, for Ti_3SiC_2 because here, since 1972, different synthesis methods where proposed ranging from chemical vapor deposition (CVD) to solid state reaction methods, achieving, an unexpectedly soft material. The efforts to produce a bulk dense carbide have shown even more ambiguous and different

attempts always produced secondary unwanted phases, such as TiC and sometimes SiC. Nowotny first devised a viable procedure to produce highly dense bulk samples, reaching levels of 80-90% of purity: he performed a variety of tests on them, showing the stiffness (Young's modulus and shear modulus of 326 and 135 GPa, respectively) of the carbide. Again, a distinct softness was found and this, coupled with the just mentioned stiffness, produced a high stiffness-to-hardness ratio, giving material properties similar to metals (from hence designated as ductile ceramic).
Finally, more recently another compound, Ti_4AlN_3, structurally related to the previous discussed ones, was discovered and its "413" stoichiometric scheme made evident that all these materials belonged to a common family of ternary layered carbides and/or nitrides, identified by the general formula $M_{N+1}AX_N$, where N could be 1, 2 or 3, M is an early transition metal, A is an A-group (mostly IIIA and IVA) element and X varies between C and N. It has been proven[47] that such phases constitute a new class of solids, describable under the denomination of thermodynamically stable nanolaminates, because of their layered structure. The morphology of the henceforth called "MAX phases" provides remarkable values of interfacial area and, in turn, exceptional mechanical and chemical properties. Nevertheless, often bulk applications are yet unfeasible due to the combination of two main factors: the difficulties encountered in the processing of such samples, since big components can't be produced, for instance, via molecular beam epitaxy, and the thermodynamic instability of fine-scale arrangements which would prevent their use at high temperatures.

The last years of the nineties saw huge efforts to systematically synthesize and characterize all the known and theoretically expected MAX phases: the results showed properties aligned with the respective stoichiometric binary metal carbides or nitrides from the thermal, elastic, chemical, and electrical point of view, with high stiffness and good thermal and electrical conductivity. The analogies stop here, though, and mechanically the new materials exhibit a peculiar behavior, since they are readily machinable, not very hard, and particularly damage and thermal shock resistant considering they belong to the ceramic family. These unusual properties can be partly understood considering that such materials are the only polycrystalline solids where the deformation is the effects of kink and shear band deformations, coupled with the delamination of single grains. Unlike most of the ceramics, here, the dislocation movements are less hindered at room temperature and, gliding exclusively on the basal planes, they are configured as assays or positioned at kink boundaries.
Summarizing, the peculiar properties of the MAX phases are ascribable to their layered structure, the mostly metallic and strong (despite the covalent and ionic contributions) behavior of the MX bonds and the weakness, especially in shear, of the MA connections.

So far Ti_3SiC_2 and Ti_3AlC_2 are the best known and characterized compounds and the available information ranges from tensile, compressive and flexural strength (with relative temperature dependencies) to creep, hardness and oxidation resistance, from fatigue, fracture toughness and tribolocical behavior, to surface characteristics. Moreover, investigations were carried out to determine the electrical conductivity, Hall coefficient, heat capacity in a wide window of temperatures, thermal expansion and thermal conductivity, providing a detailed picture of the carbide and its potentialities.

2.1.1 Structure and bonding of MAX phases

A brief discussion regarding MAX phases crystallographic structures is considered beneficial to better understand reaction mechanisms in the step necessary to transform them into their derived 2D materials.

$M_{N+1}AX_N$ phases are recognized as layered hexagonal structures with a $D_{6h}^4 - P\,6_3/mmc$ space group symmetry where each cell is occupied by two formula units. The three possible structures, namely 211, 312 and 413 are shown in **Figure 2.1.1**: they differ mainly by the changing number of M layers interleaved with A-layers, since in 211 there are two of them, in 312 three, in 413 four, and this stratified structure is decisive for the comprehension and the tuning of the material properties.

Nevertheless, independently of the specific configuration, layers of M-species are close packed and interleaved with layers of pure A-element generating a cards deck structure from which stems the denomination of thermodynamically stable nanolaminates. The M-element produces a lattice where octahedral sites (connected through the edges) are occupied by X-atoms, whereas as for A-elements, they are positioned at the center of trigonal prisms of bigger dimensions which are hence better suited to host more cumbersome chemical species. In more detail, the crystalline lattice is then constituted by M_6X edge-sharing octahedra which are perfectly matched with the ones belonging to the related binary carbides (or nitrides) rock salt structures.

The MAX phases distinguish themselves for the presence of bonds of different nature: a strong M-X bond standing out for a mixed covalent/metallic/ionic attribute and a M-A metallic bond (relatively weak, especially in shear) giving the material a much stronger structure, in contrast with other known 2D conformations such as graphite where the van der Waals forces play a fundamental role. Consequently they are resistant to breakage through simple shear forces or similar mechanisms.

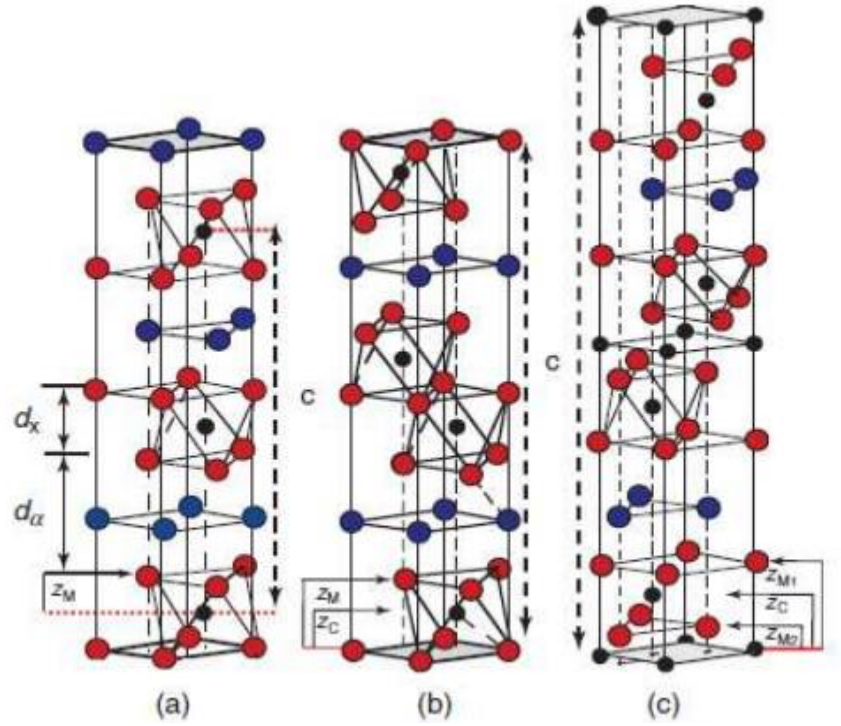

Figure 2.1.1: *3D schematics of MAX phase structures for (a) 211, (b) 312 and (c) 413 unit cells and respective c-lattice parameter depicted by vertical dashed lines. Picture credited to Barsoum M.*[47]

The three MAX phase configurations can be described as follows and reference to **Figure 2.1.2** may help for a better understanding and spatial insight:

1. 211: tree inequivalent atoms arranged in a single polymorph called α;
2. 312 four inequivalent atoms, organized in two possible polymorph α and β;
3. 413 five inequivalent atoms and three different configurations are possible, namely α, β and γ.

The most common stacking sequence has been proved to be the α polymorph for all the three possible MAX phases structures. The plane order can be better understood considering **Figure 2.1.2**a,b,d where the $(11\bar{2}0)$ planes are depicted: in all the cases the A-atoms layers act as mirror planes while the MX blocks show a herringbone shape.
As for the β configurations, similar illustration for the $(11\bar{2}0)$ planes are available in **Figure 2.1.2**c,e: the α to β transformation is quite simple for the M_3AX_2 phases since only a shear in the A-atoms layers is needed and the strong M-X bond is not affected, whereas the same is not true for the M_4AX_3 phases, where the MX octahedra are modified, requiring therefore a higher activation energy.
Finally, **Figure 2.1.2**f provides a sketch for the γ configuration showed by M_4AX_3 phases: as with the α to β transformation for the M_3AX_2 phases, the α- to γ-M_4AX_3 is generated by the shearing of A-layers and the activation energy is low again.

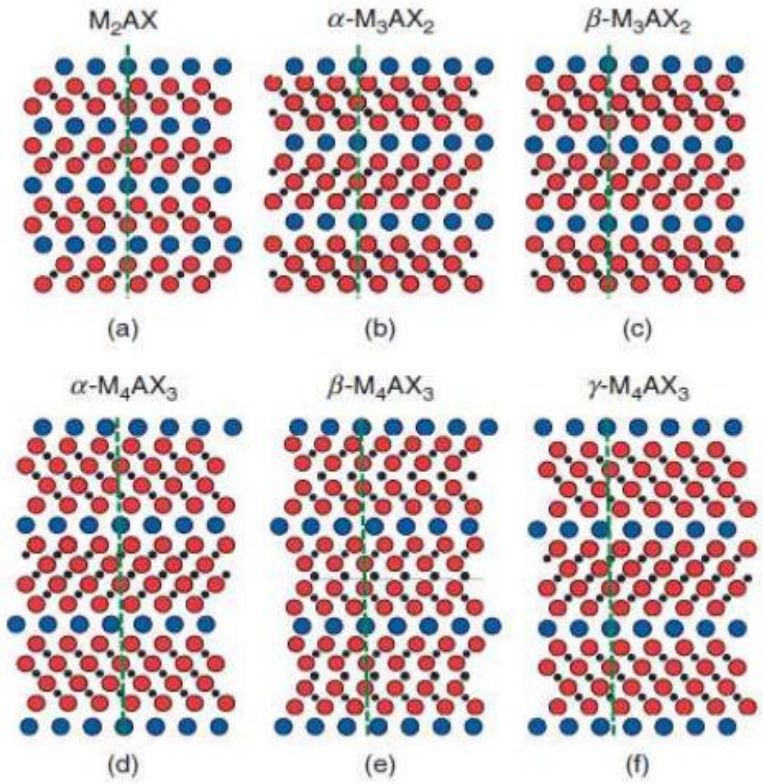

Figure 2.1.2: *2D schematics of MAX phase structures for* $(11\bar{2}0)$ *planes for the 3 different configurations possible. Picture credited to Barsoum M.*[47]

To sum up, MAX phases is a family of layered ternary metallic carbides split in turn into 3 categories: 211 has shown to be the prevalent structure so far; Al appears as the most versatile, being present in all the 3 MAX configurations with 13 compounds, whereas Ga is the most frequent for 211 structure with nine different possibilities.[47] Furthermore, the most widespread M_3AX_2 are Ti_3SiC_2, e Ti_3AlC_2 and e Ta_3SiC_2, whereas most common M_4AX_3 are Ti_4AlN_3 a Ta_4AlC_3 and Nb_4AlC_3. The layered structure is crucial to understand and optimize such compounds, not only from the mechanical point of view but also in view of chemical reactivity.

2.2 MXenes (and other 2D materials)

The concept of two dimensional (2D) material arose in the last decade thanks to the blooming of a variety of crystals with very high aspect ratio in terms of surface area to thickness. Solids comprised of a few atomic layers, with graphene as the main character, have met increasing interests due to their outstanding electronic properties and richness of their surface chemistry. After its discovery, hexagonal boron nitrides, transition metal dichalcogenides (TMDs), metal oxides, and hydroxides as well claimed their role in the scientific world, increasing the interest towards high aspect ratio structures.[10] In the same

context, only a few years ago a new family of two-dimensional early transition metal carbides or nitrides was discovered at Drexel University, named MXenes after their MAX phase-precursor and similarity to graphene.

From the MAX phase description provided above, it is easy to infer that MXenes are constituted by $M_{N+1}X_N$ layers where the intercalated A atoms plane has been acidically etched leaving adjacent 2D structures facing each other. Therefore, M is again an early transition metal, whereas X represents carbon and/or nitrogen. The general formula for such materials is though $M_{N+1}X_NT_x$ where N can assume the values 1, 2, or 3, and T is constituted by some surface terminations such as, typically, -O, -OH, and -F. The known MAX phases are more than 60 and theoretically, MXenes should be a subset of such number; nonetheless MAX phases can be a blend of different elements combined and positioned in one of the three possible sites in the crystalline lattice (a solid solution of M atoms to give $(Ti_{0,5},Nb_{0,5})_2AlC$, for instance), so extending hugely the number of potential MXenes compositions.
The idea of MXene fabrication stems from the evidence of a difference in binding energy between the two types of layers constituting MAX phases. Despite the high toughness shown by the starting MAX phases, the A layers bond is weaker than the M-X one and this suggested that employing proper chemical reactants, typically acids, a selective etching was possible. However this was not the only way to fabricate MXenes, and other techniques have been investigated, such as heating of the precursor under vacuum, in molten salts and in a few molten metals[48]. Nonetheless, usually the high temperatures achieved caused the de-twinning of the $M_{N+1}X_N$, resulting in the formation of the corresponding 3D rock salt structure. At the same time, trials with strong etchants at lower temperatures ended in the removal of both A and M atoms, with the production of a specific derived carbon, or in the formation of a ternary metal fluoride phase in case HF was used.

It was 2011 when first was reported the etching of Al-layers from the 3D structure of Ti_3AlC_2 through reaction at room temperature with HF[8]: the result was the removal of Al and its replacing with either -O, -OH and/or -F atoms, and a general weakening of the mutual interactions between adjacent $M_{N+1}X_N$ layers, meaning, in other words, the possibility of separating them readily. The material has been named MXene, to highlight the origin from the parent MAX phase and to draw attention on their 2D nature, in analogy with graphene.
To date, the best characterized MXenes are Ti_3C_2, Ti_2C, Nb_2C, V_2C, $(Ti_{0,5},Nb_{0,5})_2C$, $(V_{0,5},Cr_{0,5})_3C_2$, Ti_3CN and Ta_4C_3[10]: as mentioned above, the N value can range among 1,

2 and 3, therefore the MXene sheets are made of 3, 5, or 7 atomics layer, depending on whether M_2X, M_3X_2, or M_4X_3, are involved.

Among others, advantages of MXenes are hydrophilicity, high electrical conductivity, tunable chemistry and structure, the ability to intercalate spontaneously organic molecules, as well as electrochemical intercalation of a variety of cations. Therefore, a deep understanding in its intercalation chemistry (so as for all the 2D materials) is very meaningful in order to harness to the best the potentiality of such materials.[49]

2.2.1 MXene synthesis

As outlined in § 2.2, MXene synthesis is prompted by selective etching of the A-layer of an initial MAX phase: the most studied process is based on the reaction at room temperature and for a given time, of a powder in aqueous HF under stirring conditions and on the following washing in DI water of the acidic system by multiple centrifugation and/or filtration of the products to separate the solid part by the acidic supernatant until the pH approaches 7. The effect of the whole process is the conversion of 3D MAX particles in a loosely packed structure similar to graphite. As said before, in concert with the previous nomenclature regarding hi-tech carbon literature, such multi-layered (ML) structures have been named ML-MXenes, with a further specification for systems where the number of stacked layer is less than 5, suggesting the introduction of "few-layered" MXene denomination (FL-MXene).

From the crystallographic point of view a successful etching is marked by the attenuation or even complete vanishing of all the X-ray diffraction (XRD) peaks belonging to the previous MAX phase except for the one relative to the (000*l*) reflection. Moreover, the (000*l*) peak itself, undergoes some changes, with a significant broadening and a downshift to lower angles, meaning a larger *c*-lattice parameter (*c*-LP). On the other hand, whenever the order along the [0001] direction is missing, no XRD peak is spotted, as well as, if the etching reaction does not run to completion, MAX phase peaks are combined with the new MXene (000*l*) ones. To quantify the etching yield, however, XRD analysis is not a suited technique since exfoliation translates in fading peaks and can lead to misinterpretations with regard to unreacted MAX phase still in the sample. Alternatively, EDS (energy-dispersive spectroscopy) could be used to identify possible non-etched MAX phase, through the quantification of the A/M atomic ratio, that should approach zero for a completed reaction. Nevertheless, the technique should take into account the possibility of identifying the presence of A-element, due to the formation of salts containing it, in case the etching products weren't completely removed, and for this

reason the method is subjected to some experimental uncertainty, overestimating the MAX phase presence.

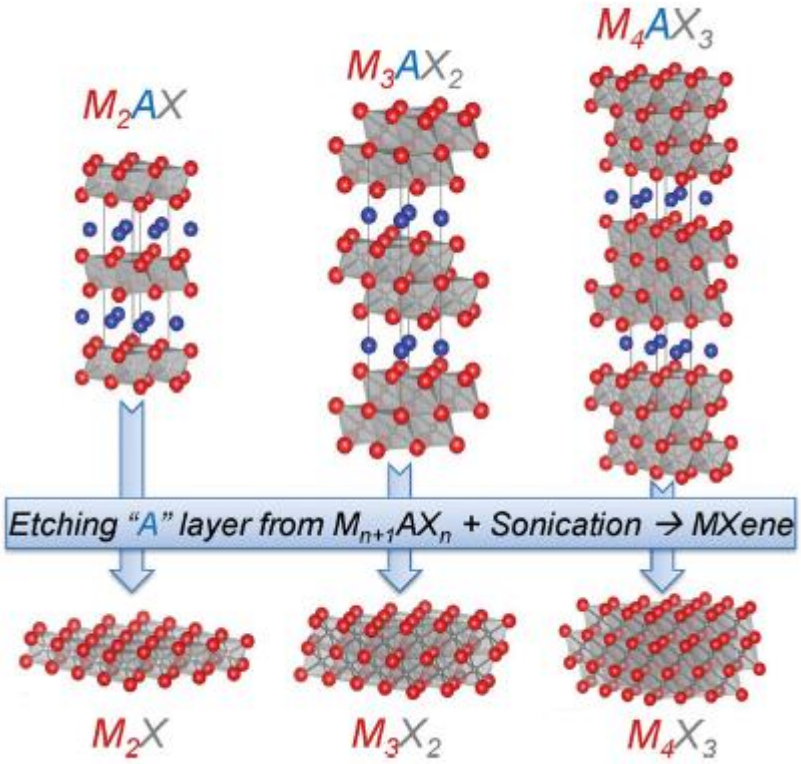

Figure 1. Structure of MAX phases and the corresponding MXenes.

Figure 2.2.1: *schematics of the structural changes occurring in the transformation from MAX to MXene. Picture credited to Naguib et al.*[10]

The MXene yield is usually calculated as the ratio between the weights of dry powder after and before the HF reaction multiplied by 100 to express it in percentage notation, and is generally included in the 60-100% range.

The delamination of MXene is possible thanks to the replacement of a quite strong A-M bond by the weaker hydrogen or van der Waals bonds, and usually after HF treatment utrasonication in a variety of solvent is enough to provide delamination. With this respect Zhan *et al*.[50] suggested that when the A-atoms layer is substituted by different species the bonds between adjacent sheets weaken and producing ultrathin flakes is easier.

Recently, Ghidiu *et al*.[51] devised a new etching technique based on a solution of lithium fluoride and hydrochloric acid where ion intercalation was able to spread MXene layers and make the material swell when hydrated. Similarly, a procedure with lithium chloride and hydrofluoric acid was tried as well, but the advantages connected to working with the less dangerous HCl and the often better results observed made the former prevail. In any

cases ion intercalation by the cation of the salt represented a breakthrough in MAX phases etching, especially when considering the delamination step and suspension in various solvents as explained in the upcoming section.

2.2.2 Ion intercalation and large scale delamination

MXene potentialities depend strongly on their processability and delamination and production of stable and concentrated colloids especially plays a fundamental role in the success of those novel materials. To accomplish those goals the presence of a salt able to provide ion exchange and intercalation has proven to be essential, so that, to date, they found place in many applications working for instance as supercapacitors electrodes with aqueous electrolytes, sorbents for pollutant ions (Pb and Cr for instance) or membranes for ionic sieving.
More generally, controlling the concentration of intercalated ions in MXenes is fundamental to enhance the material performance, especially in terms of energy storage, optics and ion-exchange to mention just a few technological fields.[52]

Just like many other layered materials for which the bonds between adjacent sheets are not very strong (e.g. graphite or clays), MXenes are easy to intercalate because $M_{N+1}X_N$ layers are glued together by weak van der Waals bonding and thus different species are allowed to penetrate and intercalate them.
The immediate effect of the intercalation is the expansion of the *c*-lattice parameter due to the obvious steric effect of the species positioned between adjacent layers, and some solvents, such as DMSO, were found to increase the interlayer distance as a result of spontaneously induced co-intercalation of ambient moisture. Long time storages of Ti_3C_2 powders intercalated with DMSO showed remarkable increase of the *c* lattice parameter (e.g. doubling of the space after three weeks) and lead to a further weakening of the bonds keeping the layers stacked, so that even a weak sonication treatment could produce a high level of delamination.

Interestingly multilayered Ti_3C_2 can be also intercalated by Li atom planes and DFT calculations suggested a structure in the form of $Ti_3C_2Li_2$ whenever a Li-abundant reaction environment is available, indicating a slightly positive enthalpy for the process, likely due to the larger size of the Li atoms in place of Al ones. The interaction between the MXene and the Li atoms counterbalances charged surface sites on MXene, giving rise to an intimate absorption of the cations provided by a strong coulombic force.
Li ions intercalation causes an increase in the structural order and XRD analysis shows an intense 002 reflection peak corresponding to a *c*-LP of 2.45 nm (for powder dried in

atmosphere) differently from what observed for the HF only etched MAX phases, where a less intense peak arises, suggesting a *c*-LP of roughly 2.0 nm. Another reason of that experimental evidence is the possible presence of dynamic H_2O layers orderly arranged thanks to the Li^+ action that organizes the material sheets into a regular array, delivering higher crystallinity.
The intercalation of other ions has been proven, employing Na, K, Rb, Mg and Ca, and a variety of different characterization methods have been used to assess the completeness of the ion exchange process.[52]

In conclusion, information about the hydration processes and specifically about dehydration kinetic could help to select proper working parameters to tune material properties, control the water intake and enhance dispersibility as well.

2.2.3 Applications of MXenes

MXenes delivers remarkable performances in a bunch of technological fields and their highly peculiar morphologies, coupled with good electronic conductivity and notable mechanical features encouraged enthusiastic efforts in researching and developing such materials. With no doubts, they have gathered great interest thanks to the possibility of tuning their properties and behaviors simply by adjusting the N value, changing the atoms across the layers and finally promoting different terminating groups to occupy the superficial sites.
The main applications encompass sensors, and more generally, electronic devices, conductive and mechanical reinforcement additives for polymers, catalysis and, foremost, energy storage device fabrication.

To date the most explored field concerns energy storage and MXenes have been tested in application as lithium ion batteries, electrochemical capacitors and fuel cells. Bare Ti_3C_2 provides efficient anodes, thanks to the enhanced conductivity provided by the metallic behavior, a smaller open circuit voltage and an improved Li-ion storage capacity. Such performance is competitive with, if not even surpassing, anatase TiO_2 or graphite, making them ideal candidates to produce high power batteries. Furthermore, the rich chemistry of MXenes, along with the possibility of tuning the composition even across the single atomic plane, deliver interesting features in terms of “ad hoc” designs for battery application, where, depending on the material selected, the electrode could work as anode or cathode in lithium ion batteries.

Another meaningful feature shown by MXene is the aforementioned ability to be readily delaminated in different solvents, such as DMSO, especially for $Ti_3C_2T_x$. Sonication of Ti_3C_2 intercalated with DMSO molecules, and dispersed then in DI water, generates a colloidal solution of few (or even single) sheets which can be easily filtrate to obtain a flexible freestanding film to be used, for instance, as electrodes in Li ions batteries. In this case, reversible capacity of 410 $mAhg^{-1}$ was found, coupled with high cycling rates, and these properties made MXenes interesting candidates to build asymmetric energy storage devices, with the goal of combining high energy densities typical for traditional batteries and high power densities provided by electrical double-layer capacitors. Enhancing the electrochemical performance is further possible by harnessing the spontaneous chemical intercalation of a variety of cations between the layer, as in this way each layer is better accessible for ions adsorption during the charge/discharge cycles.

Finally, blended MXenes were tested as additive in polymer materials (PMMA) to fabricate a conductive composite with noteworthy mechanical and thermal properties (similar results have been accomplished using graphene instead of MXene), thanks to the improved performance compared to the parent MAX phase. Moreover, the high surface area and the terminating functional groups provide an easy way to tune and enhance the interfacial properties between filler and matrix, making possible even the formation of covalent bonds.

2.3 Electrophoretic deposition (EPD) introduction

Electrophoretic deposition (EPD) is a traditional processing method for slimes of various compositions applicable in any system where suspended particles bear surface charge. The phenomenon is known since the beginning of 19^{th} century but the technique was adopted industrially only in the sixties, primarily for ceramics.[36] Lately, however, the method has also spread in the field of advanced materials and the improvements in colloid preparation allowed the production of novel inorganic nanostructured monoliths, as well as composite and coating materials where the suspended elements are, for instance, nanoparticle, nanotubes or nanorods.

The EPD process consists in two main basic mechanisms: migration of electrically charged particles starting from a stable suspension along the lines of an externally applied electric field; deposition of the moving particles on the electrode surface or on a specific substrate membrane, producing a film whose features depend on working parameters and employed solution. Finally, a further step is often required to eliminate porosity and to achieve higher density levels, consisting of heat treatments, such as firing or sintering.

In general, EPD works on all the solids reduced in powder or colloid form, as long as they are able to store charge, and examples of successful deposition are available for a wide range of material, extending from metals, to polymers and ceramics (in detail, oxides, nitrides and glasses). To improve the product quality, working solutions have to be as stable as possible, so that flocculation phenomena are prevented: this allows particles to stack and pile up on the substrate for a combination of different phenomena, such as dissolution of ions from the particles and selective adsorption of ions from the solvent, without being excessively affected by precipitation.

EPD is usually explained in the frame of DLVO theory (see below) but other models are available and the research is still working in order to describe particle interaction and kinetics, in terms of electrochemical effects and complex interactions between solvents, particles and electric field as well. Traditionally the process is performed under constant voltage conditions but, lately, theoretical developments have shown that constant current is a viable solution to excellently tune the process without experiencing the drawback of slowing the deposition rate. Within this context, numerical simulation has been tried, making available novel tools of practical interest that allow to foresee the particles interactions during the process and gives good understanding on how to optimize the working parameters.

2.3.1 Theory of suspension stability and DLVO theory essentials

As mentioned above, an essential requirement in the EPD technology is represented by the existence of a stable suspension rendered so by particles bearing surface charges. This could be achieved in several ways, but in general dissociation/ionization of surface groups (electrostatic stabilization) and adsorption of ionic surfactants (electrosteric stabilization) are the preferred routes, i.e. respectively:

1) Dangling groups can attach to the particle's surface after dissociation or ionization depending on the properties of the considered molecules and on the pH of the solution resulting in an excess either of H^+ or OH^-.
2) Surfactants molecule that can approach the particle's surface, form some kind of weak bond and hinder further particle-particle interaction due to steric effect.

As for aqueous environments Lyklema[53] found that water molecules have the ability to dissolve at least partially in non-polar solvents and undergo adsorption onto the particle/solvent surface increasing the basicity of the solid, whilst for the liquid the pH alteration is not significant; similarly Remo[54] gave confirmation of this in his studies on α-Al_2O_3, with negatively charged particles in alcoholic environment turning positive after water addition.

On the other hand, organic systems were studied by Wang *et al.*[55] (among others) who explored the behavior of some oxides (Al_2O_3 and ZrO_2 to name a few) in an ethanol solution and pinpointed a sequence of 3 steps: first, C_2H_5OH molecules adsorbs onto the basic sites of the particle, then dissociation of such molecules is observed, with hydrogens moving to the basic surface sites, and finally $C_2H_5O^-$ anions return back into the solution.

From the microscopic point of view, a charged particle is surrounded by a proper number of oppositely charged ions which ensure electrostatic neutrality, creating a system (particles + counterions) referred to as "Lyosphere". Whenever the solution is set under an external action which results in particles flowing thorough the liquid, some ions from the lyosphere leave their corresponding particle because the shear stress becomes stronger than the binding energy: this concept allows for the definition of a particular potential, evaluated at the shear plane with respect to the surface, named "zeta potential". Such entity has a deep meaning in suspension descriptions and gives insight into the stability of particles surrounded by their ionic clouds. This can be better understood considering that for high values of zeta potential the double-layer is thick and particles can not get close enough to coagulate under the action of attractive interactions such as London and van der Waals forces when particles are close to each other in a suspending media.
Sarkar' and Nicholson[56] provided a thorough analysis of particles interaction and suspensions stability starting from Poisson equation and combining it with Boltzmann equation, the latter being necessary to define the balance between energy and entropy for the ion distribution. The discussion is supported introducing a set of parameters required to define completely a colloid (i.e. a suspension of interacting particles with charges positioned on them and free ions in the solution): the charge density (σ) and the surface potential (Ψ_0) characterizing a particle, valence (z_i) and bulk ionic concentration (C_0) of the ions present in the liquid medium which represent the solvent, in turn defined by a specific dielectric constant (ε_r).
Particles in a suspension are surrounded by the "double-layer" (see the following section § 2.4 to find details) and when they get close to each other a repulsion effect is seen due to the overlapping of different lyospheres and the consequent local increasing in ionic concentration which causes, in turn, a decrease in entropy. The interaction between double-layers could be described referring to P, a parameter introduced to define the force along the separation distance D. Its value consists of the opposing contributions of two different mechanisms: P_{ES}, that is the electrostatic force occurring between the electric fields born by the facing double-layers, and P_{OSM}, expressing the osmotic force that follows from entropic variations. The former is attractive since a reduction in distance between the particles and their counterions results in a reduced Coulombic energy, whilst the latter is, repulsive due to the increased concentration of counterions (from overlapping

double-layers) which are more and more hindered in their movements causing a resulting decrease in the configurational entropy. Although both the contributions are not constant along the spatial coordinate, it is self-evident that the total force must be independent from the position if equilibrium at any point between the particles is wanted, and therefore the following equation has to be fulfilled:

$$P = P_{ES} + P_{OSM} \qquad (1)$$

This first introduction to the topic provided, a more quantitative approach is possible, beginning from the Poisson equation with the purpose to obtain the relation existing between Ψ_0 and σ, that is:

$$\varepsilon_r \varepsilon_0 \nabla^2 \Psi_0 = -\rho \qquad (2)$$

Where the variables are defined as specified before and ρ is given by $\rho = e \sum_i z_i C_i$, with C_i meaning the local concentration of ions. All this information can be combined with the aforementioned Boltzmann equation in order to take into account the effects on ions distribution (around the particle) on the two competing phenomena of energy minimization and entropy maximization. This results in:

$$\varepsilon_r \varepsilon_0 \nabla^2 \Psi = -e \sum_i z_i C_i \exp\left(-\frac{z_i e \Psi}{kT}\right) \qquad (3)$$

The remaining mathematical analysis[56] is too cumbersome for the purpose of this work but, to say it in a few words, it arises from a symmetry simplification, supposing the particle with an infinite uniformly charged surface and introducing the Debye-Huckel approximation in the form:

$$\Psi(x) = \Psi_0 \exp(-\kappa x) \qquad (4)$$

$$\frac{1}{\kappa} = \left(\frac{\varepsilon_r \varepsilon_0 kT}{\sum_i (z_i e)^2 C_0}\right)^{1/2} \qquad (5)$$

Where $1/\kappa$ is known as the Debye screening length and it is the characteristic thickness of the double-layer.

Starting from these simplifying assumptions the evolution of potential Ψ with increasing distance r can be drown as shown in **Figure 2.3.1**, as long as low potential conditions are considered. Therefore, in the region close to the particles, the model is not valid anymore and a numerical integration is required: Chan *et al.*[57], approximated the particle surface potential with the zeta potential and extended the relation between V_T and D to all the distance domain, without introducing excessive errors. Interestingly, a parallel theory (now known as DLVO) was proposed, separately, by Derjaguin and Landau[58] and by Verwey and Overbeek[59]: they described the attractive energy between suspended particles following a different path, based on the Hamaker's constant, and obtaining a model widely acknowledged and in great agreement with the abovementioned analysis method.

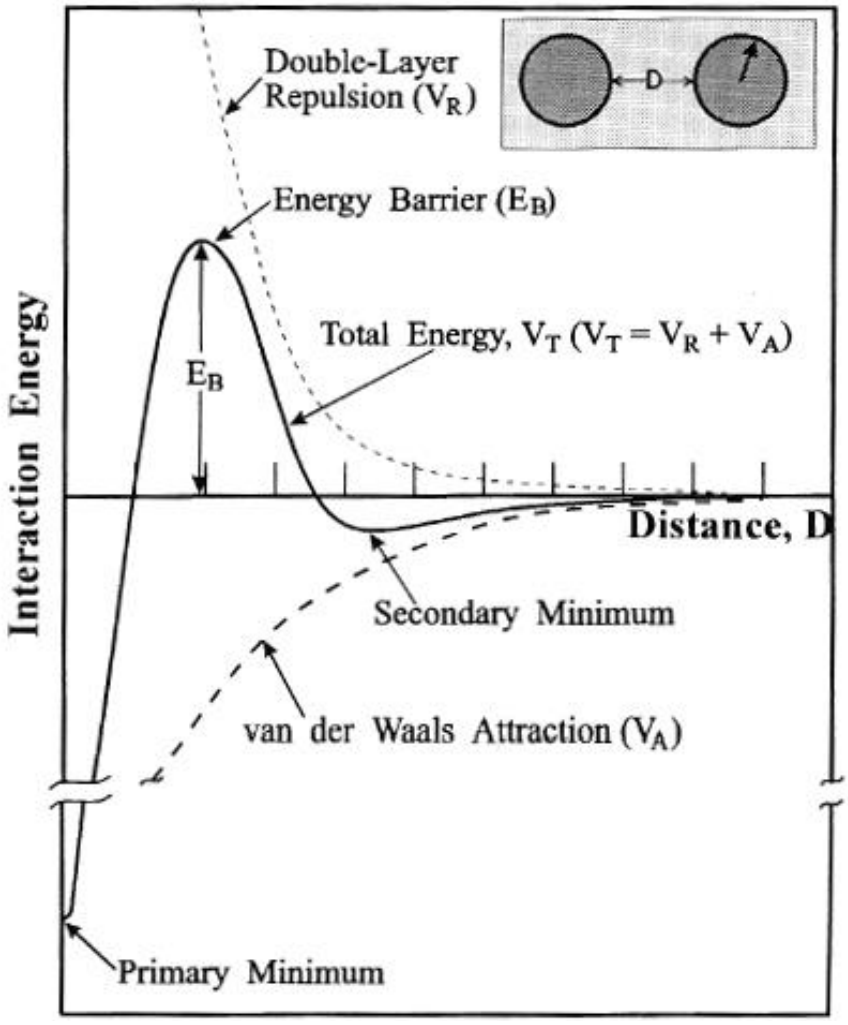

Figure 2.3.1: *plot of the interaction energy as a function of distance separating two free particles in a suspension. Picture credited to Sarkar et al.*[56]

The graph in **Figure 2.3.1** shows that the attractive forces are dominant for small distances because they follow a power law, whereas the contribution of double-layer repulsion gains prominence for increasing distances. This results in a deep primary

minimum of the total energy on the left, meaning the particles are in equilibrium when they get in contact to each other and precipitate; such potential well is marked on its right by a peak E_B that constitutes the energy barrier to be exceeded by separated particles to experience coagulation; furthermore, sometimes, as in this specific case, a secondary minimum might occur, but differently from what seen for the primary minimum, here the subsequent coagulation is not irreversible and the agglomerates could be re-dispersed.

2.3.2 EPD mechanism review

Provided some insight into suspension stability, it is now time to begin a quick review of different mechanism suggested to describe the electrophoretic deposition process.
A first significant contribute is credited to Hamaker and Verwey[60] (it is no coincidence that Hamaker gave the name to the homonym constant): they suggested a model where the deposit is created by means of continuous accumulation of single particles on the electrode surface. Starting from a stable suspension and applying an electric field the particles migrate according to their charge, forming a precipitate. This experimental evidence was explained in direct analogy with spontaneous sedimentation, simply switching from gravity to electric field when considering the action causing EPD. Under the external force, the particles drift towards the electrode and there they stack, pile up and finally accumulate into an adhering deposit, building up a solid agglomerate, thanks to the compression stresses exerted by upcoming material pushing on the already present layer.
Another remarkable contribution comes from Koelmans and Overbeek[61] who provided an analysis of suspensions hosted in polar organic media undergoing EPD. Starting from the DLVO results, they suggested that an increasing electrolyte concentration could cause precipitation in the system, but they did not consider the contribution of ions transportation, as well as the consequent possibility of electrode reaction due to the higher number of ions available. They only estimated by analytical methods the electrolyte concentration close to the depositing electrode, ascribing the observed precipitation to the crossing of the threshold which allows particle flocculation and sedimentation and to the reduced zeta potential around the electrode.

It is worth noting that several different research teams (Brown and Salt[62] as well as Hamaker and Verwey themselves to mention two) suggested models to pinpoint the minimum field strength required to observe deposition, but all of them did not predict accurately the measured values as they usually exceeded the latter by factors of 5 or more. Again Hamaker and Verwey explained the discrepancies referring to the compressing

effect of stacking particles, even though a successive work by Giersig and Mulvaney[63] regarding the deposition of a single layered gold structure discredited that theory.

Sarkar' and Nicholson reviewed the previous work on the topic and suggested a comprehensive explanation publishing a general theory of EPD. In order to accomplish this task the authors used a dialysis membrane to create a barrier between the suspension and the depositing electrode and filled the space in the middle with the suspending solvent, in order to ensure a pathway for ions. Doing so they hindered a direct interaction between the depositing electrode and the particles, and under the effect of an electric field, set by mean of a direct current, the particles flowed according to their charge, stacking on the selective membrane, whilst the ions went beyond it, closing the circuit. Given that a thick sediment was observed on the membrane, the authors were allowed to exclude particle/electrode reaction occurring in the EPD process and the previously proposed hypothesis of particle neutralization was compellingly rejected.
The suspended material was deposited on the abovementioned membrane independently from its position with respect to the electrode, and thus the precipitation for increased electrolyte concentration near the electrode was discarded as well. The phenomenon could be understood recalling the DLVO theory and adding to the curve relative to solution stability the effect of the applied external electric field. Given that F_T is the interaction force between two particles as the distance changes (the previously described DLVO curve), one can argue that the application on an external electric field by mean of a direct current causes a rigid translation of the graph by an amount F_E, where F_E indicates the force exerted on the particles by fluid friction (in other words it is the opposite of the force applied on the charged particle by the electric field). All these consideration are schematized in **Figure 2.3.2**: if at least one particle has reached the electrode or the depositing membrane, another upcoming particle undergoes a global interaction force F_T' obtained by the sum $F_T' = F_T + F_E$ as shown with the dashed curve. The deposition arises in case the attraction force outweighs the repulsion one and the minimum electric field necessary to observe coagulation could be deduced reversely by inspection of the maximum slope value assumed by the right-hand side of the energy barrier peak (**Figure 2.3.1**).

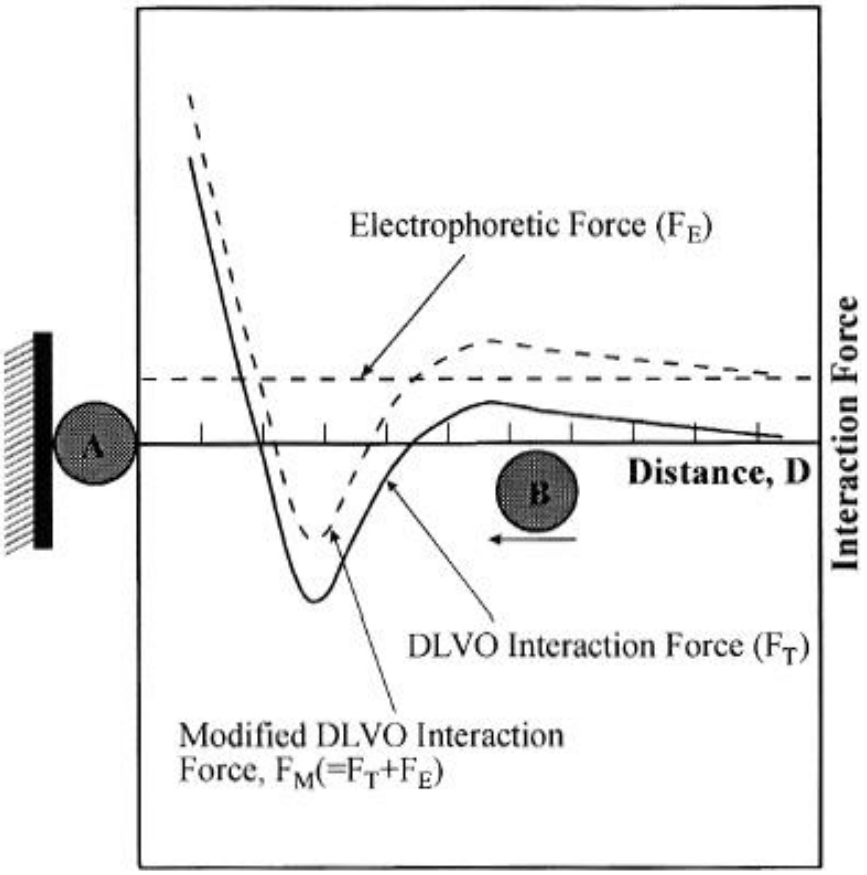

Figure 2.3.2: *plot of the force experienced by two particles in a suspension as a function of distance separating them. Picture credited to Sarkar et al.*[56]

According to the same theory, a better description of the colloidal system is achievable introducing a further parameter, *W*: it gives an estimate of the effectiveness of the energy peak in preventing coagulation and it could be obtained examining the rate of particle coagulation with changing time for different pH and dividing the slopes of each curve by the pH value for which the maximum coagulation rate is observed. A maximum W value guarantees a more stable suspension, whilst approaching the isoelectric point W and E_B decrease and the minimum is maintained over a significant pH window.

Sarkar' and Nicholson provided moreover a thorough description of charged oxide particles flow towards the depositing electrode during the EPD process: fluid dynamics, coupled with electric field, distorts the lyosphere thinning the double-layer in front of the agglomerate and thickening it on its rear, modifying the zeta potential across the specific surface point considered. In flowing conditions a particle is thus surrounded by an atmosphere of counterions stretched and shifted backwards and the equilibrium requires

them to fulfill the two following equations, relative to the dissociation reaction of electrolyte molecules and the deriving equilibrium constant K (at constant temperature):

$$YX \rightleftarrows Y^+ + X^- \qquad \Rightarrow \qquad K = \frac{[Y^+][X^-]}{[XY]} \qquad (6)$$

where the squared brackets indicate concentration of the specific species. With regard to the trailing hemisphere, once the particle has reached the electrode (or in alternative the membrane), the shearing force fails and the counterions extending in the longer "tail" are surrounded by a high concentrations of ions of opposite charge produced by the dissociation. This means a lack in equilibrium and in order to maintain the K value constant the recombining reactions starts, since at significant distance from the particle surface the double-layer is loosely bound and the original YX specie is easily formed. This causes a decrease in counterions present in the tail of the atmosphere surrounding the particle and promotes the deposition of the next incoming particle which can now encounter a lower double-layer thickness and thus a smaller energy barrier for coagulation.

2.3.3 Fundamentals of kinetics in EPD

From the processing point of view, a deep understanding in EPD kinetics, in terms of deposition rate, layer thickness, composition and material properties, is a substantial requirement. Again, Hamaker embarked first in the project of unravelling the issue and he noticed a linear correlation between weight deposited with EPD and amount of transferred charge. The voltage drop from the depositing surface was investigated and it was found to decrease steeply in the space region closest to the electrode, showing a highly resistive effect of the sediment layer. Such insulating effect provided by the ceramic material caused a current drop throughout the process due to the layer thickness increasing with time. Nonetheless it was consistently proved by experimental results that deposition yield was proportional to transferred charge and this suggested a kinetic law where the deposited mass is expressed as:

$$w = \mu CAEt \qquad (7)$$

Being w the weight of the deposit, C the suspension concentration, A the depositing surface, E the applied electric field, t time of deposition and μ the proportionality constant, defined as the electrophoretic mobility of the particle.

The same quantity could be estimated by integration, considering an infinitesimal depositing surface dS where a dw weight has grown in a dt time, as follows:

$$\int dw = \iint fu\, dSC\,(t)dt = fu \iint dSC(t)dt \qquad \textbf{(8)}$$

Compared to the previous relation, here, the variable f has been introduced as an "efficiency factor", meaning the ratio of particles contributing actively to the deposit formation (it should approximate 1 if the colloid is stable and the z potential is high), u is the velocity of the particles considered on an eaverage value and $C(t)$ is the concentration of the particles in the suspension with changing time. Such equation is in agreement with the experimental results for a steady state process and within a specific voltage window, where the lower boundary is given roughly by the minimum voltage required for deposition and the upper one is set by the voltage up to which the ohm's low is fulfilled. In ideal conditions, with homogeneous suspension and concentration varying for no other mechanisms than EPD, Equation **(8)** could be solved using the mass balance as boundary condition (i.e. $C(0) = w_0/V$ at time $t = 0$ and $C(t) = (w_0 - w(t))/V$ at $t \neq 0$, with w_0 indicating the initial weight of the solid dispersed in the suspension of volume V) giving:

$$w(t) = w_0\,(1 - e^{-kT}) \qquad \textbf{(9)}$$

$$\frac{dw}{dt} = w_0 k e^{-kT} \qquad \textbf{(10)}$$

where k is a kinetic parameter defined as $k = Sfu/V$.

As discussed previously EPD can be performed following two different procedures:

- Constant voltage, if the potential is kept constant between the two electrodes. This translates though in a mutable EPD potential, since as the material is deposited, the resistance increases and the electrical field available for further deposition is weakened, slowing down the process even to zero if the driving force is completely depleted.
- Constant current, if the electrons flow is adjusted (and maintained constant) in order to provide an unchanging electric field to the EPD process and prevent variations in deposition rate due to resistance increase.

Sarkar' and Nicholson showed that although under constant current conditions the previous equations fit satisfactorily the experimental data, the agreement between theory

and practice is not preserved if a constant voltage is applied. This implies the need to introduce a further parameter, to take into account the decrease of deposition rate with time, represented by I_N, namely the normalized deposition current changing with time, and this restores the curve fitting with experimental data.

Based on what discussed above, therefore, the kinetic integral (Equation **(8)**) under constant voltage operations needs to be adjusted as the concentration $C(t)$ and the particles velocity, $u(t)$, are both functions of time. This translates into:

$$\int dw = f \iint dSu(t)C(t)dt = f \iint dS\mu_e E(t)C(t)dt \qquad \textbf{(11)}$$

$$\int dw = k' \int E(t)(w_0 - w(t))dt \qquad \textbf{(12)}$$

where $E(t)$ indicates the voltage drop per unit length of suspension in the direction perpendicular to the depositing electrode whereas k', the new kinetic factor, is now expressed as $k' = Sf\mu_e/V$.

Moreover, the authors proposed a new model to describe the changing voltage drop in the system as the material is deposited, defining a new fictitious distance, L_{eq}, which would separate the electrodes in the hypothetical conditions where the resistance was given by a thicker amount of suspension rather than the sum (calculated on the original length L) of the suspension resistance coupled with the effect of the growing deposited layer. In analytical form this means:

$$L_{eq} = L + L_{dep}(R_r - 1) \qquad \textbf{(13)}$$

Where L_{dep} and R_r constitute, respectively, the thickness of the deposit and the ratio of deposit resistivity to the suspension's one. Now, the first variable could be expressed as a function of density, ρ, and weight, w, of the deposit, as follows:

$$L_{dep} = \frac{Volume\ of\ deposit}{Depositing\ area} = \frac{w(t)/\rho}{S} \qquad \textbf{(14)}$$

Combining the last two equations a new expression for L_{eq} is provided:

$$L_{eq} = L + \frac{w(t)/\rho}{S}(R_r - 1) = L + w(t)R' \qquad \textbf{(15)}$$

Where the parameter R' is defined consistently:

$$R' = \frac{(R_r - 1)}{\rho S} \qquad \textbf{(16)}$$

This allows to obtain a new relation for the voltage drop per unit length, $E(t)$:

$$E(t) = \frac{V_{app}}{L_{eq}} = \frac{V_{app}}{L + w(t)R'} \qquad \textbf{(17)}$$

And thus the deposition equations could be rewritten as:

$$\int dw = k' \int \frac{V_{app}}{L + w(t)R'}(w_0 - w(t))dt \qquad \textbf{(18)}$$

The last equation could be solved giving:

$$w(t)R' + (w_0R' + L)\ ln\left(\frac{w_0 - w(t)}{w_0}\right) + k't = 0 \qquad \textbf{(19)}$$

The agreement between Equation **(19)** and the experimental data resulted adequate as well as it was with the already discussed model based on the variable kinetic factor[56]. Interestingly, if R_r is set as 1 then $R' = 0$ and the constant voltage equation degenerates into the constant current equation, strongly supporting the validity of the developed theory.

All these theories, proposed in slightly different forms also by other research groups[64] are good descriptions of experimental data only for short depositing time, whilst for longer experiments only the constant current conditions preserve the agreement between theory and observations, since for constant voltage the particle velocity decreases due to lowering of the potential drop, making it difficult to develop equations able to predict the system behavior.

In conclusion constant current provides better control and is the best choice from industrial point of view because it provides a higher deposition rate whenever $R_r > 1$ even though, to date, the constant voltage working conditions are the most used. This might be due to the simplicity of equipment required to perform such a process, but could also be ascribed to the benefits produced by controlling the applied potential and not the

current, whose effect depends strongly on the electrode area, as the charge carried is effect of the particle concentration.

2.3.4 EPD applications of interest for this work

Given the extreme simplicity of the mechanism on which the EPD process is founded, i.e. an electric field controlling the motion of charged particles, it is not surprising that such technique has encountered success in a host of applications. As a matter of fact, the process is very versatile and it is economically sustainable since the concept is easy to engineer. Moreover, the deposit can be shaped consistently with the design requirements, scaling up the system to industrial size, when needed, and achieving various configuration and even complex 3D structures.[65]

Currently, EPD is of great interest both in academia and in industry, and many reports and patents have been issued, but here a brief introduction to the applications of this process will be devoted only to those fields which might share some features with what researched in the present study. Nevertheless, it is worth mentioning that EPD on advanced ceramics (i.e. the topic discussed in this work) is inserted in a wider category of colloidal processing method and it is used to synthetize bulk components as well as coatings, films, functionally graded materials and composite laminates.

Beginning from ceramic slimes deposition, advances in suspensions preparation improved the fabrication of highly homogeneous materials with remarkable results for monolithic and free standing objects, hollow bodies and complex 3D shapes. What's more, recently the practice involved the nanoparticles systems as well, and now highly controlled and fine microstructures are easily achievable, allowing to precisely tune the sediment properties and its evolution during the following sintering step.

To date, silica and silica-alumina colloids are the most common materials to fabricate *via* EPD even though a variety of functional ceramics are nowadays treated with this technique, being $BaTiO_3$, ZnO, alumina, pyrite (FeS_2), diamond, yttrium, zirconia some examples. Titania (TiO_2) deserve a specific dissertation because of its remarkable role in many strategic fields of research and industry development. In 1994, Matthews *et al.*[66] fabricated a titania thin film deposited, under constant current, on a conducting glass supposed to work as the active material in a prototype photovoltaic cell. Other than that, examples of porous titania films were produced, employing different kind of substrates and materials: good result were accomplished, with high degree of particle packing and homogeneity in the microstructure, even in the case of constant voltage conditions, smooth surface finish and thicknesses of few micrometers.[65]

Moreover, EPD proved to be an excellent route in applications concerning composite films production of ceramics coupled with other materials, such as, for instance, a cobalt oxide nanostructured film[67] in a combination of EPD preceded by a cathodic electro-synthesis of cobalt hydroxide. Changing the working parameters, the properties of the films could be tuned and the subsequent heat treatment resulted in a decomposition of the precursors and in the formation of the desired oxide film. The method can be applied to a variety of different systems and combination of disparate electrochemical processes are nowadays possible, in combination with EPD, to achieve better insights into the production of functional and structural composite films.

Finally, a brief dissertation is devoted to EPD carried out on metallic nanoparticles and metallic phase nanostructured systems, despite the smaller amount of publications available compared to the literature regarding the world of functionally graded ceramics. Deposition of metallic nanoparticles is a remarkable way to fabricate advanced materials where the electronic, optic, magnetic, thermal and photocatalytic properties are tunable based on the selection of specific process variables.
The most inspected materials have been Au, Ag, Pt and Pd, but functional application of semiconductor nanoparticles such as CdSe are included in the list.[68] The applications are multiple, and 2D and 3D configurations could be found in Raman scattering films, photovoltaic applications, optical gratings, a variety of coatings, diodes, sensors nanostructured electrodes and much more.
Metallic nanoparticles EPD found place in the production of electronic devices and a process for depositing nano-sized silver to create electrode layers for electroceramic application has been proposed. Using silver powder with a diameter of 10 nm an outstanding control of surface roughness and particle packing was achieved starting from a suspension with a non aqueous dispersant medium.[69] The result was the production of multi-layerd structures with noticeable electrical conductivity and a thickness around only two times the diameter of the starting powder.
Finally, EPD allowed the production of novel reactive oxides dispersed intermetallic coatings, obtained starting from a combination of EPD and conventional sedimentation and the initial formation of oxide particles from the plating bath: the products, namely oxidation resistant coatings with intermetallic phases, shown a high industrial relevance and are likely to gather further interest in the upcoming years.[65]

In Conclusion: EPD has proven to be a versatile and cost effective technique for material processing with remarkable control over microstructure, stoichiometry, microscopic and macroscopic dimensions. In the last years, these advantages have triggered a thriving research activity and in the future, a great development in industrial production is

expected. Potential areas for new application are likely to extend from fabrication of nanostructured and hybrid materials to functionally graded materials and laminated nanoceramics. Many material categories might be involved and especially the electric, dielectric, super- and semi-conducting, magnetic and biomedical fields might benefit from such developments. More generally, all areas where the EPD has shown relevance and advantages compared with competing processing techniques in commercial and industrial activity have to be considered for future expansions. Nonetheless further modelling and research are needed to ensure a better understanding of the phenomena and help scientist to overcome the annoying trial and error empirical approach currently necessary to set experiments.

2.4 Electrochemical capacitors

As well established, a capacitor is an electric component primarily devoted to energy storage (even though other applications are possible) and the basic layout consists of two conductive plates facing each other with a dielectric material layer positioned in between. Under an applied voltage, charge starts flowing and collecting on the boundaries of the circuit, i.e. the capacitor's plates, but it is prevented from short circuiting tanks to the presence of the insulating material, providing an easily and feasible route to physically store energy.

A quite similar phenomenon, though reproduced on microscopic scale, is the fundamental on which electrochemical capacitors (contracted form ECs, sometimes referred to under the trade names "Supercapacitors" or "Ultracapacitors") in their most common - symmetric - structure are based: the operation principle consists in employing a solid material characterized by high values of the specific surface area (SSA) in the role of active component for an electrode that is soaked in a proper electrolyte to produce a miniaturized capacitor, thanks to the interfacial formation of an electrochemical double-layer (details provided below).

In view of what just stated, such an electrochemical phenomenon can be harnessed to store energy and the scientific community has been aware of the formation of a double-layer at the interface between a solid and an electrolyte when a potential is applied, since the late 19th century. Nevertheless, the first commercialized double-layer effect based capacitor appeared only in 1966[70]; since then, however, a thriving market has bloomed and a number of patents, journal articles, and dedicated meetings has arisen. The second milestone in the ECs market was the NEC's SuperCapacitor^{TM} released in 1978 under license from SOHIO and, starting from the backup power devices application, the next generation design found place in wireless communication, regenerative energy capture

processes, and many other fields where their battery-complementary properties gave practical advantages.[70]

As a matter of fact, ECs have the same objective as traditional batteries, namely energy storage, but differently from the latter, the former does not usually rely on chemical reaction to generate electrical energy and the idea is rather to achieve high capacitance values thorough a physical mechanism of electrons collection and ions flow. More precisely, however, the improvements in the primary understanding of ECs operation have pinpointed two different contributions to the overall capacitance of such devices:

- Double-layer capacitance, due to the formation of the so-called Helmholtz plane, that is a separation of charge of opposite sign at the interface between a solid electrode, made of a conductive material, and a proper electrolyte, namely a wetting solution in contact with it.
- Pseudocapacitance, ascribable to electrochemical processes where some kind of electrosorption or intercalation redox reactions occurs, but their rates are so quick that the ions movements result in a highly reversible charge transfer at the electrode.

Although both mechanisms contribute simultaneously to the total capacitance shown by ECs and their ratio can range hugely, usually the double-layer capacitance is widely predominant, so much that electrochemical double-layer capacitors (contracted forms EDLCs) deserves a specific dissertation.

As inferable from before, in contrast with batteries, which, again, rely on chemical reactions, mass transfer and phase growing to generate electrical energy, the energy storage properties of ECs, and foremost EDLCs, stems from their traditional capacitors counterparts: charge is collected physically (instead of chemically like in batteries) thanks to a couple of electrodes immersed in a proper liquid that work along the lines of the plane plates of massive capacitors, producing a high reversibility and a remarkable cyclability, translated, in turn, in reproducibility of charge-discharge cycles. With more detail, for this category of devices the energy storage is based on the charge separation established spontaneously between the electrode and the electrolyte when an external voltage is applied: the formation of an electric double-layer at the interface between a high specific surface area active material and a liquid electrolyte allows huge values of the capacitance and exactly from this peculiar configuration arises the common denomination of such devices.

The capacitor-like behavior is observed because the charge transfer across the electrode interface is mainly hindered, at least as long as operations are carried under a voltage threshold of 3V: the value should be theoretically enough to trigger one or more electron transfer processes from a thermodynamic point of view, but kinetics considerations show

how the rates of such reactions are so small as to be considered negligible and cause the electrode to experience a net charge on its walls. According to the models developed by Grahame toward the middle of the past century,[7] the electrode is constituted by a solid plate collecting electrons and by an electrolyte wetting the solid wall, where ions of the proper charge, flow and accumulate forming a diffuse double-layer to preserve electroneutrality. The limited thickness (on the orders of nanometers or even less) of the space separating the opposite charges and the high surface areas involved provide capacitance value much higher than what observed in conventional capacitors, and the properties could be further tuned acting either on the electrode or on the electrolyte or even on both of them.

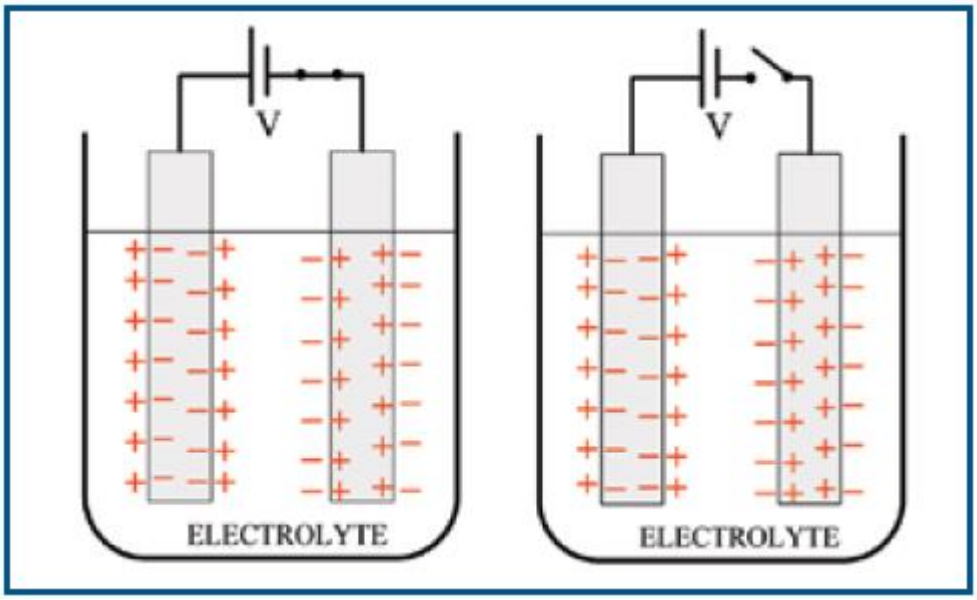

Figure 2.4.1: *schematics of a double-layer capacitor in a proof of concept configuration. Two electrodes are inserted in a beaker and a voltage is applied causing charge separation that persists even after the electric circuit is opened. Picture credited to Miller et al.*[96]

The fundamentals of EC can be better explained starting from a thought experiment where two electrical conductors are inserted in a beaker containing an electrolytic fluid. If the two solid components are connected by an external electrical circuit, no voltage can be measured, but if the device is equipped with a battery and the switch is closed, current flows according to the EMF (electromotive force) available until the complete balance is achieved and charge separation occurs at both the liquid-solid interfaces (see **Figure 2.2.1**). In other words, two capacitors are working in series, connected through the in between present electrolyte and the behavior is even more remarkable when, under applied voltage, the switch is open and charge persists at the interfaces, resulting effectively in a storage. This means solvated ions in the electrolyte are attracted to the solid surface by an opposite charge placed on the solid surface, giving rise to the

aforementioned electric double-layer: the charges are spaced by a thin separation layer, usually ranging on the order of few angstroms and a SSA up to thousands of squared meters per gram makes theoretically possible the fabrication of capacitors with capacitances of several kF.

Such a high SSA is yet the reason of the relatively slow response of ECs compared to traditional capacitors where the charge is quickly stored on the conductive plates. This can be understood considering the schematic illustration (**Figure 2.4.2**) of the hypothetical circuit characterizing the inside of a pore supposed to be cylindrical for the sake of simplicity. The behavior of its cross-section filled with electrolyte resembles the one of a RC circuit with a multiple time constant equivalent model: under an applied voltage, the electric double-layer at the interface between solid and liquid builds up but while the solid wall of the nanoporous material are conductive and the charge distributes evenly and promptly across them, the same does not happen for the electrolyte. As a matter of fact, the charge carried by the electrolyte in form of ions has to face a variety of obstacles along its path to get from the mouth of the pore to the further regions of the cavity and this clearly translates in a higher series resistance and in a decrease of the process efficiency. Nevertheless, the responsivity of energy storage devices compellingly challenges the quite slower performances of traditional batteries.

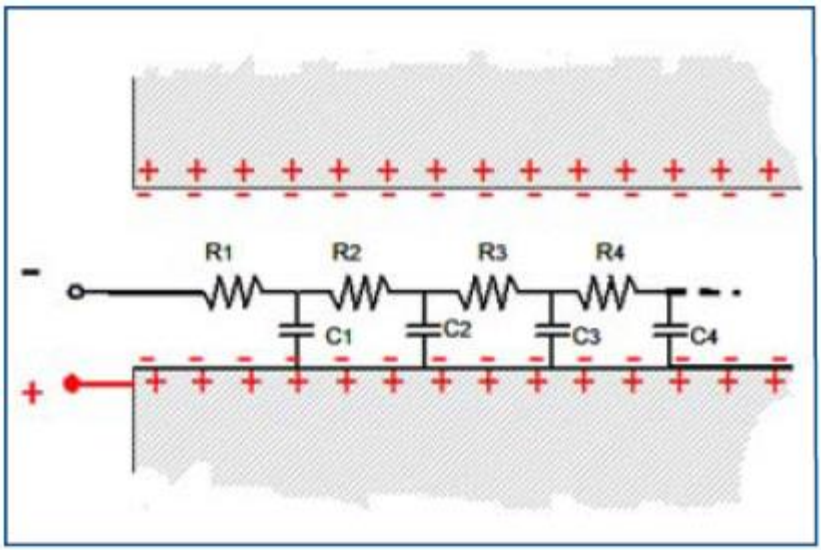

Figure 2.4.2: *schematics of the idealistic equivalent circuit for an electrolyte-filled cylindrical nanopore in an electrochemical capacitor carbon electrode. Picture credited to Miller et al.*[96]

The required high values of SSA for the electrodes are usually achieved resorting to materials characterized by high levels of porosity, such as, as main example thanks to its up to 2000 m^2/kg impressive value, treated porous carbon (obtainable easily starting from coconut shells with a quite inexpensive process). With such a high value for SAA

capacity, up to 200 F can be reached occupying a space much smaller than a traditional capacitor would do, simply constructing a EDLC based on two carbon electrodes matched in series and connected by a suitable electrolyte.
Even though the latter is the most common active material, lately a variety of alternatives have been proposed and especially carbon nanotubes and nanofibers and carbon nanoporous structures above all have gathered the attention.[71]
Another key parameter is represented by the electrolyte used to wet and connect the electrodes: not surprisingly, it can have different compositions and be either aqueous or organic, citing for instance sulfuric acid or acetonitrile, respectively[72]. Different substances, though, have found success in different periods and during the last decades, they have experienced an evolution starting from the early H_2SO_4 and KOH, which provided narrow operating window voltage below 1V, and moving towards organic electrolyte, such as ammonium salts dissolved in acetonitrile or propylene carbonate, thanks to the remarkable increase of the ranged cell voltage up to 2.7 V. Thus, the operating voltage is determined by the breakdown potential of the electrolyte and for many applications single cells must be series-connected, just as happens for batteries, to provide the voltage drop required by the powered equipment.

The other class of ECs, as mentioned before, does not rely exclusively on the electric-double-layer and is referred to as pseudocapacitor: they stand out for a fast reversible (faradaic) surface redox process which occurs thorough an effective electron transfer, yet coupled with a still remarkable formation of the electric-double-layer, that allow these devices to store even more energy than EDLCs (for instance gravimetric capacitances of 1358 F/g have been observed[72]). Unfortunately the excessive cost of the active material usually employed, namely RuO_2, prevents currently industrial application: to overcome its expensiveness, different other active materials have been suggested and especially polymers able to store energy thanks to the doping and de-doping of ions from the electrolyte, as well as transition metal oxides, are meeting a moderate success. Currently pseudocapacitors can reach energy densities of about 30 Wh/Kg, and this remarkable value (with respect to EDLCs) have driven efforts devoted to identify suitable materials able to preserve an outstanding charge-discharge cyclability while increasing the charge storage capacity.

As mentioned before, the pioneering ECs of 30 years ago were based on a symmetric design where two identical electrodes faced each other, immersed in an aqueous electrolyte that imposed operating voltage window limited to circa 1.2 V/cell.
Most recently, however, a further and more successful class of ECs, represented by the "asymmetric hybrid capacitors", has arisen thanks to the series combination of different

behaving electrodes. It is about a category of devices where a battery-like (or pseudocapacitor-like) faradaic electrode is paired with a capacitor-like non-faradaic electrode in order to combine the peculiarity of both and accomplish the goal of creating a device which shows both high energy (battery) and high power (capacitor) output. Generally, the capacity of the battery-like electrode is much higher than its traditional counterparts, and this allows to produce devices characterized by twice the capacitance of a symmetric design, because the potential of the former electrode is almost fixed, whereas the latter experience an almost linear change of potential with charge. Bearing in mind that the energy stored in a capacitor is proportional to the square of the cell voltage, matching, for example, an anode doped with Li ions and a cathode of activated carbon provides a remarkable energy output, since the chemistry of the Li redox reaction by the just described electrode combination can produce an operating voltage of approximately 4V, i.e. a value much higher than what available for traditional ECs.

In general, advantages offered by ECs can be gleaned from any Ragone plot, where the comparison with batteries shows an outstanding specific power, balanced though by modest levels of specific energies. Such behavior is ascribable to the earlier illustrated mechanisms of charge storage and releasing, that are intrinsically fast because based on physical charge separation instead of on any major change in the structure of the electrode material due to electron transfer. This gives a hint for storage devices design, because ECs becomes thus attractive whenever any rapid velocity change is experienced, i.e. abrupt accelerations and heavy power duties, but can't provide long lifetimes, in perfect complementarity with batteries and fuel cell performances. The charge discharge time is on the order of seconds or less, but the process is reversible and, thus, a single charge-discharge cycle takes place in a very short time compared to other kind of energy storage devices.

The other stunning benefit brought by ECs is the high reversibility of the process which is credited to their basic operating principle: the storage mechanism does not lead to any volume change (differently from batteries where the electrochemical transformation of active masses is observed) neither any major chemical reaction occurs, providing robust devices with excellent cyclability (up to many millions of cycles) and from many point of view they can improve the batteries properties, reducing both the system volume and the maintenance needed.

Another major advantage is their ability to store energy that is usually lost in form of heat during cyclic processes, as happens for cars in breaking and accelerations: although for light vehicles batteries are able to provide the required instantaneous energy, things change when the weight is increased, for examples in busses or trucks, or when the loads

are particularly heavy as for cranes, and the ECs can show in this field their supremacy over traditional batteries.
Furthermore, the charge-discharge efficiency of ECs is high, and this allows a small amount of energy loss throughout each cycle, providing a device that can promptly remove the unwanted produced heat without any noteworthy cost ascribable to the possible residual heat extraction system. Finally, ECs show advantages even from the point of view of safety, meant in terms of easiness in the state-of-charge (SOC) assessment, since their aging occurs smoothly, or better linearly, with a gradual decrease in performance with time, free from any sudden drop (as sometimes happens when working with traditional batteries).

In conclusion, ECs are energy storage devices where two electrodes are soaked in a proper electrolyte to build an electric circuit resembling a couple of capacitors series-connected. Usually the electrode is made of an active material characterized by high SSA, like a treated carbon powder, and the charge accumulated on its highly extended walls attracts an equivalent amount of opposite sign charge in form of properly charged ions, inducing the formation of the so called electric double-layer close to the solid surface. The limited thickness of the double-layer, coupled with the high surface area available provide a remarkable energy density compared with those of traditional capacitors, with high specific and volumetric capacitances, and produces a formally unlimited charge-discharge life. The only limitation is due to the restrictions in the applied voltage, since the electrolyte is not always stable and the operations should be carried under its breakdown potential; nevertheless, further developments are expected and non-symmetric combinations of the electrodes have partially overcome the issue.

Chapter 3

Materials and methods

This chapter provides general information regarding the synthesis of pristine MAX phases starting from precursors' powders, the etching procedures and the technique adopted to carry out the electrophoretic deposition (EPD) of the MXenes sheets after their dispersion in water or dimethyl sulfoxide of propylene carbonate. Details about the characterization methods, comprising X-rays diffraction (XRD), scanning electron microscope (SEM), Fourier transform infrared spectroscopy (FTIR), dynamic light scattering (DLS) and four probe film conductivity measurements are provided. A description of the Swagelock cell assembly, used for electrochemical testing of EPD electrodes is given as well.

3.1 General steps in MXene colloidal solutions fabrication

Films of various thicknesses and features were produced starting from delaminated MXene solutions of different concentrations and compositions. The MAX phase precursors, i.e. metallic powders and graphite, were mixed and reaction sintered to form ternary carbides. The as-obtained materials were then milled and etched with different acidic solutions to remove the Al layers and yield multilayered MXenes. Finally, the sheets were intercalated with various solvents promoting the delamination either by manual shacking/vortexing or by sonication. In some cases, both techniques were combined, to produce a suspension concentrated enough to successfully undergo EPD.

3.1.1 Main steps in the synthesis of bulk MAX phases

MAX phases of various compositions were fabricated employing their parent compounds in form of as-received powders (see **Table 3.1.1** to find a summary of materials, purity, particle size and source), for the metallic species as well as for the carbon (graphite) fraction. After weighing the proper amount of each desired specie (weighing scale model: Setra 5000, accurate to the nearest 0.01 g) the powders were poured in plastic bottles along with either new or thoroughly cleaned zirconia milling balls to carry out the mixing

phase, using a mechanical mill for different treatment times, as specified in the following chapters.

Powder	Purity (wt. %)	Particle size	Source
Carbon	99	-300 mesh	Alfa Aesar, Ward Hill, MA, USA
Aluminum	99.5	-325 mesh	Alfa Aesar, Ward Hill, MA, USA
Titanium	99.5	-325 mesh	Alfa Aesar, Ward Hill, MA, USA
Tantalum	99.97	-325 mesh	Alfa Aesar, Ward Hill, MA, USA
Niobium	99.8	-325 mesh	Alfa Aesar, Ward Hill, MA, USA
TiC	99	–	Alfa Aesar, Ward Hill, MA, USA
Ti_2AlC	92	-325 mesh	Kanthal, Sweden

Table 3.1.1: *list of the powders used to synthetize MAX phases in this study, combined with their respective source and characteristics.*

According to the lab know-how, only some of the powder mixtures were cold pressed to obtain a pre-compacted brick before proceeding with the sintering process. Variable amounts of powder, generally ranging between 10 and 20 g were poured in a cylindrical pressing die made of hardened steel, evenly distributed in order to avoid the presence of air embedded in the material and pressed with a punch of 25 mm diameter exerting forces of tens of kN and generating pressures of hundreds of MPa, depending on the materials and on what the individual compositions required to end in a free-standing disk.
Powders, whether pre-compacted or not, were moved to an alumina boat (and spread evenly across all the available space if not compacted) to undergo reaction sintering and obtain MAX phases as final products.
The crucible was inserted in a tube furnace always coupled with a second boat containing a small amount of Ti powder, with the aim of gettering possible oxygen molecules present in the reaction chamber. To further prevent oxidation, the furnace was purged with Ar for 1 h before starting the sintering process. With the flow of Ar constant, the heat programs were started according to what suggested as optimal practice by previous works. The heating process consisted of a ramp to reach the soaking temperature, a holding phase at the treatment temperature and the passive cooling to room temperature RT. The resulting sintered bricks where ground into fine powders with a titanium nitride milling bit and sieved to obtain powders of particle size < 38 mm (-400 mesh) to be used for following MXene synthesis. Furthermore, the bigger particles left were ground again in the mortar and pestle and sieved repeating the process until the wasted material was reduced to the minimum.

3.1.2 General procedure to etch MAX phases into MXenes

The MAX phases were treated with acidic solutions, either as-received or diluted by deionized (DI) water in order to obtain milder reaction conditions. The purpose was to selectively etch the A-atoms – Al in most cases - which are bonding the $M_{N+1}X_N$ layers to produce multilayered (ML) MXenes. To enhance the sheet delamination and water intercalations once the MAX phase was taken apart by the removal of the A-atoms layers, lithium salts dissolved in the reaction batch were used as well.
The chemical species used to carry out the wet chemistry synthesis are summarized in **Table 3.1.2**, as well as their respective source and initial concentration, where it has to be specified that the latter were assumed to be the average rounded to the nearest integer in case ranges were provided instead of single values: hydrofluoric acid, HF, for instance, was available in concentration between 48 and 51 wt.% and therefore 50 wt.% was taken to be its representative value.

Chemical compound	**Source**	**Concentration**
Hydrofluoric Acid (HF)	Fisher Scientific, Fair Lawn, NJ, USA	48-51 % in H_2O
Hydrochloric Acid (HCl)	Fisher Scientific, Fair Lawn, NJ, USA	37 % in H_2O
Lithium Chloride (LiCl)	Alfa Aesar, Ward Hill, MA, USA	98%
Lithium Fluoride (LiF)	Alfa Aesar, Ward Hill, MA, USA	98.5 %

Table 3.1.2: *list of chemical compounds employed in the wet chemistry reactions, combined with their respective source and concentration.*

Dealing with concentrated acids is dangerous and precautions have to be taken: HF especially poses high health risks and a thorough knowledge of the safety data sheet as well as wearing a proper attire (apron, sleevelets and face shield added to the usual chemical lab safety equipment) are recommended. The reactions were all carried out under a fume hood and thermostatic baths were used, for both safety and products quality considerations.

The fundamentals of the etching reactions are comprised by a few standard steps and are based on immersing the MAX powders in the acidic solutions contained in a reaction vessel, although variations might be introduced to accomplish specific goals. For the present work, plastic bottles of different sizes (30, 60, and 120 mL) were drilled first with a little hole in their lid to provide venting and avoid pressure build up. The selected amount of acid was then poured in the jar, making sure of having chosen a proper size to prevent excessive rise in the liquid and subsequent overflow during the reaction. As mentioned above, in some cases, ion intercalation was stimulated by adding to the acid either lithium chloride or lithium fluoride depending on whether the etchant was HF or

HCl respectively, and some stirring was then provided manually. Thereafter the MAX powders, always sieved through a -400 mesh (see the following chapter to know the specific amount for each MAX phase), were poured in the acid solution being careful that the process was carried out very slowly. Using a metallic spatula fractions of grams were added at regular time intervals allowing sufficient time between each other for the heat generated by the exothermic etching reaction to be removed.
Completed this last stage, a magnetic stir bar was dropped in the reaction vessel and, once the bottle was closed, a gentle whirling movement was manually applied before placing the batch on stirrer for a time depending on the specific acid and MAX phase involved. Most of the time, according to the synthesis conditions and safety regulations, the reaction vessel was partially immersed in the oil of a thermostatic bath (working as a secondary container) at temperatures slightly higher than RT, in order to both enhance the reaction kinetic and, in parallel, provide heat removal in case of strongly exothermic reactions.

At the end of a pre-specified time, the reacted powders needed to be washed from the acidic solution in which they were soaked in. For this purpose, the reacted mixture was split evenly in two centrifuge tubes (50 mL each) and DI water was added, filling both of them completely to dilute the acid. Then the solutions were centrifuged at 3500 rpm (2300 rcf) for two minutes to precipitate the powders and after that the so-generated supernatant was poured in a proper acid waste container. The centrifuge tubes containing only the black sediment were filled again with DI water and vigorous shaking was provided, both manually and using a vortex mixer, to re-disperse the powders, repeating the centrifuging and decanting steps until the supernatant after centrifugation remained dark, which typically occurred after the liquid achieved pH > 6.

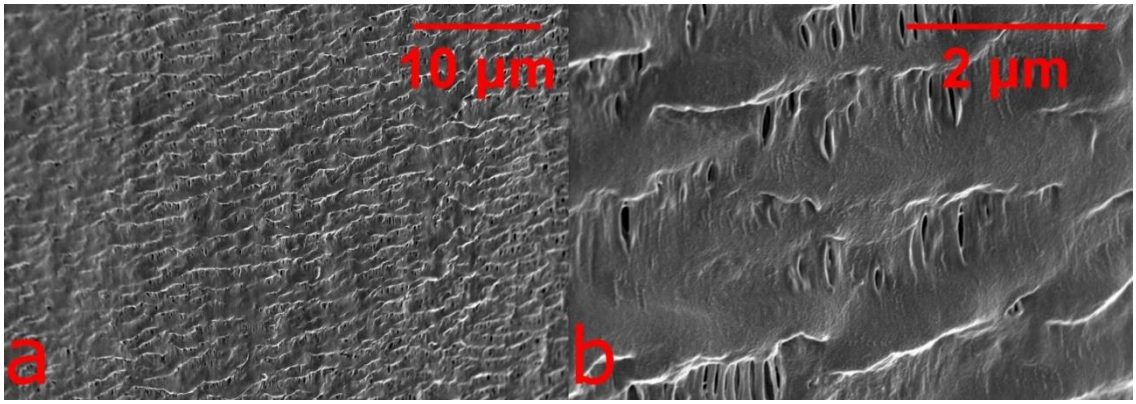

Figure 3.1.1: *SEM images of the polypropylene membrane used for vacuum filtration. Pictures were taken using the following instrument parameters: EHT 1.50 kV, working distance 3.3 mm and magnification 2.5K and 20K respectively for a and b.*

After obtaining a neutral solution the powders were finally vacuum filtered, unless dispersed in water and sonicated right away, as described in § 3.1.3: the device, connected to a pump, allowed the powder to be separated from the liquid phase (mainly water) thanks to the action of a glass porous filter and of a nanoporous polypropylene membrane (SEM images in **Figure 3.1.1**) laid down on the latter, that let the liquid be drained, preventing the powders from being sucked in as well.
The deposit produced in that way was then extracted from the vacuum filtering device, still on the porous membrane and let air dry for further synthesis steps and/or analysis.

3.1.3 MXenes delamination and suspension

For this specific work propylene carbonate, PC (Alfa Aesar, 99 %), dimethyl sulfoxide, DMSO, (Fisher Scientific, ≥ 99.7) and DI water where used as dispersing media of the single/few-layered MXene particle obtained after delamination. Except for the cases when the just washed sediment was re-dispersed in water and sonicated right away with the working parameters specified later, independently on the solvent the basic procedure for particle delamination comprised, in chronological order: weighing of the powder to be suspended and storage of a small amount for XRD analysis; pouring of the powder in a plastic bottle containing the dispersing agent as well; magnetic stirring of the mixture for varying time lengths (step for PC only), sonication and, finally, centrifugation of the suspension at 3500 rpm for 60 or 10 minutes, for water and PC respectively, to separate through precipitation the bigger particles from the effectively delaminated sheets. At this stage the supernatant, appearing as a black solution, was pipetted, and not poured to avoid the risk of dragging some bigger particles into the liquid, in a proper container and stored to undergo the EPD trials.
As mentioned above, to enhance the delamination yield, solutions were sonicated at the stage preceding the final centrifuging, but the MXenes inclination to be easily oxidized required specific precautions to carry out this treatment minimizing the damages suffered by the material. Following the best available indications from the previous work and the lab know-how, the sonication was performed in any case under argon and in an ice cooled water bath so that oxygen concentration was kept low as well as the temperature, namely another well-known oxidizing factor. The procedure followed two slightly different paths depending on the nature of the dispersing medium, since working with organic solvents can turn out to be dangerous due to diffusion of potentially harmful vapors:

- Water solutions, most of the times immediately after the washing step at the end of the etching reaction described above, were poured in a centrifuge tube or in a bigger glass jar whose lid was drilled with two holes, one for purging the vessel with the inert gas (Ar) and the other to provide venting. The piping coming from

the tank was connected to a plastic pipette oriented upside-down, cut at its top and immersed in the MXene solution in order to create a homemade bubbler. The gas flow was regulated to ensure an efficient purging, but to avoid solution overflow, and kept active during the whole treatment time, while ice cubes were added periodically to keep the system cool.

- PC and DMSO solution were stored in a glass container sealed with a rubber cap. Safety consideration lead to a different way of purging the "reaction" vessel, since a continuous system pouring organic vapors in the external environment was deemed to be potentially hazardous for the lab environment. As such, a syringe needle connected to the Ar tubing was used to puncture the rubber lid and slightly pressurize the inside of the container; a 20 mL syringe was then used to withdraw the gasses from the vessel, the rubber cap providing hermetic sealing, and the exhaust was channeled into a fume hood. The process was repeated 5 times in total and at the end the oxygen concentration in the glass container was considered low enough not to affect the delamination process. In this case too, during the sonication the temperature was kept under control and ice cubes were added as needed.

In all cases, the colloidal solutions were vacuum filtered in order to analyze with XRD the intercalated spacings with ions and molecule depending on the solvent. Delaminated MXenes always produced a film essentially constituted of individual or few flakes that, in the literature, is referred to as MXene paper, a designation that will be applied henceforth for this work as well.

3.2 MXenes EPD

The electrophoretic deposition was performed in a custom cell (**Figure 3.2.1**) comprised essentially by two glass slides coated with a conductive transparent layer, an O-ring to separate them and provide room where to inject the solution (spacing 3 mm when unused and 2.7 mm when compressed into the equipment) and a plastic rectangular chassis with 4 screws at the corners that could be tightened to assemble the device and ensure the seal through a rubber gasket.

This layout causes the charged particle to flow towards the oppositely poled surface, whenever a voltage is applied through the two clips connected to the electrodes. As mentioned above, the depositing substrates, with thicknesses of 1.6 mm and lateral dimensions of 25 x 25 mm^2, were comprised of glass slides. Several different coatings were tried, such as ITO (indium tin oxide), the cheaper FTO (fluorine doped tin oxide) or even sputtered platinum obtained in house. The goal was in general to ensure conductivity

without affecting the transparence of the systems, namely a very appreciated feature since the discussed equipment is specifically studied to visually observe the process evolution during its progress.

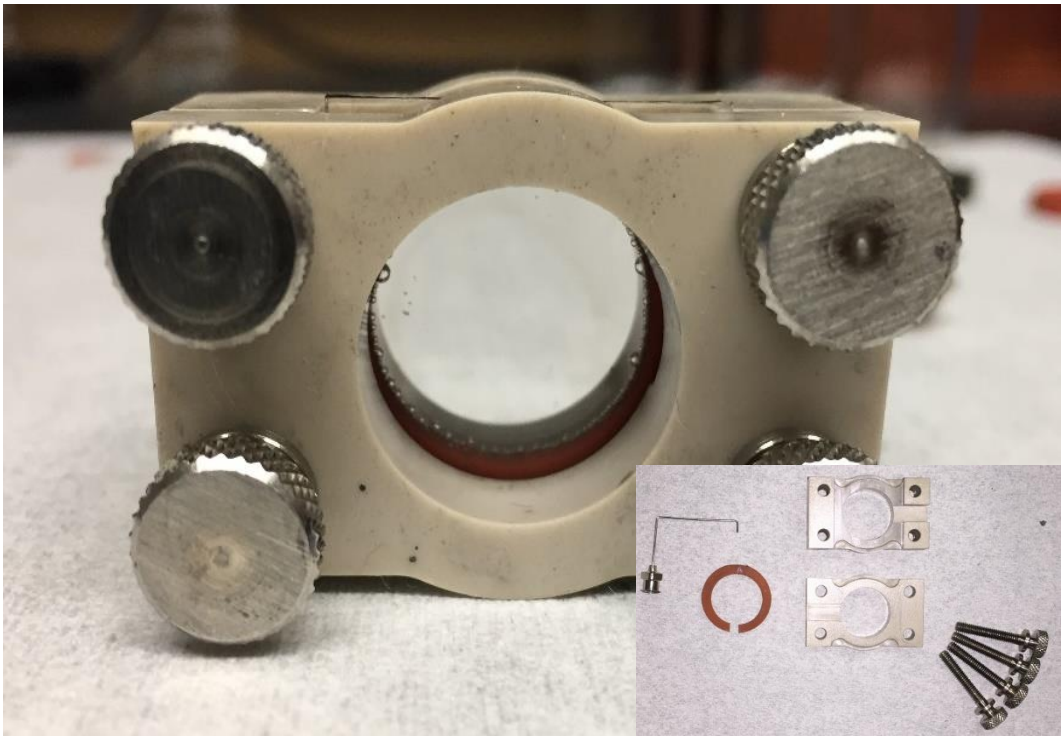

Figure 3.2.1: *digital photo of cell used for electrophoretic deposition; inset shows gasket separating the two electrodes, screws, draining conduct and the same cell armors disassembled.*

The deposition process is forerun by the cleaning of the substrates, which even when they are coming directly from the manufacturer, whether they are already coated or are just pristine glass slides to be subsequently sputtered with platinum, can yet have some dirt residues on their surfaces. To get rid of any kind of impurities the following standard washing procedure was followed: the substrates were first cleaned in a 10 % Hellmanex III (Hellma) solution by sonicating them for ten minutes in an upright sample holder, such as a slide washer vessel, and discarding the liquid at the end of the treatment. At this stage DI water was added and the system underwent sonication for a minute before discarding the fluid and repeating the process for a total number of three times. Finally, the sample holder was filled with ultra clean ethanol (300 Proof, Decon Laboratories, King of Prussia, PA) and sonicated for 1 minute, repeating the procedure two more times replacing the ethanol after each cycle.

The substrates were then removed from the vessel with ultra clean tweezers and blasted dry with a nitrogen gas gun in order to remove any possible last dirt residues, rather than letting them reside on the substrate after the evaporation of the solvent. A few times, a further step was added to this cleaning procedure and an UV-Ozone treatment inside an

inert atmosphere glovebox was performed, but the final EPD results did not seem to be significantly affected by this last step.

The fully constructed EPD apparatus, was filled with 0.7 mL of colloidal suspension and several voltages or currents were applied for different times using an Agilent E3616A DC Power Supply. The DC current were measured at 1 s intervals using a Hewlett-Packard 34401A Multimeter. After deposition, the voltage was held constant for a few seconds while the excess solution was evacuated from the bottom of the cell with a syringe fitted with a stainless steel needle. The glass substrates were carefully removed taking care not to disturb the deposit and were either air dried or dried at elevated temperatures in a vacuum oven. Free-standing MXene films were easily detached from the electrodes after drying.

Because of PC's high boiling point (242 ºC), the as-deposited films had excess solvent that could not be removed by passive drying at room temperature and needed to be annealed under a mechanical vacuum to obtain free-standing films (the other non-aqueous solvent, DMSO, did not provide sufficiently concentrated colloidal suspensions and in not discussed henceforth). Several annealing temperatures were tried, but ultimately 35 °C under vacuum for 30 min sufficiently dried the samples to allow easy film detachment from the substrates. Nonetheless mass measurements showed that 160°C for at least 12 h, was required to reach a final stable mass, where presumably all the PC was either expelled or reacted with the sample.
Those heat treatments were performed using a Precision Model 19 vacuum oven: deposited films and substrates were placed in a glass beaker and covered with aluminum foil with some small apertures cut on it to allow for venting. First vacuum vas pumped and then the temperature was ramped towards different soaking values and held for prespecified time before passive cooling to RT.

3.3 Electrochemical cell assembly

The electrochemical measurements were carried out on free-standing MXene films produced by EPD or vacuum filtration without further preparation. These films acted as the working electrode in a 3 electrode Swagelok cell, according to the following procedure.
All the cell components were separated from each other and washed with two sonication treatments in DI water for 5 minutes each time and after that everything was placed in a beaker and dried overnight in a low temperature oven. As for the two precious metal thin layers (gold and platinum) used to improve the conductivity between the active material

and the metallic component of the electrode, they were washed following the same procedure, but further steps were added whenever needed, such as manual rubbing with ethanol and a paper towel or even mild acidic treatment in HCl to dissolve any potential impurities contaminating the material surface.

Ensured a sufficient level of cleanliness for all the parts, as a first step of the device assembly, a plastic sheet was inserted in the cylindrical space of the Swagelok cell in order to avoid electric shortcut insulating the system through wrapping the metallic rods used to push the electrodes against each other. At this stage, one of the two stainless steel rods was inserted in the cell and secured in its proper position thanks to the tightening of a bolt and the additional help provided by specific sealing rings.
The active part of the supercapacitor was assembled on weighing paper out of the cell to simplify the procedure and ensure good alignment between the electrodes, laying down both working and counter electrodes on the metal rod top surface (with the cell held in a vertical configuration) in a single shot, warding off the hassle of working in the narrow space provided by the testing device.

A little piece (less than 1 mm^2) of MXene paper was cut from the initial cake, independently of whether it was obtained by EPD or by vacuum filtration, and weighed on a high precision weighing scale (Mettler Toledo UMX2, accurate to the nearest 0.001 mg). The cut out portion was then photographed laid on a background dense grid to use as scale reference: this allowed, as long as the form was fairly tetragonal, to easily analyze the image with a proper software (ImageJ) and obtain an estimate of the area, information useful to roughly evaluate the areal load as well as the film thickness, provided an approximate value of the surface density was available.

To build the testing cell, a layer of YP-50 activated carbon (Kuraray, Japan), intended to work as the overcapacitive counter electrode, was rolled to a thickness of around 100 μm and cut in circular form using a punching tool of proper size (few millimeters in diameter). The little cake was then laid down on the small platinum sheet and a gentle pressure, usually applied with the roll itself, was used to make the two components stick to each other. The separator was positioned above the activated carbon, and a droplet of the electrolyte solution was added to improve adhesion. As a last step, the small MXene layer and the gold sheet was stacked, following the just mentioned order, on the top of the separator, completing the assembly of the five-components system necessary to perform the electrochemical tests.
The whole pile was positioned inside the cell, and pressure was applied inserting the second rod from the opposite side of the cylinder and screwing the bolt until all the

components were fixed in place. The tightening process was carried out carefully, since the spinning of the metal rod could have caused the rotating element to apply a torque shearing stress on the inner materials, potentially disrupting the MXene sheet and its small-scale structure.
Finally, from the top aperture of the Swagelok cell all the system was flooded with the electrolyte (H_2SO_4 1M) and a rubber cap was used to seal the device and allow the insertion of the reference electrode (Hg/ H_2SO_4, in saturated K_2SO_4, ChI Instruments).
The system was finally connected in a three electrode configuration to the potentiostat, plugging two metallic pins in the rods in contact with working and counter electrodes, while a small clamp was used for the reference electrode.

3.4 Material characterization techniques

X-ray diffraction (XRD) was conducted on a powder diffractometer (Rigaku SmartLab) in the 3-65° 2θ range using a step size of 0.02 or 0.04° and dwell time of 0.7 s per step.

Scanning electron microscopy (SEM) with 100, 1000, 8000 and 17000X magnifications and energy dispersive X-ray spectroscopy (EDS), using 30 s scans, were conducted on dried, free-standing MXene films on a Zeiss Supra 50VP microscope equipped with an Oxford EDS system. Optical profilometry was performed with a Zygo Newview 6000 using the 10X objective at a working distance of 7.4 mm. Film weights were collected with a calibrated balance, accurate to the nearest 0.1 mg.

Electrical resistivity measurements were performed on free-standing MXene films in a nitrogen-filled glove-box (< 100 ppm O2 and moisture) using a Keithley 2634B SYSTEM Sourcemeter in a linear 4-point probe configuration with probe spacings of 2.3 mm. The reported resistivity values represent the average of three measurements per film using the method reported by Smits [73]. The errors reported are associated with the standard deviation in the three measurements and variations in film thickness.

Phase Analysis Light Scattering was used to measure the zeta-potential and electrophoretic mobility of the MXene flakes. Based on the solvent used, colloidal suspensions were diluted either in DI water or PC and the solution was analyzed using a Brookhaven NanoBrook Omni. Zeta-potential measurements were performed with a bias of 4 V alternating at 2 Hz.

Electrochemical tests were conducted using a potenitostat/galvanostat (Bio-logic VMP3). CVs were obtained at scan rates in the 2 to 200 mV/s range after an initial pre-cycling of

the cell 1000 times at 10 mV/s. The pre-cycling step was necessary to stabilize the CVs to a constant value of current and shape. The gravimetric capacitance values, C_m, were calculated assuming:

$$C_m = \frac{1}{m\Delta E}\int_{E_1}^{E_2}\frac{i}{\nu}dE \qquad (20)$$

where m is the working electrode's mass, ΔE is the potential window, E_1 and E_2 are the potential limits, i is the measured current, and ν is the scan rate. Volumetric capacitance values were computed by multiplying the gravimetric capacitance by the electrode's density.

Galvanostatic cycling was conducted at a constant current corresponding to a current density of 10 A/g based on the mass of the MXene films for 10,000 cycles each. Capacitance retention values are reported as percentages of the initial 1st cycle capacitance.

Chapter 4

MXene synthesis and delamination

The current chapter deals with MAX phases sintering and their subsequent reaction in acidic environments to etch the A-layers and produce the 2D MXene flakes. Delamination of resultant MXenes in water and non-aqueous solvents is also discussed, along with mobility and Z-potential of the as-produced colloidal suspensions.

4.1 MAX phases sintering

The MAX phases have been used as precursors for the following MXene production and their delamination in order to obtain stable and concentrated (i.e. at least more than 1 mg/mL) colloidal solutions. According to previous studies the sintering process was carried out either after cold pressing or, in only one case, under pressureless conditions, anyway aiming always at the best tradeoff between the maximum purity possible and the highest time efficiency. The literature, again, provided guidelines to produce good quality MAX phases, suggesting to slightly increase the initial concentration of the A-group with respect to the stoichiometric value, in order to prevent the formation of unwanted secondary phases such as the metal binary carbides above all.

4.1.1 Ti_3AlC_2

As the most studied and reliable specie among all the known MAX phases, titanium aluminum carbide was synthetized several times exploring different processing conditions in order to achieve the highest possible purity.

Thanks to the lab know how, production of Ti_3AlC_2 was possible either starting from the powders of the three elements mixed in proper molar ratios or reacting commercial Ti_2AlC with commercial TiC. However, sintering Ti, Al and C in a 3:1:2 proportion caused the formation of an excessive amount of intermetallic impurities and the drawback was overcome by a two steps procedure, wherein the 211 transitional compound was first fabricated, drilled into a powder and then re-reacted with pure TiC to obtain the final 312 phase. To discuss this in more detail, the Ti_2AlC intermediate was produced using a

2:1.1:1 composition of Ti:Al:C which was ball milled for 48 h before sintering in the tube furnace, under a flowing Ar atmosphere. The powders were fired for 2 h at 1350 °C, using a heating ramp of 5°C/min and then passively cooled to room temperature.

The X-ray diffractogram relative to the just described material is available in **Figure 4.1.1**: in red the profile measured for the actual Ti_2AlC is shown, whereas black represents the theoretical peaks for the same material and blue is relative to its 312 counterpart, again calculated theoretically. Interestingly, as depicted by the dashed vertical lines (colors consistent with those of the profile from where they are originating), despite the initial composition chosen to actually produce Ti_2AlC, the peaks observed for the real powders are at times broader than expected, asymmetric, or even present for 2θ values where nothing would be expected, such as 2θ≃42° or 2θ≃56°. Comparison of these anomalies with the abovementioned Ti_3AlC_2 theoretical profile, though, sheds light on the actual composition of the discussed powder, indicating that a portion of the starting mix reacted to produce the 312 phase.

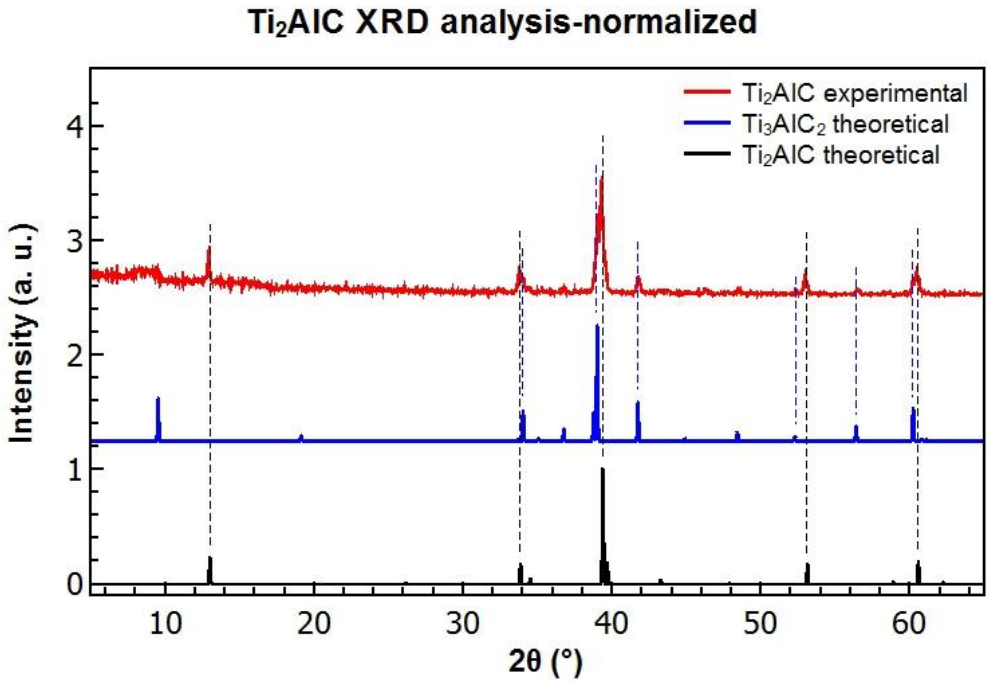

Figure 4.1.1: *X-ray diffraction of Ti_2AlC obtained from mixing of starting elements powder, combined with theoretical spectra for both Ti_3AlC_2 and $TiAlC_2$. As shown by the vertical lines in blue and black consistently with what indicated in the chart legend, some 312 phase is contained in the produced 211.*

Thus, such a starting composition not only proved to be inappropriate to effectively produce highly pure Ti_2AlC but also introduced a new issue in view of the following 312 material production. The non-negligible amount of final 312 phase already present in the 211 reactant caused a molar ratio of 1:1 between the described Ti_2AlC and TiC to be evidently disproportionate, requiring more investigations in this regard.

A similar problem was encountered when using commercial MAXTHAL powders (Kanthal, Sweden), consisting primarily of Ti_2AlC as the majority phase with Ti_3AlC_2 impurities, instead of in-house sintered Ti_2AlC, just due to the same reasons previously mentioned. Considering the large availability of such commercial intermediate in the lab stock, the optimization of Ti_3AlC_2 production by direct reaction between such powder and commercial TiC was deeply explored through a sequence of steps which could be summarized as: sintering of a 1:1 molar proportion between the two components, XRD scanning of the so-produced powder, performing of the Rietveld refinement, composition correction and, finally, reaction of the proper mixture to obtain a pure final Ti_3AlC_2 powders.

Figure 4.1.2 shows, again, theoretical spectra for both Ti_3AlC_2 and TiC in black and blue respectively; the 312 phase obtained by mixing a 1:1 molar ratio of commercial Ti_2AlC; commercial TiC depicted in yellow. A quick comparison with the blue profile demonstrates how some impurities are still contained in the produced powders especially due to the little peak present at $2\theta \simeq 36.4°$ which is very likely due to a titanium carbide fraction. Rietveld refinement provided the tool to calculate how much Ti_2AlC commercial powder was to be added to the "1:1" mixture and after the proper adjustment sintering of a new batch produced the material whose diffractogram is available in red at the top of the stacking (**Figure 4.1.2**).

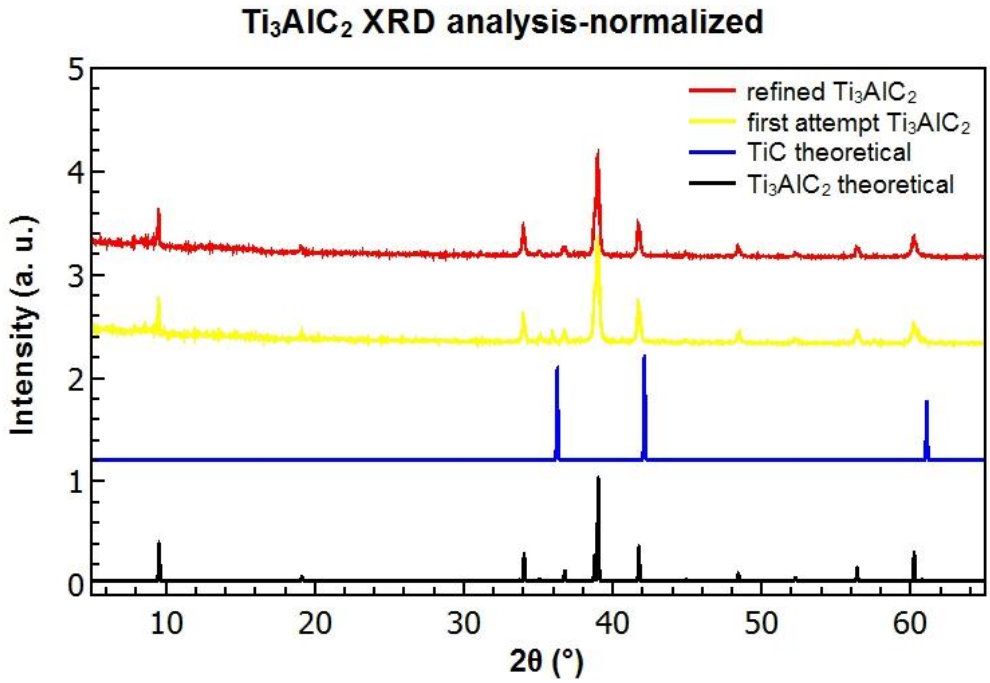

Figure 4.1.2: *X-ray diffraction of Ti_3AlC_2 obtained from mixing of commercial Ti_2AlC and commercial TiC in 1.1 molar proportion (yellow) and after Rietveld refinement, combined with theoretical spectra for both Ti_3AlC_2 and TiC.*

This time the TiC peaks were very difficult to pinpoint and this sustained the discussed analysis quality, which effectively provided a sufficiently pure material in view of future experiments.

For the sake of completeness, though, it has to be said that the actual 312 powders used to carry out all the studies discussed from now on throughout this work came from yet a different batch where the starting composition was obtained, again, from mixing of commercial Ti_2AlC and commercial TiC. This was due not only to the higher purity achieved in this different sintering (albeit same conditions as the previous batch were used), but also to the need of having a sufficiently large amount of MAX phase before starting any kind of study, given the risk of altering or even jeopardizing the experimental observations in case of not using the same initial batch. **Figure 4.1.3** shows the excellent matching between the synthetized MAX phase peaks end the theoretical predictions, not only in peak position but also in terms of peak amplitude, peaks showing moreover a very narrow FWHM which proves the quality of the signal collected and hence of the material purity.

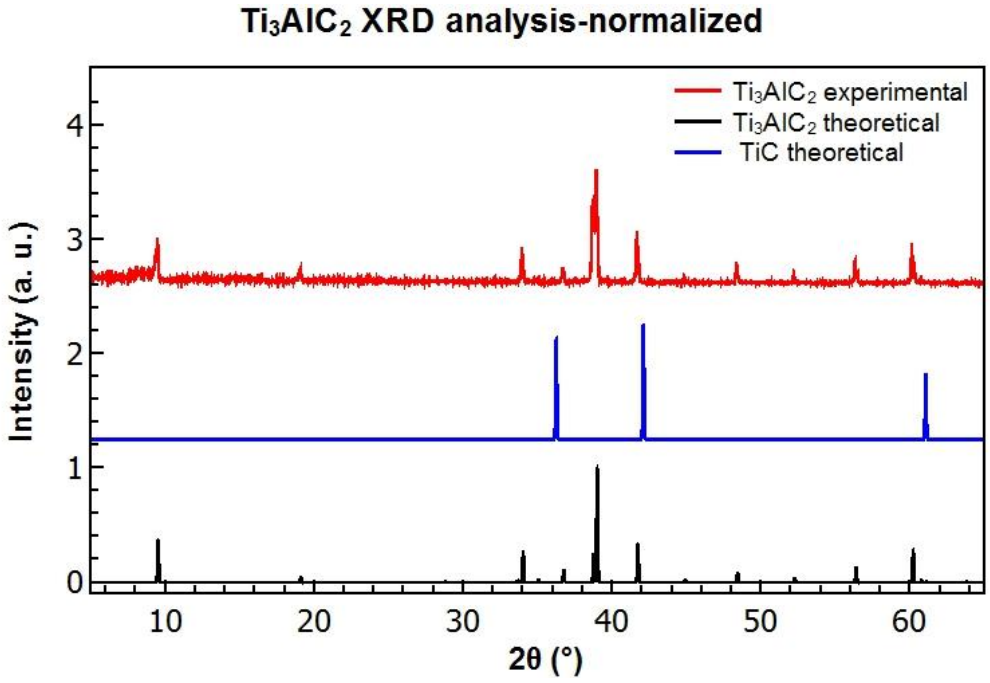

Figure 4.1.3:*X-ray diffraction of the Ti_3AlC_2 used from now on throughout the whole study in order to the guarantee results based on a constant and highly pure material. Powders, as before, were obtained from mixing of commercial Ti_2AlC and commercial TiC. The image reports theoretical spectra for both Ti_3AlC_2 and TiC as well.*

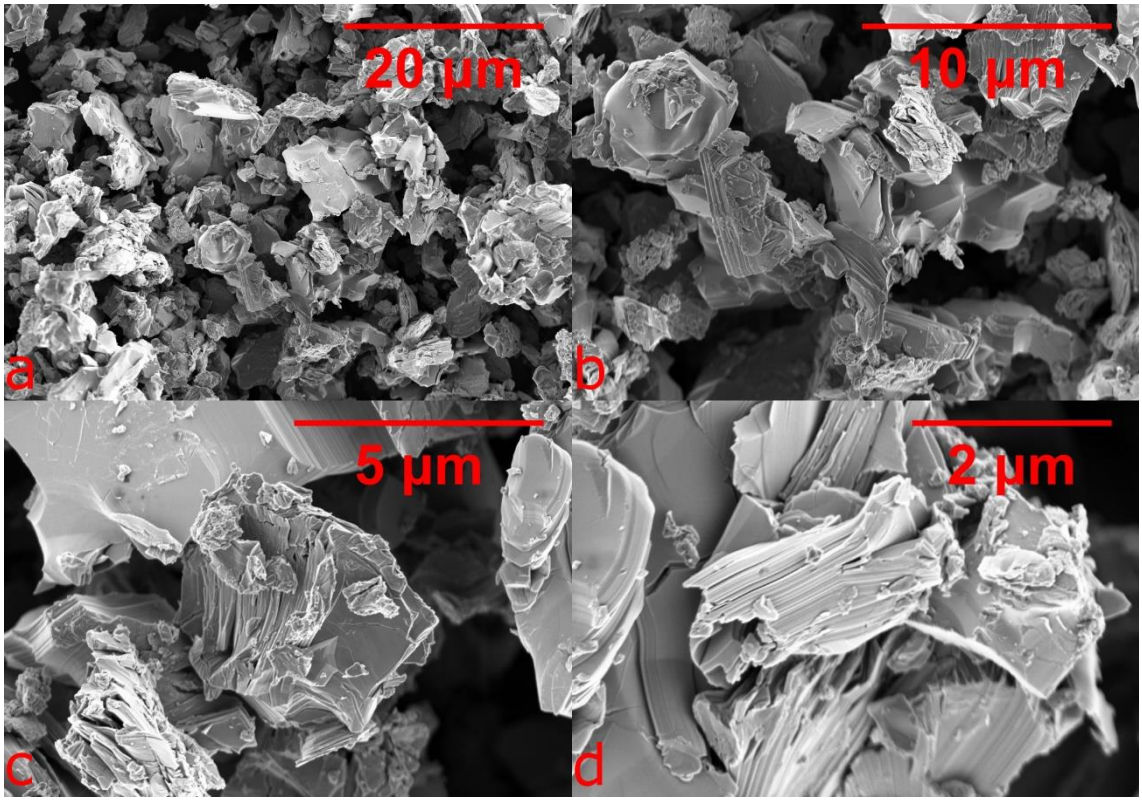

Figure 4.1.4: *SEM images of Ti_3AlC_2 powder with particle size smaller than 38 µm obtained by sintering for 2 h at 1350 °C a commercial Ti_2AlC and commercial TiC refined mixture. Pictures were taken using the following instrument parameters: EHT 1.50 kV, working distance 3.3 mm and magnification 2K, 5K, 10K and 20K respectively for a, b, c and d.*

The so-obtained and sieved Ti_3AlC_2 powders were characterized through SEM imaging using EHT 1.50kV, working distance 3.3 mm and magnification 2K, 5K, 10K and 20K as instruments parameters (**Figure 4.1.4**). From the pictures, two observations are worth making with regard to the following etching undergone by the powder. First, it is evident that the average particle dimension is smaller than what expected for the selected sieve mesh, with most of the agglomerates found in the 5-10 µm range, assuring the absence of significant kinetic barriers due to mass transfer towards the material core during the subsequent reaction. Moreover, the highest magnification pictures reveal something already known from theory, that is how MAX phase particles are packed structures, where adjacent layers stack on each other thanks to the gluing role played by A-atoms; **Figure 4.1.4**d in particular shows well this feature as well as how even without acidic treatments some portions of the particle are already exfoliated and partially opened just due to the shear effects of the drill mill and following manual sieving.

4.1.2 Ta_4AlC_3

The MAX phase world was then explored aiming at the production of a 413 member, selecting specifically Ta, Al and C, with the hope to overcome, thanks to the EPD process, the brittleness issue encountered when Ta-C films are produced resorting to the conventional vacuum filtering method.

Production of Ta_4AlC_3 was carried out starting from the powders of the three elements mixed in proper molar ratio keeping in mind that sintering Ta, Al and C in a 4:1:3 proportion causes the formation of an excessive amount of intermetallic impurities. Hence, a powder constituted by a 4:1.75:3 composition of Ta:Al:C was adopted and, before sintering under Ar atmosphere, the mixture was ball milled for 48 h and then cold pressed at a pressure high enough to produce a self-standing brick, namely 200 MPa. Thereafter, the pre-compacted disk was fired for 1 h at 1500 °C, using a heating ramp of 5°C/min and then passively cooled to room temperature. Owing to the high temperature reached, the Al was likely to evaporate and an excessive element loss in the mixture was contrasted both increasing by 75% the theoretical Al amount in the premixed composition and covering the reaction vessel with a graphite sheet.

The X-ray diffractogram of the material is shown in **Figure 4.1.5**: in red the profile measured for the actual Ti_4AlC_3 is shown, whereas black represents the theoretical peaks. Their comparison demonstrates how the sintered 413 MAX phase is highly pure and definitely eligible for further etching reaction and colloidal suspension production.

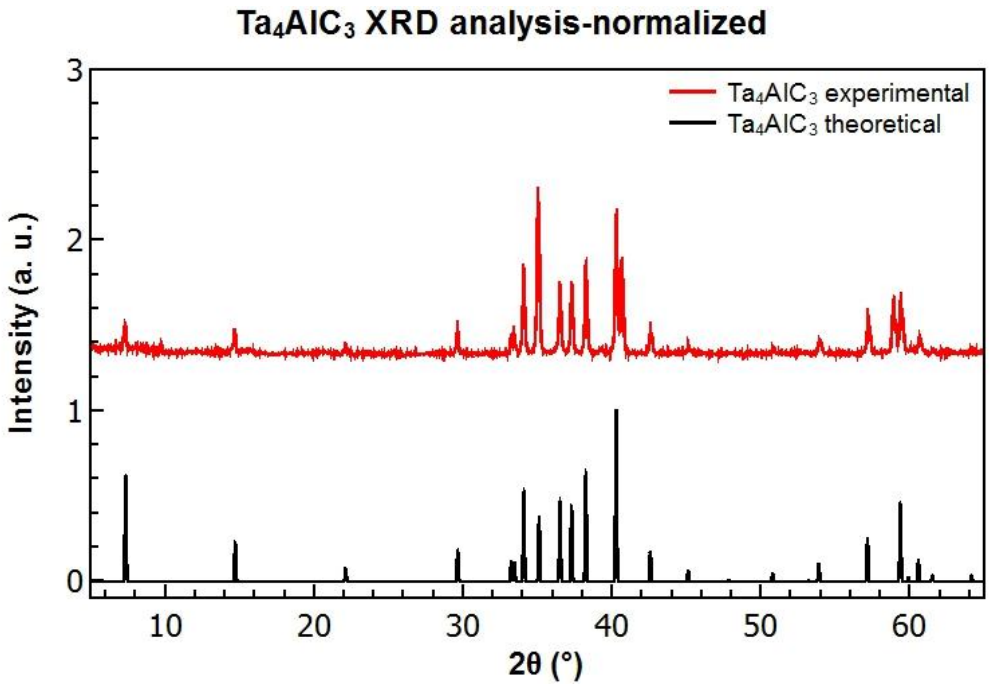

Figure 4.1.5: *X-ray diffraction of Ta_4AlC_3 obtained from mixing of starting elements powders, combined with its theoretical spectrum.*

4.1.3 Nb_2AlC

The MAX phase fabrication relative to this study was completed with the synthesis of a 211 compound so that a member was available for all the three different possible MAX structures. Production of Nb_2AlC was obtained following the guidelines discussed in the previous sections and thus the theoretical molar proportion 2:1:1 among Nb, Al and C respectively was adjusted adding 10% molar to the Al component. As with Ti_4AlC_3, the powder mixture (*viz.* Nb:Al:C with a 2:1.1:1 ratio) was ball milled for 48 h and then cold pressed at a pressure high enough to produce a self-standing brick, namely 100 MPa.
Subsequently, the pre-compacted was fired for 4 h at 1600 °C, using a heating ramp of 5°C/min and then passively cooled to room temperature. Again, due to the high temperature reached the Al element proved to be likely to evaporate but the excessive element loss in the mixture was contrasted this time only by covering the reaction vessel with a graphite sheet.
The X-ray diffractogram relative to the just described material is available in **Figure 4.1.6** where in red the profile measured for the actual Nb_2AlC is shown and black represents the theoretical peaks. Their comparison demonstrates how the sintered 211 MAX phase is sufficiently pure and appropriate, on paper, for further experiments. Nonetheless the project of Nb_2AlC was abandoned in its early stages even though an inspection of Nb_2C propensity to be delaminated in colloidal suspension and undergo EPD film fabrication is an easily predictable future development.

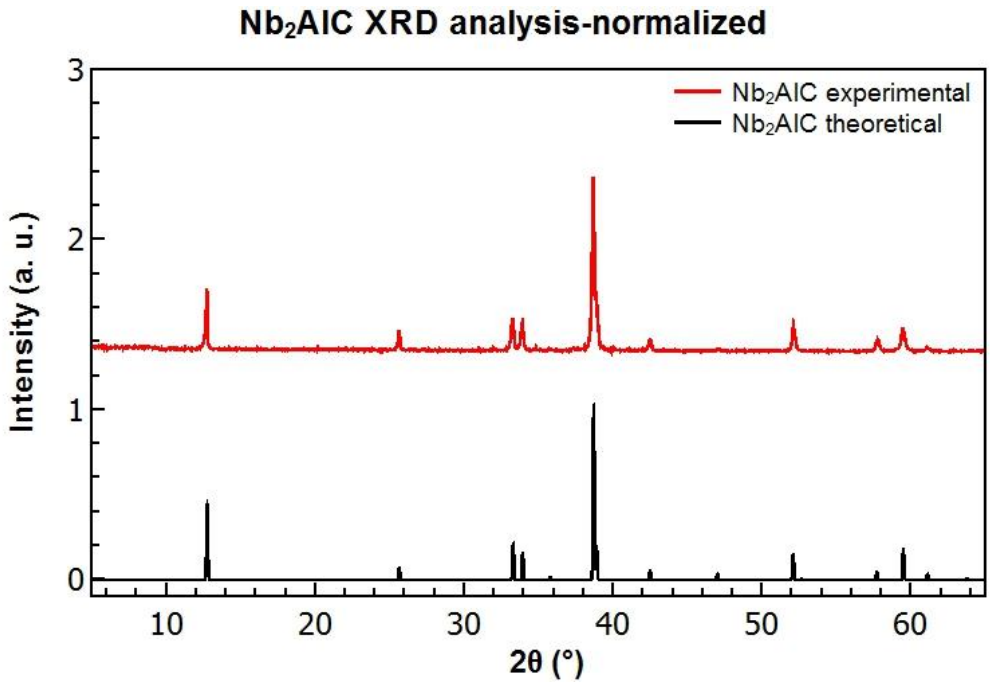

Figure 4.1.6: *X-ray diffraction of Nb_2AlC obtained from mixing of starting elements powders, combined with its theoretical spectrum.*

4.2 MXene synthesis (exfoliation)

The MAX phase bricks were generally ground and sieved to obtain powders of particle size < 38 μm: this would increase the reaction kinetic and improve the MXene yield, i.e. the extraction speed of the A-group layers from the stacked MAX structure.

At this point a terminological specification is required and the difference between "exfoliation" and "delamination" in clay layered materials is introduced, as discussed by Gardolinski and Lagaly [74] and recalled by other works.[75] Exfoliation arises when a large particle is decomposed in smaller elements, while delamination occurs when the aforementioned layered elements are completely separated into individual layers. Keeping this in mind, MXene synthesis starting from the parent MAX phase is, by definition, an exfoliation process, with the initial particles broken down to smaller and multilayered entities.

In view of the subsequent delamination step, the etching reaction was carried out employing either HF/LiCl or HCl/LiF [76,77,22] environments previously pinpointed as the best currently available methods to boost the few layers MXene yield or, to say it in other words, the concentration of the derived colloidal suspensions (the second recipe worked generally best). Anytime the bonds between adjacent layers in packed structures are rather weak, as happens generally for clays, and MXenes as well, the intercalation of extraneous species, either organic or inorganic or even ionic, is possible, allowing the layers to increase the distance separating them, as easily proven by XRD analysis through an inspection of the *c*-LP values. Therefore, the weak bonds linking adjacent sheets of exfoliated structure of loosely bound $M_{N+1}X_N$ layers can be disrupted either mechanically or chemically performing that processing step defined as delamination.

4.2.1 Ti_3C_2

According to the preview given above, etching of titanium aluminum carbide (312) was achieved using two different methods. 2 g of Ti_3AlC_2 powders, of particle size < 38 μm, were slowly added to a premixed 20 mL mixture of 50 wt.% aqueous HF and LiCl solution containing 2.18 g of LiCl in order to achieve a molar LiCl to Ti_3AlC_2 ratio of 5:1. The reaction system was stirred for 24 h at 35 °C and then the reacted powders were washed several times in DI water until the supernatant remained dark after centrifuging. Alternatively, the same procedure was performed changing only the acid/salt environment. In this case 2 g of Ti_3AlC_2 powders (again with particle size < 38 μm) were slowly added to a premixed 20 mL mixture of 12 M aqueous HCl and LiF solution containing 2.32 g of LiF in order to achieve a molar LiF to Ti_3AlC_2 ratio of 5:1. The reaction batch was stirred for different amounts of time (i.e. 24, 72 and 144 h) at 35 °C and then powders were treated following the same procedure described for the HF/LiCl

system. In agreement with what specified above, between the two procedures the former provided poor etching yields and was soon abandoned, being completely outperformed by the latter, and for this reason it will not be discussed in the present work.

When the powders were added to the HCl/LiF mixture, the reaction produced most of the times small bubbles presumed to be H_2, and only in a few episodes slight evidence of heating was found, despite the slow powder adding, anyways never exceeding the temperature of the thermostated bath which was kept at all the times hotter than the reaction vessel. As-synthetized $Ti_3C_2T_x$ was characterized via SEM (see **Figure 4.2.1**) at different magnifications and beyond 7K X it is possible to notice the multi-layered structure produced by the etching process with basal planes fanned out and spread apart, producing a morphology already observed for MXenes obtained via HF treatment.[75]

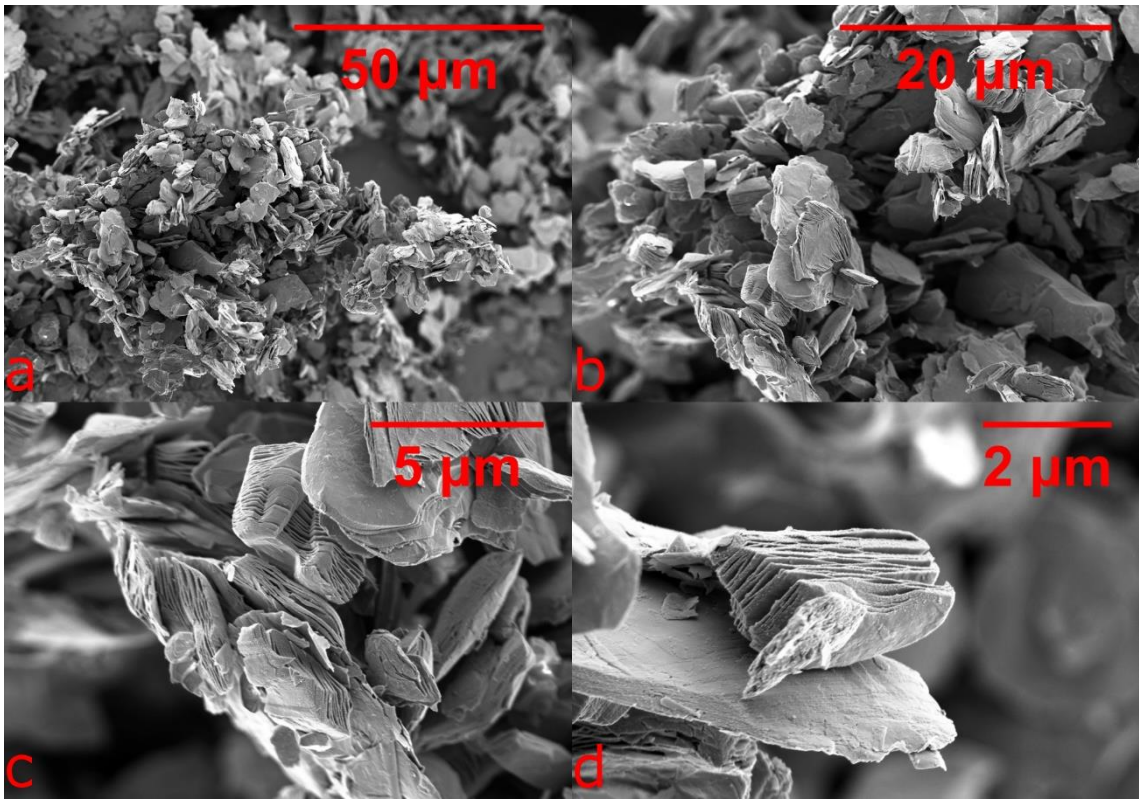

Figure 4.2.1: *SEM images of $Ti_3C_2T_x$ powder produced by 1 day etching of Ti3AlC2 with particle size smaller than 38 µm obtained by sintering for 2 h at 1350 °C a commercial Ti_2AlC and commercial TiC refined mixture. Pictures were taken using the following instrument parameters: EHT 1.50 kV, working distance 3.3 mm and magnification 1K, 2.7K, 7K and 13K respectively for a, b, c and d.*

To quantify the extent of Al etching, the composition of the$Ti_3C_2T_x$ powders were subjected to EDS analysis, which showed that the Al content has reduced with a concomitant increase in O, F and Cl. The atomic Ti : Al : C : O : F : Cl atomic ratios obtained – normalized to Ti = 3 - were ~ 3.0 : 0.1 : 1.8 : 0.9 : 0.9 : 0.2, respectively. This suggests that Al layers were replaced by O, F and Cl, as well as that some portions of the salt present in the solvent wasn't likely removed by the washing step. Nevertheless, this

possible residue amount of salt did not affect remarkably the material properties and hence no further procedures were performed.

However, the main purpose of the current section is to pinpoint the ideal etching conditions to obtain a high multi-layered MXene yield and, subsequently, the most concentrated colloids possible.

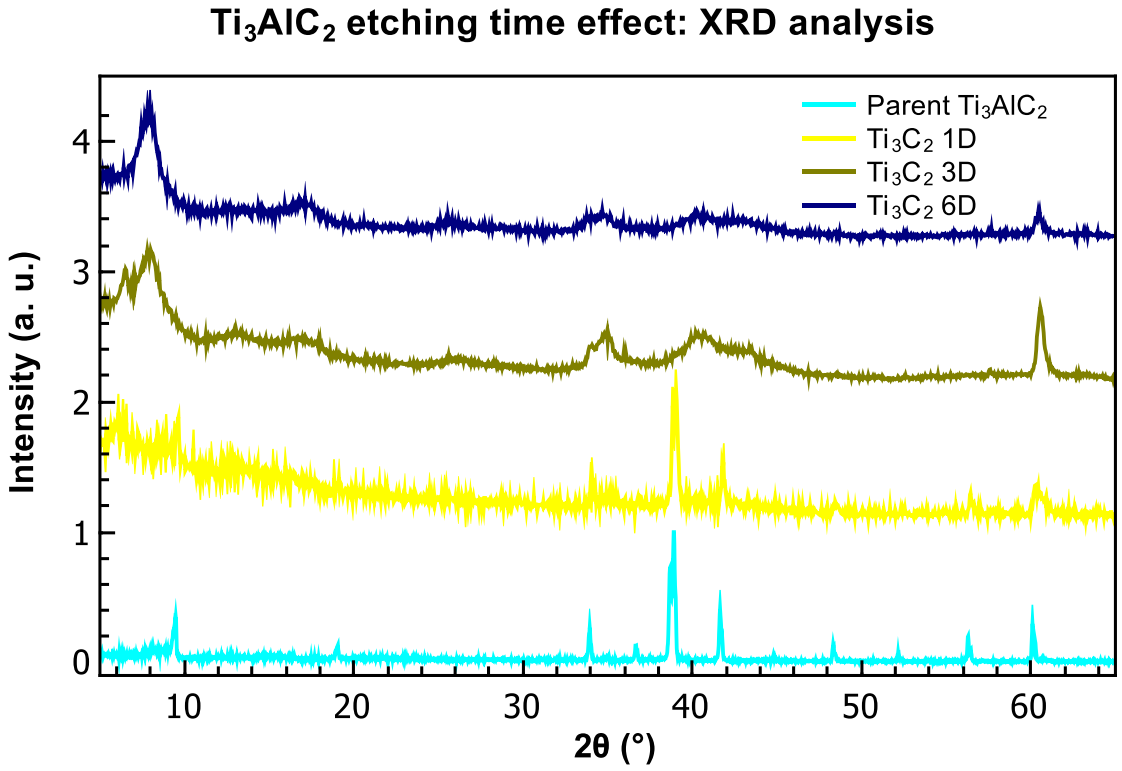

Figure 4.2.2: *X-ray diffraction of multi-layered $Ti_3C_2T_x$ obtained from the parent Ti_3AlC_2 (depicted in light blue at the bottom, same as the one in* ***Figure 4.1.3****) after 1, 3 and 6 days of etching.*

Figure 4.2.2 shows diffractograms for MXene powders etched in HCl/LiF for 24, 72, and 144 h in their multi-layered form after vacuum filtration and air drying, combined with the diffractogram of the parent Ti_3AlC_2: after 24 h of reaction already, good parts of the MAX phase peaks (in light blue) disappear and with longer times, not only those peaks are progressively flattened but also new peaks specific of the MXene start raising.
Therefore, 3 d appear to be the threshold between complete and incomplete MAX phase conversion, with the 1 d sample still showing a good fraction of Ti_3AlC_2 present and the 6 d one proving the almost complete transformation to $Ti_3C_2T_x$. Interestingly, the diffractogram relative to the 3 days etched sample shows multiple peaks in the 6 to 10 2θ range and according to the work of Ghidiu *et al.*[78] this was ascribed to partial deintercalation of water present between the MXene layers that resulted in the presence of more than one basal spacing.

As described better in the following pages, 3 d was considered the optimal solution to produce concentrated colloidal solutions, despite the slightly higher MXene yield of the 6 d etched sample, whereas as for 1 d etched powder good suspensions were achieved some times but issues in the reliability of the process would require more studies.

4.2.2 Ta_4C_3

To produce Ta_4C_3, 1 g of Ta_4AlC_3 powders, of particle size < 38 μm, was slowly added to 15 mL of 50 wt% aqueous HF and the mixture was stirred for 72 h at room temperature. The product was washed 5 times until the pH was > 6 with a 3500 rpm for 2 min treatment and then the sediment was vacuum filtered. As synthesized powders were analyzed with XRD and the relative diffractograms are given in **Figure 4.2.3** along with the profile of the original MAX phase. Although the etched sample shows many peaks belonging to the parent Ta_4AlC_3, 72 h of reaction proved to be sufficient to start MXene conversion as some original peaks disappear, others are lowered and above all, the basal plane peak translates from its starting position to $2\theta = 5.92$, meaning a d spacing of around 15 nm.

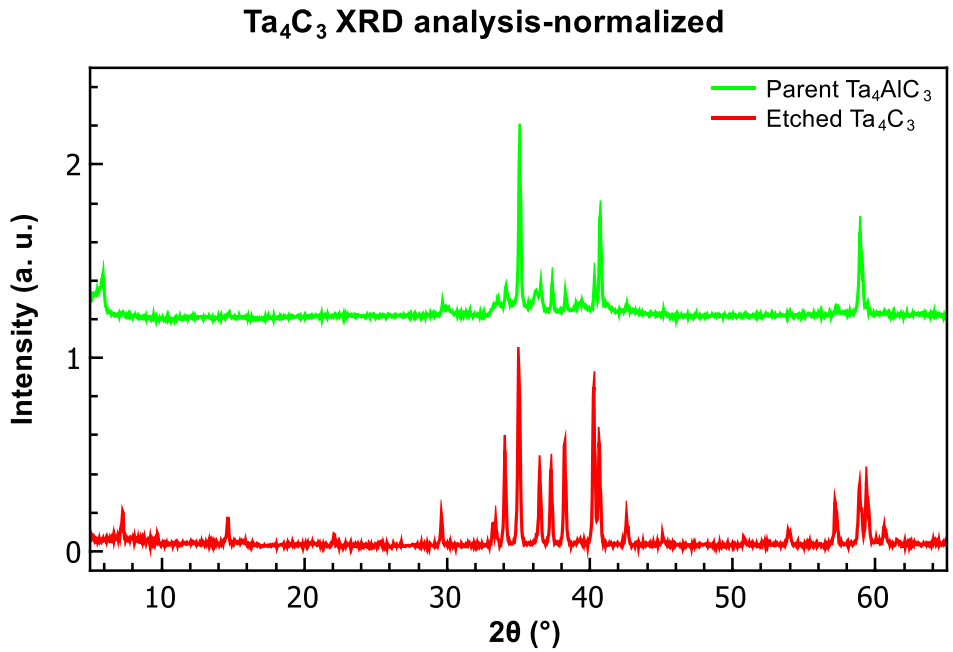

Figure 4.2.3: *X-ray diffraction of multi-layered Ta_4C_3 obtained from the parent Ta_4AlC_3 (depicted red at the bottom, same as the one in* ***Figure 4.1.5Figure 4.1.3****) after 72 h of etching.*

For the sake of completeness, the tantalum carbide dried powder was split into two samples (0.3 g each) and dispersed in 10 mL of PC and DMSO, respectively. Both the containers were magnetically stirred for 3 d and afterwards a centrifugation of 3500 rpm for 10 minutes was performed: in any cases no colloidal suspension was found. The XRD diffractograms showed that the basal peak positions were unaltered, confirming that no

solvent intercalation in between the layers occurred and thus explaining the lack of formation of a colloidal solution. Some phenomena must have prevented interaction between the solvent and the surface groups and the positive results provided by $Ti_3C_2T_x$ system deflected research efforts so that no further investigations were carried out on Ta_4AlC_3.

4.3 $Ti_3C_2T_x$ delamination

Once $Ti_3C_2T_x$ multilayered flakes were obtained, the last step in consistently producing colloidal suspensions suitable to undergo EPD was their delamination to obtain either single- or few- layered (i.e. delaminated accordingly to the definition provided in § 4.2) "MXene flakes". This goal was achieved thanks to the discovery of the intercalation effect, as the intercalation of Li ions (see § 4.2.1) provided by the salt presence increases interlayer distances weakening the bonds connecting the single sheets to each other. $Ti_3C_2T_x$ suspensions were produced both in water, the most common and environment friendly solvent, and in propylene carbonate, PC, to overcome the limitation set by aqueous systems electrolysis whenever a high enough potential is applied.

4.3.1 Aqueous suspensions

Aqueous suspensions of $Ti_3C_2T_x$ were produced after Ti_3AlC_2 etching following two different procedures that proved to be essentially equivalents in terms of final concentrations of the obtained suspensions. At the end of the washing stage the MXene powders were either: i) sonicated right away and then centrifuged or ii) vacuum filtered, air dried, and only after this intermediate step, sonicated and centrifuged. The second procedure was carried out both to save the multi-layered powder necessary for XRD analysis and to observe the effect of drying on the final achieved concentrations. In general, depending on the time allowed for water evaporation (from 12 to 48 h) the produced MXene mass exceeded from 20 to 40 wt% the initial MAX phase mass: this was ascribed, principally, to a small amount of water still intercalated between the layers, the presence of terination groups such as -OH, -O and -F which substituted for the original Al atoms and the presence of a certain amount of LiF contaminating the sample (EDS detected the presence of Cl, part of which might have been terminations, however).
At the end of centrifuging, the black supernatant, namely the delaminated $Ti_3C_2T_x$ solution, was pipetted out and stored to undergo EPD tests. However before final use, small volumes from all solutions were vacuum filtered to obtain an estimate of the produced concentrations: particle loadings ranging from 0.2 to 15 mg/mL were achieved (measures performed after 2 h of vacuum annealing at 85 °C to get rid of residue water),

introducing a remarkable reproducibility issue. Nonetheless, after many trials, 3 d of etching and 1 h sonication (independently from the presence of the intermediate drying step) was found to be the best procedure to consistently obtain concentrations > 5 mg/mL, although more investigation to identify the key parameter to reinforce the MXene colloids fabrication are still required.

In this respect a note is added regarding a peculiar case of dispersion failure: following apparently an identical procedure as the one described so far, the fluid extracted from the jar at the end of sonication appeared to be like a dense sludge, and after 1 h of centrifuging no phase separation was detected, being the initial slime still present. The material was examined immersing a clean pipet in it and a gradient of viscosity was found, but even at the top of the centrifuge tube the material wasn't properly liquid. The formation of such a jelly substance was attributed to MXene swelling due to water intercalation and the subsequent formation of a 3D framework which did not allow the excess water to be separated from the heavier particles.
Furthermore, in the dispersion-failure frame, it has to be reported that 30 min only of sonication (20 mL water and 0.5 g MXene) did not result twice in a colloidal suspension with all the particle settled in the centrifuge tube after only 15 min of treatment at 3500 rpm. Speaking about the centrifuging step, surprisingly it was noticed that to achieve a neutral pH a number included between 7 and 12 subsequent washes was needed, independently from whether the acidic solution was contained in 1 or 2 centrifuge tubes (i.e. the powders were rinsed either with a volume of water or with the double of that value): this aspect is to date not fully understood, even though it was partially justified thinking of kinetic barriers to the H^+ ions removal, so neglecting as a first approximation the influence of the water amount involved in the process.
To conclude the discussion of issues related to MXene suspensibility, a final result is worth discussing: two etching were set up and located on the same stirring plate, trying to follow identical procedures and reduce to the minimum possible differences which might have affected the result. Nonetheless at the end of the sonication and centrifugation concentration, measurements provided two rather divergent values, showing that a fundamental process aspect is currently overlooked.

Although isolated, these observations confirm what has been already noted about the several parameters affecting the colloids production and pave the path for further work in this direction.

4.3.2 Non-aqueous suspensions

Non-aqueous suspensions of $Ti_3C_2T_x$ were produced after Ti_3AlC_2 etching by soaking washed powders in two organic solvents, *viz.* DMSO and PC. Following the guidelines described in § 3.1.3, at the end of the washing and vacuum filtering steps, different procedures were chosen to accomplish such goal and carry out a systematic study on the influence of several process parameters, such as amount of water still present in the air dried material, days of etching underwent by the Ti_3AlC_2 powder, days of mechanical stirring in the solvent and enhancing effects of the sonication step.

Before going in deep with the treatise on the aforementioned aspects, it is woth noting the total and consistent failure of DMSO to create colloidal suspensions, regardless of whether either HF/LiCl or HCl/LiF etching solutions were used. Even after 6 d of treatment, and independently from the sonication step, 10 min of centrifuging at 3500 rpm were always enough to settle all the particles and leave the solvent completely clear. For this reason DMSO was rejected and more efforts were devoted to PC, which since the preliminary studies offered a remarkable ability to suspend MXene and allowed for more thorough investigations.

Given that colloid concentration was a critical factor for EPD feasibility, as better explained in the next chapter, the first part of the present work dealt mainly with enhancing this factor. The first variable was identified in the amount of time spent magnetically stirring the powders in PC, followed by air drying of the vacuum filtered multilayered powders. Keeping all the other sensitive parameters constant, and especially the length of etching process, 3 d of mixing were deemed to be the minimum time necessary to achieve a concentrated suspension, whereas 5 d were chosen as the optimal value, since longer times did not enhance the final concentrations. Henceforth the stirring was kept constant at 5 d and the other three parameters were investigated. A summary of the results is given in **Table 4.3.1**, where the concentrations of the solutions are showed for each treatment, with the rows varying etching times and columns describing different colloids synthesis.

The influence of drying on the multilayered powders suspensibility was investigated starting from a totally wet sludge, removed with a spatula right after the end of the washing procedure: 2 grams of material were immersed in 15 mL of PC and let stir for 5 d then sonicated in g atmosphere for 1 h, but even from visual observation a poor suspension was evident, so that after centrifuging at 3500 rpm for 10 min the supernatant looked completely transparent and a null concentration was estimated (column named Wet/sonicated in **Table 4.3.1**). Set this as the maximum amount of water contained in the multilayered particles, progressive dryings were performed and finally the optimum to enhance MXene particles loading in PC suspensions was pinpointed, with the normally

achieved concentration showed in the column named "dried" of **Table 4.3.1**. Such values were possible performing a controlled drying steps, before pouring the powder in PC according to a ratio of 1 g of $Ti_3C_2T_x$ per 30 mL of solvent: after vacuum filtering the optimal value of water wt% retained in the sediment to observe maximum particle loading was found to be around 25 % of the MXene powder, assuming, grossly, an approximate mass conversion of 1:1 between Ti_3AlC_2 and $Ti_3C_2T_x$. Furthermore, this procedure showed best results in terms of final colloid concentrations when an etching of 72 h was performed ad this working condition was hence selected whenever a high particle loading was required. At times, a final sonication step of 1 h in Ar environment was performed to maximize suspension concentrations and a remarkable value of 13 mg/mL (similar to what observed in water) was achieved more than once.

Etching time	Wet/sonicated	Dried	Dryed/sonicated
24 h	0 mg/mL	2 mg/mL	4 mg/mL
72 h	0 mg/mL	6 mg/mL	13 mg/mL
144 h	0 mg/mL	Gel or 5 mg/mL	Gel or 10 mg/mL

Table 4.3.1: *summary of PC colloidal concentrations achieved for different working parameters.*

Interestingly, 6 d etching resulted once in a jelly-like material (as with water), independently from whether the sonication step was performed or not, at the end of the centrifuging (10 min at 3500 rpm). When this occurred, MXene soaked in PC was poured in a container and 15 mL PC were added for both the samples to dilute the suspension and vigorous manual shaking was provided: not surprisingly, the non-sonicated solution appeared less viscous and after a second centrifuge run it provided a 4 mg/mL concentration; on the other hand, the sonicated material, even after a combined centrifugation for 10 mins at 3500 first and 5000 rpm then, did not produce any change and gave again a sludge. For this reason, 30 more mL of PC were added and a 10 min 3500 rpm centrifuge treatment was run. This caused a gradient of viscosity with a liquid-like substance at the top and a sludge at the bottom of the tube, but it was not yet possible to observe a neat phase separation. The centrifugation step was intensified extending the treatment time to 1 h (3500 rpm) and at this point the liquid was eventually less viscous at the top but the concentration was poor, as the suspension did not seem highly dark and, what's more, the sludge was found again at a few cm from the top of the tube. Therefore, also with this non-aqueous solvent reproducibility issues were encountered and some phenomena aren't very clear to date, requiring father analysis if a deeper understanding in the fundamentals of colloids fabrication are desired.

Finally, a few details regarding the annealing processes used to dry the samples and calculate colloids concentrations are worth reporting: after centrifugation, 2 mL of suspension were vacuum filtered, producing a highly wet cake sticking to the filtering paper. The whole sample was placed in the vacuum furnace and treated at 55 °C for 4 h to allow the deposit to detach from its substrate without reacting with it; afterwards, the MXene film was re-placed in the furnace and a tougher annealing was performed at 180 °C for 12 h to get rid of most of the solvent and measure the effective mass to calculate a reliable concertation value. To better characterize the process, some points of the evaporation curve were collected and starting from the sample just detached from the filtering paper, it was observed that at 110 °C for 12 h, 55 % of the initial weight was removed and that, increasing the temperature up to 180 °C without changing the processing time, such percentage was pushed to 60 %. This might be useful information in case there is a suspect of reaction between MXene and PC, as working at milder temperatures could prevent material surface groups degradation.

4.3.3 Final remarks

To conclude the colloids fabrication section, some general comments and a few comparisons between aqueous and non-aqueous suspensions are provided. As specified before, vacuum filtered films were produced both from water and PC suspensions and other than weighing to calculate concentrations, some of them were characterized through XRD. Their typical spectrograms, after air drying for water and after 12 h of vacuum annealing at 180 °C for PC, are shown in **Figure 4.3.1**: both show the usual Ti_3C_2 structure with a strong basal peak and some (00*l*) multiples, especially for water. Interestingly those peaks are positioned at quite different 2θ values denoting a d-spacing of 14 nm and 11 nm, respectively for water and PC. To have a reference for EPD results (see next chapter) the same films were imaged with SEM at 5K X magnification and two examples of what observed are provided in **Figure 4.3.2**: the structure consists of tightly stacked MXene layers and no major difference is apparently generated by the use of aqueous and non-aqueous solutions.

Finally, both colloid types were characterized through dynamic light scattering and information was obtained for the electrophretic mobility and the zeta potential. Interestingly, the aqueous and non-aqueous solutions showed similar zeta potentials of -58.39 mV and -61.45 mV, respectively. The mobility, μ, of MXene in water gave $-3.04*10^{-8}$ $m^2/(V*s)$, whereas MXene in PC gave $-0.96*10^{-8}$ $m^2/(V*s)$, which are values in good agreement considering that this parameter is inversely proportional to the viscosity of the solvent and PC is almost three times more viscous than water.

Such high values of zeta potentials were welcomed in view of the subsequent EPD investigation, as they were able to provide good particle stability and prevent them from agglomeration under the application of a voltage.

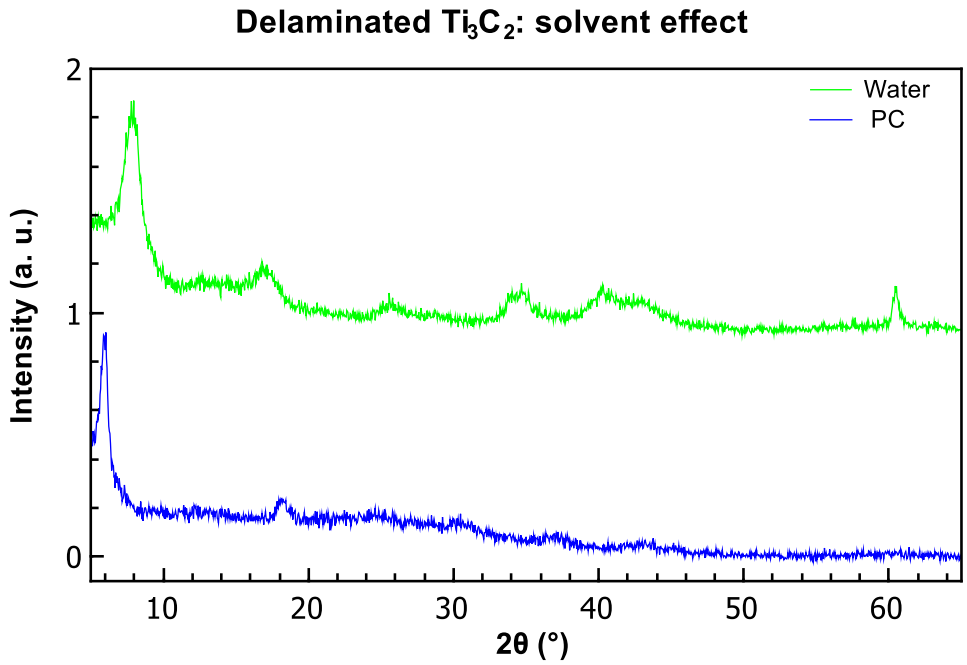

Figure 4.3.1: *X-ray diffraction of Ti_3C_2 obtained by etching the parent Ti_3AlC_2 for 6 days and delaminating it both in water and PC: spectra are taken on VF films after drying, in air for the former and in a vacuum furnace for 12 h at 180 °C for the latter.*

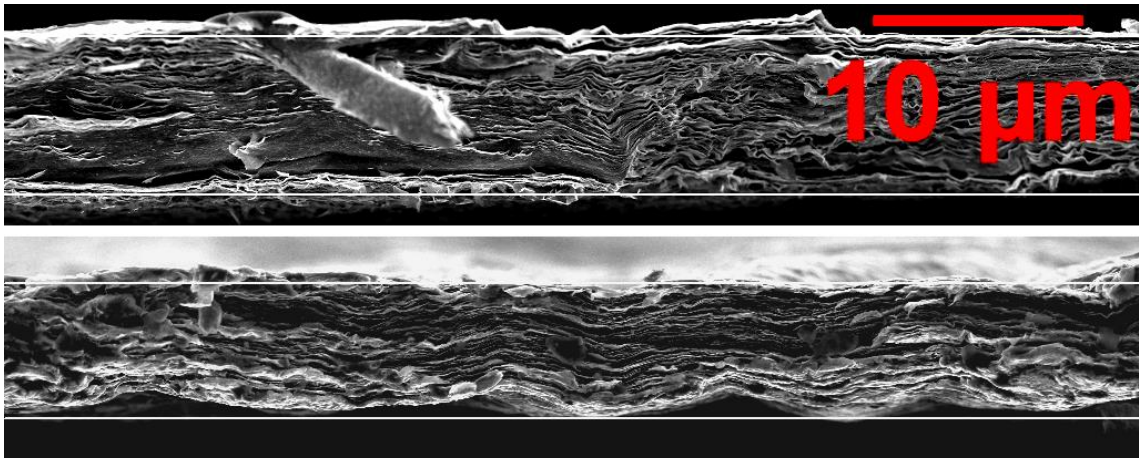

Figure 4.3.2: *SEM images of vacuum filtered $Ti_3C_2T_x$ film produced from water (top panel) and PC (bottom panel) solutions. Powders were etched for 6 days in both the cases and PC solvent was removed performing a vacuum annealing at 180 °C for 13 h. Both the pictures were taken using the following instrument parameters: EHT 5 kV, working distance 4 mm and magnification 5K.*

Chapter 5

EPD studies

The present chapter provides a detailed description of EPD tests and characterization of the film produced from both aqueous and non-aqueous colloidal suspensions.
In the first section, water solution behavior under several EPD working conditions is inspected through several characterization techniques: XRD diffractograms were used to determine the level of structural order and possible flake misalignments across the film with changing applied voltages; SEM imaging, general visual observations and current measurements provided information about the film quality and parasitic processes occurring simultaneously with EPD; weighing of the deposited mass after air drying permitted to fit with a kinetic model the mass deposition trend of the suspended particles under both constant voltage and current conditions. Similar studies are discussed following the same flow for PC solution, in the second section. Nevertheless, issues introduced by the solvent high boiling point required the use of vacuum annealing before any kind of further exploration and therefore effect of different heating treatments are herein discussed as well.
Note that how discussed through the previous chapter, only $Ti_3C_2T_x$ gave actual colloidal dispersions and for this reason, from now on the remaining of this work deals with this particular member of the MXenes world.

5.1 Aqueous suspensions

Electrophoretic deposition was first of all explored for $Ti_3C_2T_x$ dispersed in water with a particle loading of 13 mg/mL (at times referred to as “concentrated”) and a half diluted version of the same solution (i.e. approximately 6.5 mg/mL, at times referred to as “diluted”). Besides the good understanding behind delaminating MXenes in aqueous environment this solvent was chosen, despite electrolysis issues during EPD, because of its cost effectiveness and ease of industrial treatment compared to other possible organic molecules; what’s more, the principle of electrophoresis requires that particles are electrically charged which is easier to obtain in a strongly dissociating solvent, like water.

The two solution were tested under several working conditions, but the main experimental campaign consisted of a constant voltage exploration, where several potential values and deposition times, up to 10 minutes, were tried, as explained later. Before any other investigation the main aim was to assess the lowest potential capable of forming an effective deposit, and after some trials 3 V was compellingly identified as the lowest boundary for the EPD process to occur, as little to no deposition was observed. Though electrophoresis was still likely happening at such low voltages, the high zeta potentials measured herein suggests that the electric field was insufficient to overcome interparticle repulsion needed to form a solid deposit at the electrode-suspension interface.[79]
To summarize, 3, 5, 10, 15, 20 and 25 V were tried, while, as for times, experiments were performed for 5, 10, 30, 60, 120, 300 and 600 seconds. Nevertheless, a "proof of concept" constant current series of tests was carried out at a current density of 2.3 mA/cm^2, a value chosen in order to drive electrophoresis and collapsing particle in a film structure, still preventing excessive electrolysis promoted by the increasing voltage applied throughout the experiments. The purpose in this case was both to study the process kinetic proving what stated by Sarkar *et al.*[56] and finally to inspect the product quality of deposits fabricated despite the continuously changing voltage – up to levels where electrolysis was occurring - necessary to keep the current constant.

5.1.1 Overview

Water solution characterization started from some visual observations of the deposited films, right after the process and at the end of the air drying, combined with SEM analysis at different magnifications. Nonetheless, to gain some insights into the basics of the EPD phenomena a current vs time measurement was performed at first on both available concentrations, testing the behavior at 5, 10, 15, 20 and 25 V. **Figure 5.1.1** shows the current density variations with time data collected for the 13 mg/mL water solution in the 5 to 25 V range, as just described.
Initially, the deposition current shows a remarkable drop with increasing time for all voltages which does not surprise considering that current is, among other things, certainly effect of the ongoing particle deposition and is expected to be higher at the beginning when suspension loading is greater and, in turn, a larger charge flow is fostered. Nonetheless the graph deserves some more comments, as, except for the lowest voltage (5 V), which shows a monotonic decrease until a final plateau, all the other potentials applied produce a halt of this drop, represented by a small hill with a relative maximum before a subsequent final decreasing, which suggests the presence of some undesired electrochemistry. Even though this phenomenon is not fully understood, some insight was provided by the visual observation of bubble formation getting more and more vigorous

with increasing potentials. This evidence of electrolysis was furtherly tested performing an experiment where the EPD cell was filled with pure DI water and the current was measured across an extensive time window. Results of this test are shown in the inset in **Figure 5.1.1** and corroborate the electrolysis theory, showing an increasing current trend associated with the electrochemical phenomenon, immediately after a brief initial decrease ascribed to a little conductivity provided by a few impurities present in the water. Hence, it is possible to assume that after a short activating time, the electrolysis phenomenon started occurring in parallel with the EPD process, gaining more and more importance as the solution loading was decreasing. In light of this, the observed current densities measured at potentials ≥ 10 V are now less mysterious and the well observed in the curve after a few seconds can be imagined as corresponding to the electrolysis start.

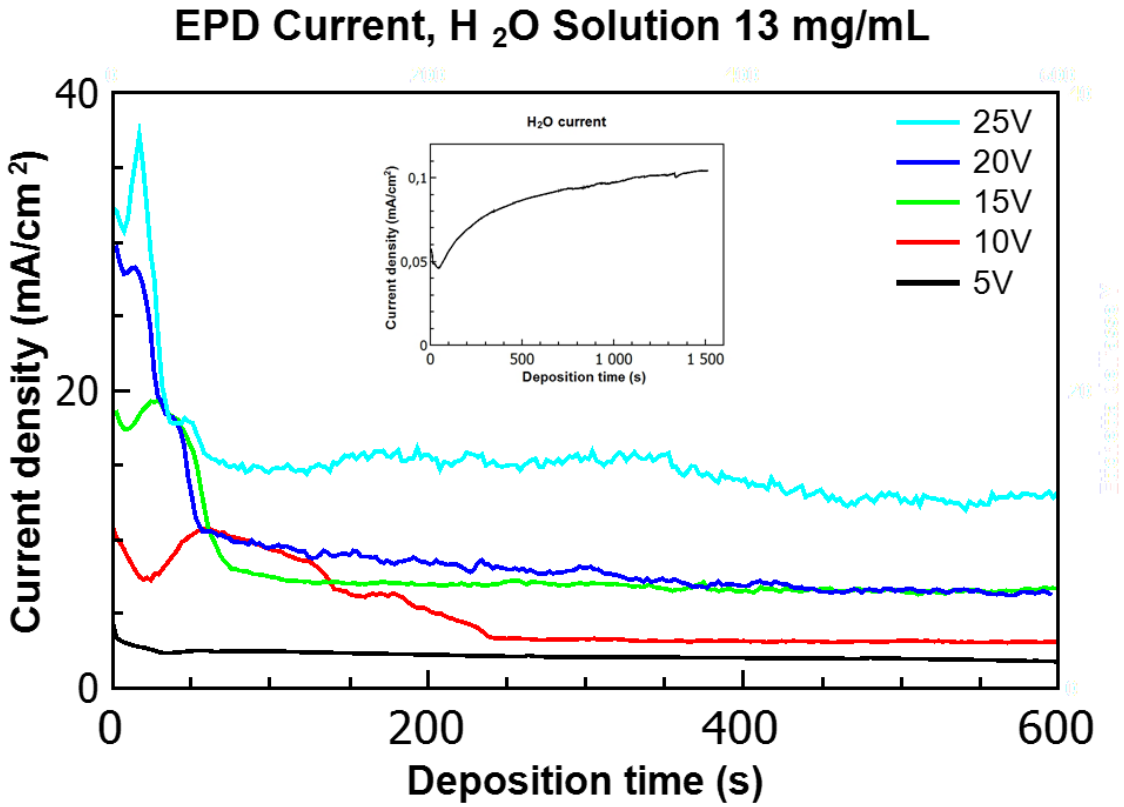

Figure 5.1.1: *time dependence of deposition current density at 5, 10, 15, 20 and 25 V up to 600 s for $Ti_3C_2T_x$ dispersed in H_2O solvent (13 mg/mL). Inset shows the behavior of the same system under a potential of 5 V for pure H_2O (no particles suspended) in order to have insight into possible background effects.*

Interestingly, despite the mentioned variations in the derivative values for different voltages, after a finite and relatively short amount of time, all the curves approach a plateau and it is fair to state that in approximately 3 minutes all the transient phenomena related to EPD come to an end. Afterwards, all the voltages produce an approximately flat current signal, providing good evidence that a steady state process was taking place and that all the possible deposition was over: the behavior in this second stage is

justifiable again considering the ongoing electrolysis, since the fully developed parasitic process controlled electrically the system once the electrophoresis depleted the solution from particles until its nominal conclusion. Those plateaus did not lay at the same current level, except for the unexpected case of superimposed 10 and 15 V, indicating that the electrolysis occurring during the steady state phase was generally dependent on the applied voltage, with higher potentials driving more gas evolution. To date, the observed behavior throughout the final stage of EPD process is explained only qualitatively in terms of different electrolysis intensities, but more work is required to understand its fundamentals and the overlapping of 10 and 15 V. Nevertheless, this analysis provided useful information about the EPD mechanisms and characteristics and allowed an aware choice of the time range to consider for further analysis. Therefore, 10 minutes were deemed more than sufficient to appropriately describe the process and depositions of 5, 10, 30, 60, 120, 300 and 600 seconds were performed on both concentrated and diluted solutions at 5V along with a constant current test (current density 2.3 mA/cm^2) on the diluted solution only, yet considering the same time intervals.

Figure 5.1.2 shows photographs of the FTO substrates after deposition and drying in air for the systematic study carried out on diluted water solution (6.5 mg/mL) at 5 V and different times. Within a few minutes after the process, the films started to show drying effects, loosing progressively all the visible humidity in less than half a day, with time ranges depending clearly on the EPD duration (longer depositions resulted in a higher amount of material on the substrate and, in turn, in more water to be evaporated). Not surprisingly, a growing in the deposited mass amount with processing time is easy to catch even from visual observation and all the films are adhering to their substrate, showing a peculiar behavior compared to many other cases, as discussed below. Nevertheless, the films could be easily scratched and peeled off the FTO coated glass, not only showing a poor adhesion with it, but also giving proof of a greater intrinsic mechanical strength than interfacial's one.
Similar considerations are still valid for **Figure 5.1.3** which shows photographs of the FTO substrates after deposition and drying in air for the systematic study carried out on diluted water solution (6.5 mg/mL) at 2.3 mA/cm^2 and different times. In this case, though, for times longer than 10 seconds the as-produced films detached spontaneously from the substrate during drying, likely owing to material contraction which proved to be unbearable by the weak interfacial bond. Such an interpretation is supported by the fact that constant current conditions, as better explained later, sustain a higher deposition rate than constant voltage and thus, for a given time, more material is generally present in the film, resulting in a bigger stress during drying.

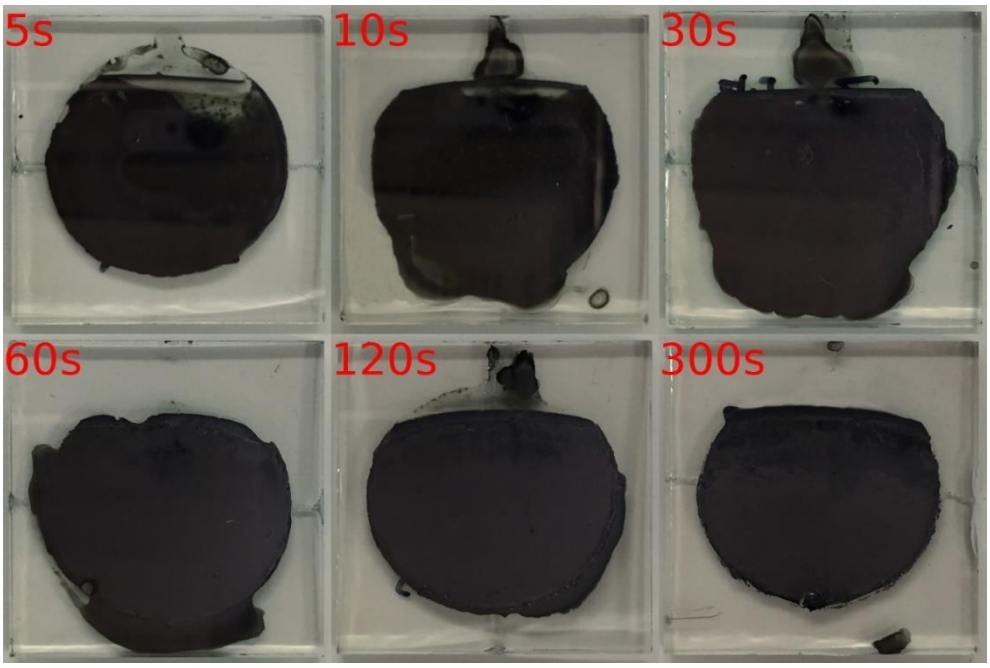

Figure 5.1.2: *digital photo of $Ti_3C_2T_x$ films fabricated from water diluted solution at a potential of 5V applied for different deposition times as specified in the upper-left corner for every sample.*

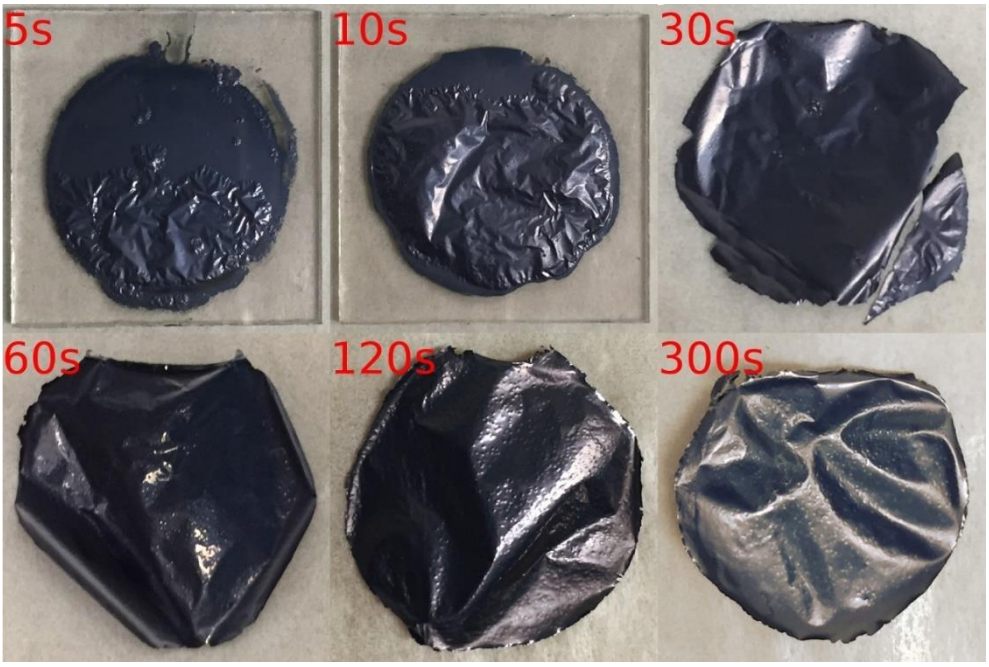

Figure 5.1.3: *digital photo of $Ti_3C_2T_x$ films fabricated from water diluted solution with a current density of 2.3 mA/cm^2 applied for different deposition times as specified in the upper-left corner for every sample.*

Finally, both the selected constant voltage and constant current conditions did not produce significant bubbling throughout the process, giving evidence of an electrolysis process at

least controlled if not completely hindered by kinetics barriers. This positive outcome in terms of processing reflects also in the films quality because no major turbulence affected their growth, providing a rather uniform and flat surface with properties not excessively affected by parasitic phenomena.

Furthermore, the morphological characterization was extended with a series of depositions from concentrated water solution at 5, 10, 15 and 20 V for a fixed time of 120 s in order to inspect the influence of applied potential on the final film microstructure. The micrographs in **Figure 5.1.4** show increasing surface roughness, film inhomogeneity, and occurrence of macropores with diameters on the order of several hundreds of micrometers, growing in size with higher voltages. These experimental observations are justified based on two different aspects, one stemming from electrolysis effects and the other from coagulation of individual particles when a voltage is applied. As already discussed, during the EPD process current was progressively diverted from acctual deposition by a parasitic process, namely water electrolysis at potentials greater than 5 V, which resulted in the formation of hydrogen and oxygen gases at the cathode and the anode, respectively. This continuous turbulence and outgassing, more stimulated by increasing voltage, caused pin holes in the deposits, poor adherence to the substrate, and decreasing homogeneity, due to entrapment of bubbles within the deposit. Nevertheless, this apparent drawback set by electrolysis of the aqueous medium disrupted on the other hand the even MXene stacking observed for 5 V deposition, suggesting potentially surprising results in term of charge storage specific capacity provided by an electrode made from such films, thanks to its opened structure where MXene flakes are exposing their side and not their top face. The second explanation for the observed morphologies is credited to a previous research [80]: when a "high" voltage is applied, despite the high stability ensured by the remarkable zeta potential value, particles start to coagulate in the middle of the suspension and move towards the oppositely poled electrode in form of aggregates bigger than the original flakes dimensions. Furthermore, at such high deposition voltages, the coarser particles are driven to move more quickly and when they collide onto the electrode they don't have enough time available to sit realizing the best-packed structure possible and adjusting their position as needed, therefore generating a non-homogeneous structure. Nonetheless, this interpretation will be partially retracted in the section relative to the PC suspensions study, since in absence of mayor water electrolysis smooth structures were observed even at the highest voltages.

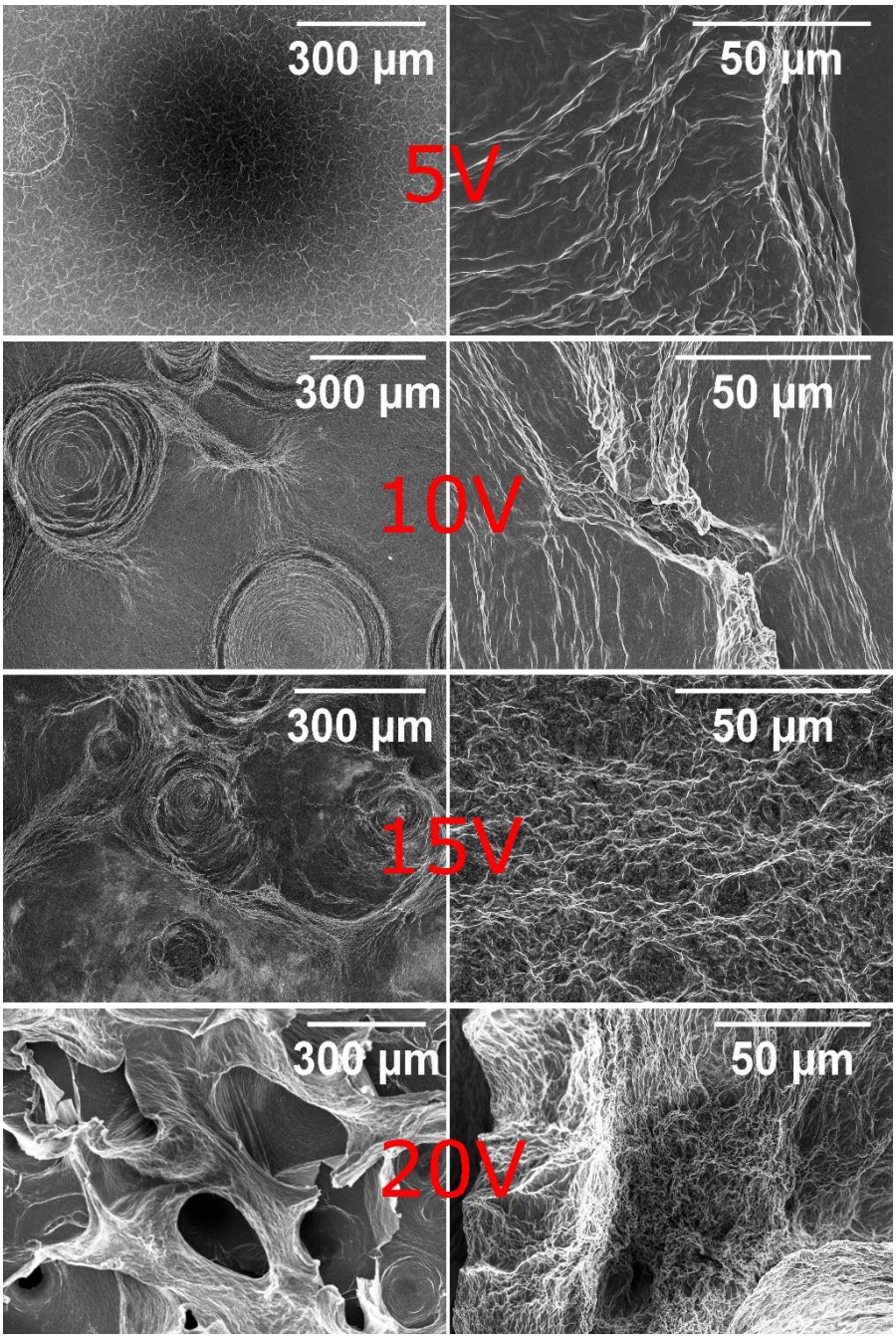

Figure 5.1.4: *surface morphology SEM images of $Ti_3C_2T_x$ films (after 2 d of spontaneous air drying) deposited from water solution (13 mg/mL) at different voltages for a constant time of 120 seconds. Single rows represent an individual film depicted at two level of magnification (low on the left and high on the right) to understand macroscopic and microscopic features. Pictures were taken using the following instrument parameters: EHT 5 kV, working distance 3 mm and magnification 0.1K (left column) and 1K (right column).*

5.1.2 XRD

The structural observations provided by SEM imaging were essentially confirmed by XRD analysis, performed on air dried films obtained from concentrated water solution EPD at 5, 10, 15 and 20 V for a fixed time of 120 seconds (see **Figure 5.1.5**). The four diffractograms show that the basal (00l) peaks intensity is quite high at 5 V, but reduces monotonically as the voltage is increased. The interpretation of this observation is that the amplifying gas evolution above 5 V likely disrupts the oriented coagulation of $Ti_3C_2T_x$ flakes, which otherwise occurs parallel to the electrode at lowest voltages, validating the considerations reported in § 5.1.1. Moreover, at most voltages, aqueous EPD films had a c lattice parameter (c-LP) of 22-23 Å, whereas values ranging from 25-30 Å have been reported in literature for $Ti_3C_2T_x$ films made by other methods from aqueous suspensions.[23,27] The reasons for the lower c-LP and asymmetry in the shape of the (002) basal peaks are not clear at this time but could be the result of water being forced out as flakes come together to form a deposit.

Finally, it is worth noting that some peaks related to the substrate and detected for the lowest voltages are alive even at 20 V despite the increased film thickness due to a dense pattern of pinholes prejudicing the film continuity and directly exposing the FTO coating to the X-ray beam.

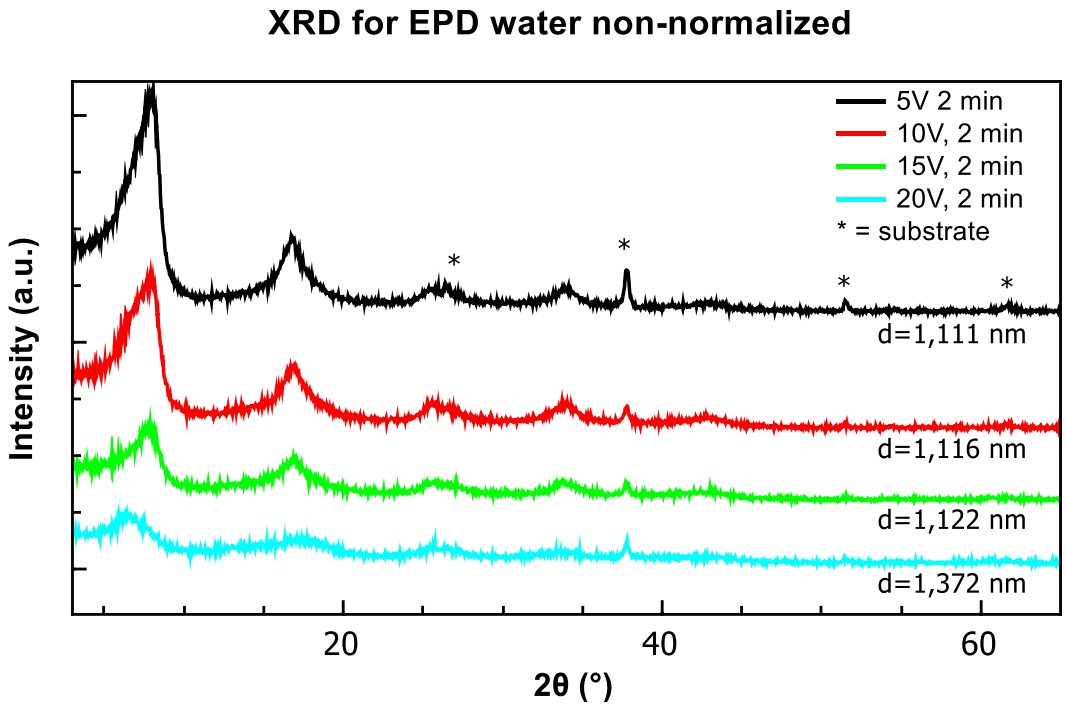

Figure 5.1.5: *X-ray diffraction of $Ti_3C_2T_x$ films on FTO substrate after EPD from aqueous (13 mg/mL) suspensions for 2 min at 5,10,15, and 20 V. Asterisk are placed above peaks related to substrate coating and d-spacing calculated from Bragg's law are reported beneath each spectrogram.*

5.1.3 EPD Kinetics

In this section, kinetic of EPD process for water solution is discussed, although only some major hints will be provided, as a more comprehensive dissertation is given in § 6.1.
Briefly, concentrated and diluted water solutions underwent EPD at an applied potential of 5 V for a set of 7 different times, 5, 10, 30, 60, 120, 300 and 600 s in order to plot the deposited mass vs deposition time graph depicted in **Figure 5.1.6**.
At the end of deposition, the substrates were placed in a clean drawer using an empty CD case to store them yet allowing for air drying. After 2 days the interparticle water (note that interlayer H_2O molecules were still partially adsorbed as shown by the above mentioned XRD analysis carried out on samples treated similarly) was considered completely removed from all the films and the weighing step was performed. The plot shows that independently from the specific concentration, the experimental points lay following an approximately exponential trend, which is reasonable, as during deposition the particle loading in the suspension was progressively depleted and therefore less particles were available to increase the deposit mass. This resulted in an asymptotic behavior approaching, for long times, the theoretical maximum, given by the total mass suspended in the colloidal solution.

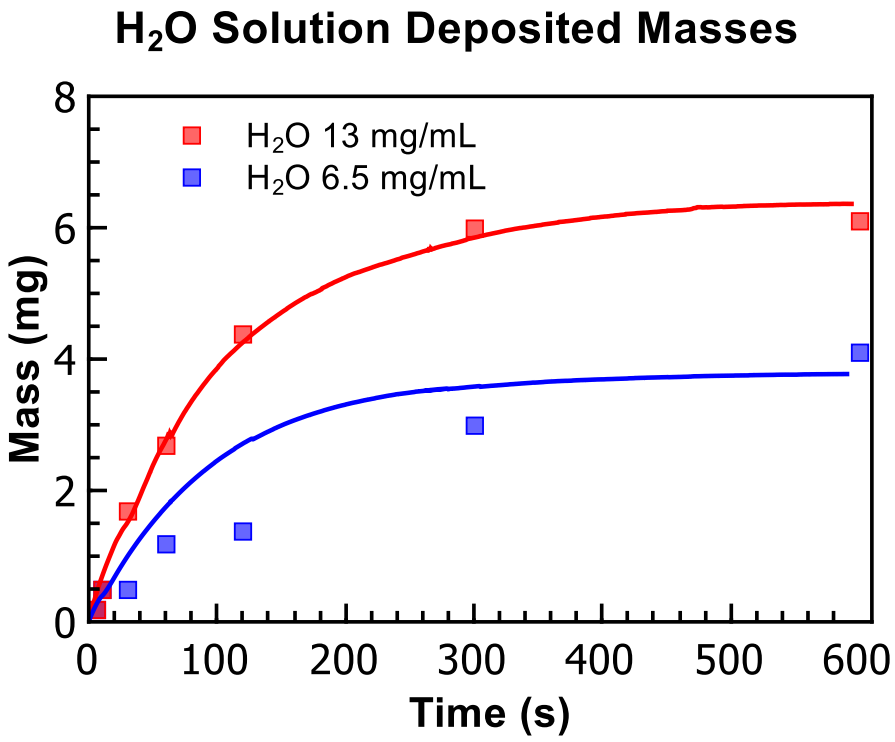

Figure 5.1.6: *kinetics of the EPD process under an applied potential of 5 V for both concentrated and diluted suspensions of $Ti_3C_2T_x$ in water. Mass deposited after spontaneous air drying throughout 2 days is plotted against the time allowed for deposition, along with the suggested fitting model.*

Along with experimental points **Figure 5.1.6** depicts the two corresponding fitting models derived according to the work published in 1996 by Sarkar *et al.* to describe the EPD kinetics.[56] Based on considerations similar to those presented here, they suggested to shape the curve with an exponential model tending towards the maximum possible value of mass deposition. For a constant voltage configuration, however, especially for particles which are not conductive once collapsed onto the electrode and separated from their ions cloud (which is not true in this work, though) the basic model needs to be adjusted with a changing-with-time factor in the exponential argument which, representing the normalized current across the experiment, accounts for the drop in current density caused by the increasing resistance of the growing deposit.

The quality of this interpretation was confirmed by a further constant current test where, using a current density of 2.3 mA/cm^2 the diluted water suspension was deposited following the same time subdivision proposed in the study at the fixed voltage. Experimental points and the fitting curve are shown in **Figure 5.1.7**: again, the shape is clearly asymptotic, tending towards the particle weight suspended in solution, but in this case the constant current boosts the deposition rate and the crude exponential model is sufficient to fit the data. As said at the beginning, however, all this discussion will become clearer in § 6.1, where a deeper scientific interpretation of these phenomena is provided.

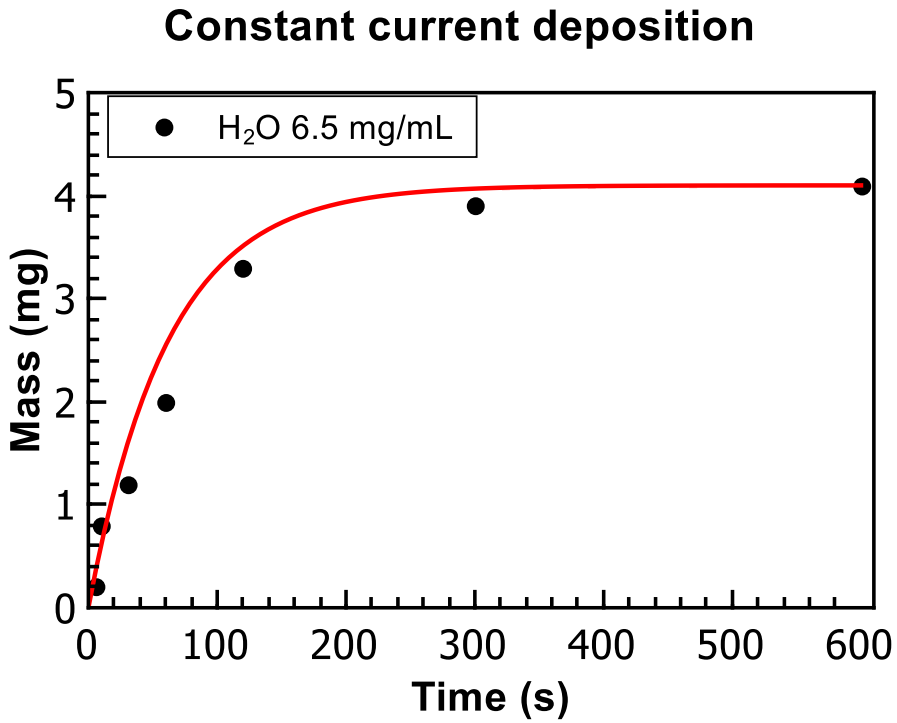

Figure 5.1.7: *kinetics of the EPD process under an applied current density of 2.3 mA/cm^2 for diluted suspensions of $Ti_3C_2T_x$ in water. Mass deposited after spontaneous air drying throughout 2 days is plotted against the time allowed for deposition, along with the suggested fitting model.*

5.1.4 Film thickness

Besides deposited mass, film thickness not only is an alternative parameter in terms of process kinetics, but also a critical industrial feature, as tailoring a coating in terms of thickness is most of the times more meaningful than adjusting its mass. Nonetheless, it is crucial to report that differently from mass, which is a rather absolute feature once the working conditions are set, deposit thickness is affected among other things by gravity in a non-stirred system like the one studied herein. Therefore, the film's vertical cross-section presents a gradient, with thicknesses clearly lower on top and progressively increasing until a maximum value towards the bottom. It is hence evident that an incontrovertible thickness characterization was impossible and despite all the efforts made, some error was introduced from the beginning by the measurement practice. As discussed in Chapter 3, two different techniques were adopted to carry out the measurements, choosing the more appropriate for the specific sample, namely optical profilometry when films were still adhering to the substrate and SEM cross-section imaging whenever deposits were freestanding after drying. In order to minimize the effect of the aforementioned thickness gradient all the samples were analyzed at half of their height.

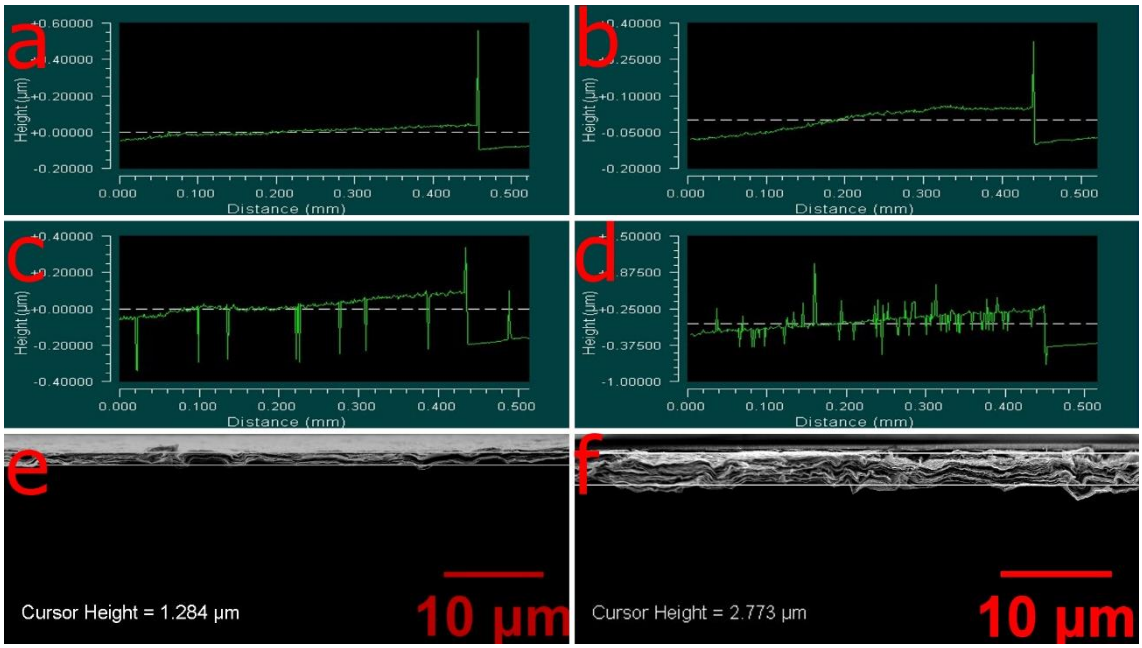

Figure 5.1.8: *example of thickness measurements conducted on deposited films produced from suspensions of $Ti_3C_2T_x$ in water at 5V for 5, 10, 30 60, 120 and 300 s showed in a, b, c, d, e, and f respectively. From a to d results came from profilometry, whereas the others were obtained via SEM imaging, with the following instrument parameters: EHT 5 kV, working distance 3 mm and magnification 2 K for both e and f.*

Figure 5.1.8 provides an example of thicknesses measured through the two different methods on films fabricated from the diluted water solution in the systematic study with

an applied potential of 5 V and different time intervals: while the first two rows are results plotted directly from the profilometer software and don't tell much about material characteristics, the bottom row shows SEM cross-section measurement and a few more considerations are necessary. Differently from what sought, $Ti_3C_2T_x$ appear orderly stacked with particles planes parallel to each other, forming structure comparable with the MXene paper produced by vacuum filtration. On the other hand, however, this proves that at low voltages even a water suspension is capable of producing smooth film surfaces with a homogeneous and controlled microstructure and a process easy to scale up for several applications. Furthermore, more investigations are required to characterize cross-sections of films produced at higher voltages and what found so far from SEM top views is encouraging in the frame of energy storage and supercapacitors development.

Finally, **Figure 5.1.9** provides a thickens overview for the same samples depicted in **Figure 5.1.6**: the shapes assumed by both the solution concentrations tested are reasonable and resemble what already experienced for mass. This does not surprise given that assuming grossly a direct proportionality between thickens and mass through a factor given by the areal density, then both parameters are likely to follow a similar trend, as will be better explained in § 6.1.

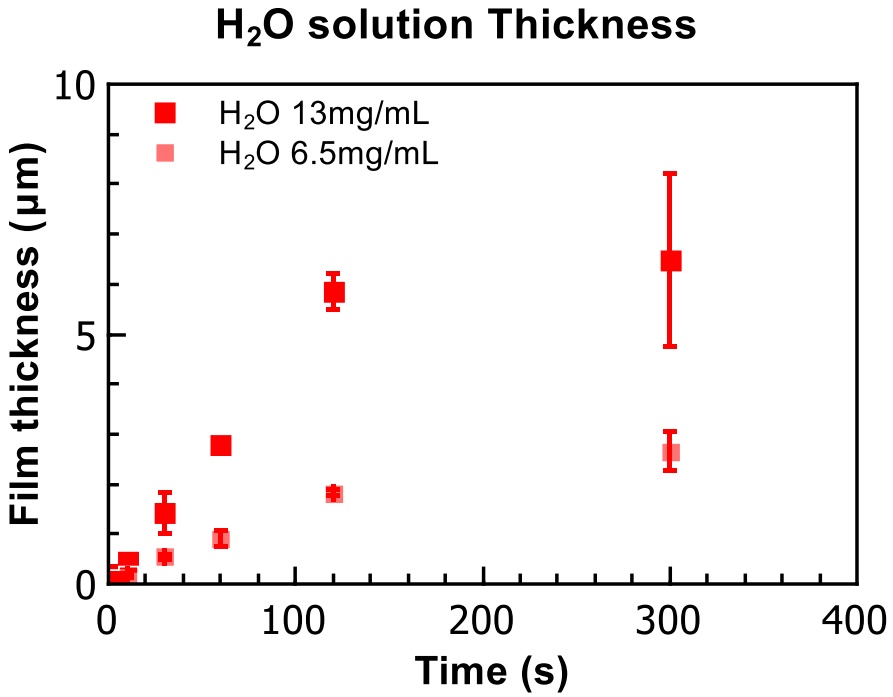

Figure 5.1.9: *film thickness after spontaneous air drying throughout 2 days as a function of deposition time under an applied potential of 5 V for both concentrated and diluted suspensions of $Ti_3C_2T_x$ in water.*

5.2 Non-aqueous suspensions

Study of electrophoretic deposition was then extended to $Ti_3C_2T_x$ dispersed in PC with a particle loading of 13 mg/mL (at times referred to as "concentrated") and a half-diluted version of the same solution (i.e. approximately 6.5 mg/mL, at times referred to as "diluted"). In this case, a third concentration of 2 mg/mL was also used to fabricate films that were characterized via XRD. This second kind of MXene solution was introduced to overcome the electrolysis issues encountered using water with and achieve a stable deposition, based on the fact that, reaching 5.6 V, PC has a much larger electrochemical stability window.[81]. The results description and discussion will follow the same structure proposed for the treatise regarding water suspensions and some observations will be repeated in order to render this section self -sufficient. Furthermore, comparisons with what observed for water will be provided, except for kinetics and thickness which are treated extensively in the next chapter.

The two solution with particle loadings of 13 and 6.5 mg/mL were tested under several working conditions, but the main experimental campaign consisted of a systematic constant voltage explorations, where several potential values and deposition times, up to 10 minutes, were tried, as explained below. Moreover, the same solutions were tested for fixed time and different voltages, spanning the 5-25 V range with a step size of 5 V. As with water, before any other investigation the lowest potential capable of forming an effective deposit was researched: 3 V was compellingly identified as the lower boundary for the EPD process to occur, since little to no deposition was observed. Though electrophoresis was still likely happening at such low voltages, the high zeta potentials measured for PC suggests that the electric field was insufficient to overcome interparticle repulsion and that the formation of a solid deposit at the electrode-suspension interface was hence hindered.[79]

To summarize, 3, 5, 10, 15, 20, 25 and 30 V were tried, while, as for times, experiments were performed for 5, 10, 30, 60, 120, 300 and 600 seconds. The purpose in this case was to characterize the EPD stability at applied potentials higher than 5 V, investigate the process kinetics trying to model it with the theory published by Sarkar *et al*.[56] and to inspect the product quality of deposits. In addition, the possibility of treating the solvent at higher voltages without the danger of major parasitic phenomena paved the way for another kinetic study where given a fixed time several potentials were applied producing a linear growth of the mass that was easy to accommodate recalling the Hamaker's law.[82]

5.2.1 Overview

PC solution characterization started from some visual observations of the deposited films, right after the process and at the end of different vacuum annealing treatments, combined with SEM analysis at several magnifications. Nonetheless, to gain some insights into the basics of the EPD phenomena a current vs time measurement was performed at first on both concentrated and diluted suspensions, testing their behavior at 5, 10, 15, 20 and 25 V. **Figure 5.2.1** shows the current density variations with time collected for the 13 mg/mL PC solution in the 5 to 25 V range, as just described.

Following a behavior comparable with what experienced in the aqueous system, the deposition current shows a noteworthy decrease during the initial stage of the process. However, this is aligned with what expected considering that current was, at least produced by the ongoing particle deposition and was supposed to be higher at the beginning when suspension loading was greater and, in turn, a larger charge flow was triggered. While curves for 5, 10 and 15 V lower smoothly and almost monotonically, a quite different behavior is adopted by the remaining two higher voltages, where for times longer than 100-200 s broad local maxima in the currents are observed, suggesting a small contribution from electrochemical side reactions. Nonetheless this phenomenon was not fully understood as no bubbling was observed in the suspension at any of the voltages used, in contrast with the aqueous suspensions. To shed more light on this unclarified aspect, a reference test was set up, performing an experiment where the EPD cell was filled with pure PC only and the current was measured across an extensive time window. Results of this test are shown in the inset in **Figure 5.2.1** and are apparently in contrast with electrolysis occurrence, as the measured current immediately decreases towards negligible values, presumably after the few ions present as impurities were initially moved towards the oppositely poled electrode providing a small conductivity. What discussed seems to contradict the initial hypothesis, but the two observations might be conciliated by speculating the presence of mild electrolysis of either water intercalated between MXene sheets or PC itself, stimulated indeed by the presence of suspended particles which might activate this process lowering the kinetic barriers. Such an interpretation is supported by the aforementioned broad peaks, which, somehow resembling water behavior, would suggest the beginning of the parasitic electrochemical process at a certain point during the deposition process when a high enough potential is applied. Besides the current secondary maximum at “high” voltages, this test highlighted a second feature shared with the aqueous system: after a period of time required by the process to stabilize, close to the end of the experiment the current signals approach progressively a plateau value (even though for 20 and 25 V a longer experiment would be necessary to totally confirm this statement), providing evidence that a steady state process was taking place and that all the possible deposition was finally over. The

behavior in this second stage is justifiable again hypothesizing an ongoing electrolysis, which would control the mechanisms once no more particle were available to sustain the electrophoretic current flow.

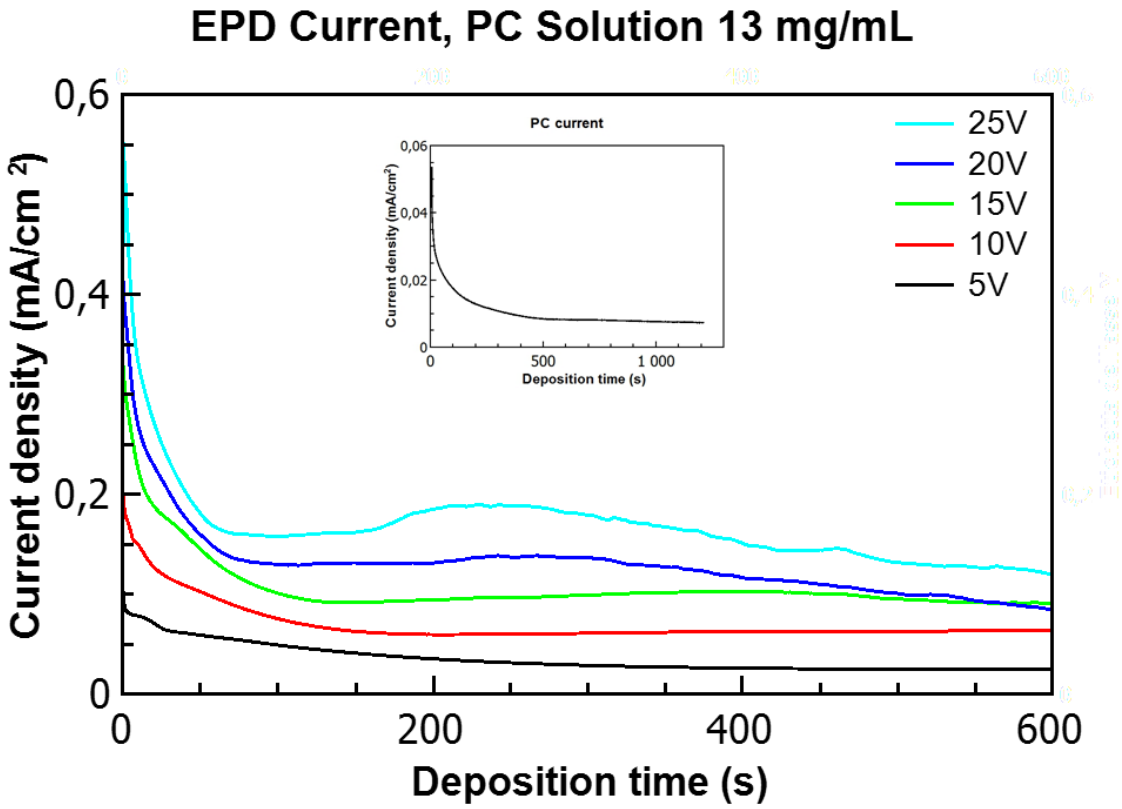

Figure 5.2.1: *time dependence of deposition current density at 5, 10, 15, 20 and 25 V up to 600 s for $Ti_3C_2T_x$ dispersed in PC solvent (13 mg/mL). Inset shows the behavior of the same system under a potential of 5 V for pure PC (no particles suspended) in order to have insight into possible background effects.*

Those final and approximately constant currents, do not assume the same value, except for the unexpected case of partially superimposed 15 and 20 V, indicating that the supposed electrolysis occurring during the steady state phase was generally dependent on the applied voltage, with higher potentials driving more gas evolution. At this stage, all this considerations are confined to the qualitative level and are explained only in terms of different electrolysis intensities, but more work is required to understand their fundamentals and the different shapes assumed at different applied potentials. Nevertheless, this analysis provided useful information about the EPD mechanisms and characteristics and allowed for an aware choice regarding the time range to consider when designing the further analysis. For this reason, 10 minutes were deemed more than sufficient to appropriately describe the process and depositions of 5, 10, 30, 60, 120, 300 and 600 seconds were performed on both concentrated and diluted solutions at 5V.

Figure 5.2.2 shows photographs of the FTO substrates immediately after deposition for the systematic study carried out on concentrated PC solution (13 mg/mL) at 5 V and

different times. All films looked evidently wet, sticking to the substrate, and air exposure did not provide the necessary drying therefore, compared to water, PC introduced a new issue related to the solvent elimination. As with vacuum filtered films form PC solutions (see previous chapter for details) an annealing effect study was necessary and to prevent MXene oxidation vacuum conditions were chosen for all the annealing treatments. The research produced different guidelines based on the specific objective targeted, i.e. either reducing the film mass to a nominally minimum value, corresponding to a stage when all the PC was presumably evaporated if not reacted with the solid phase, or allowing for films delamination removing the minimum possible amount of solvent. This second option was pursued after preliminary XRD analysis showed that intense annealing treatment caused a complete collapse of MXene flakes to form a closely packed and layered configuration similar to what commonly achieved thorough vacuum filtration and thus presumably not enhancing the charge storage specific capacity of the material. After many trials the evaporation kinetic was characterized finding that a vacuum annealing at 160 °C for 12 h allowed the highest mass reduction possible, generally with a loss of 35-45 wt%, and even tougher heat treatments did not stimulate further drying. On the other hand, 35 °C for 30 min appeared to be sufficient for an easy film detachment from the substrate, even though even visual observation revealed that a good fraction of the solvent was still wetting the material rendering it moldable and slightly sticky.

Figure 5.2.3 shows digital pictures of the annealing effect on the same samples depicted in Figure 5.2.2: all the films are evidently dry, the color has changed and even from a top view one can see how thickness has shrunk. Thus, as with water solution, the drying step resulted in generation of contraction stresses often too high to be born by the interfacial bindings between film and substrate, causing film delamination. What discussed can be noticed for instance in the 5 s sample where the constrains generated by some points where the film is still bound to the glass cause the formation of waves across the film. Differently from water, though, at the end of the annealing treatment it wat always possible to obtain free standing films, either by spontaneous delamination or promoting the process with a razor blade, anyways ensuring their integrity. Moreover, it is evident that for a long enough deposition time the heat treatment alters the film, causing at first bubbles and for even longer time its complete crumpling and curling. To prevent this setback, milder annealing treatments were tried; however, despite several different heating programs designed to slow down evaporation kinetics with an initial step at temperatures lower than 100 °C before reaching the final 160 °C target, no improvements were observed, forcing to conclude that beyond a certain thickness value the PC excess was trapped in the deposit with no way to escape without bubble formation.

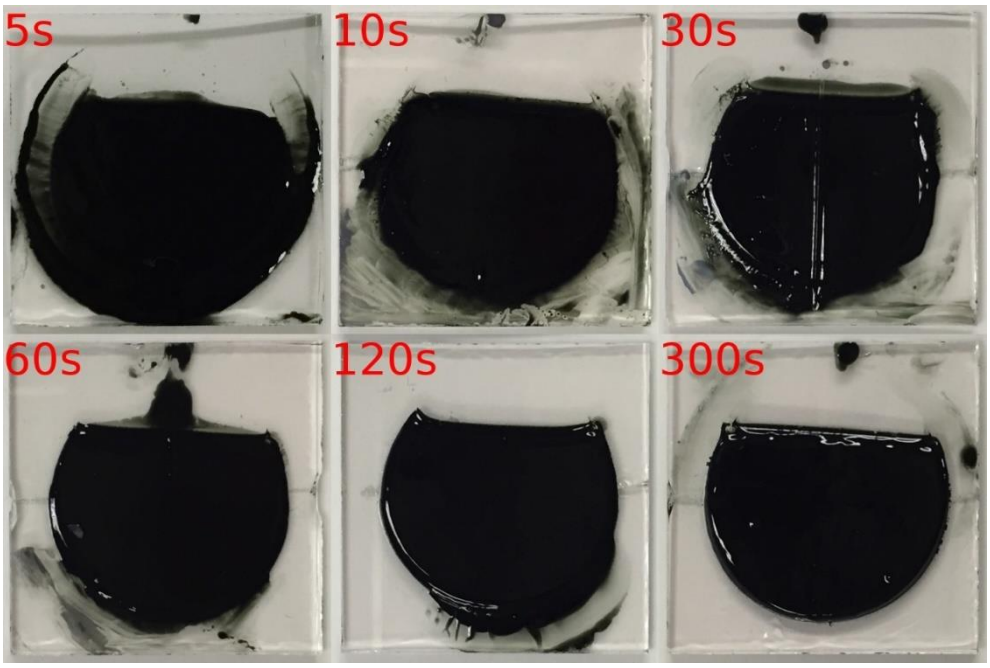

Figure 5.2.2: *digital photo (right after deposition) of $Ti_3C_2T_x$ films fabricated from PC concentrated solution at a potential of 5 V applied for different deposition times as specified in the upper-left corner for every sample.*

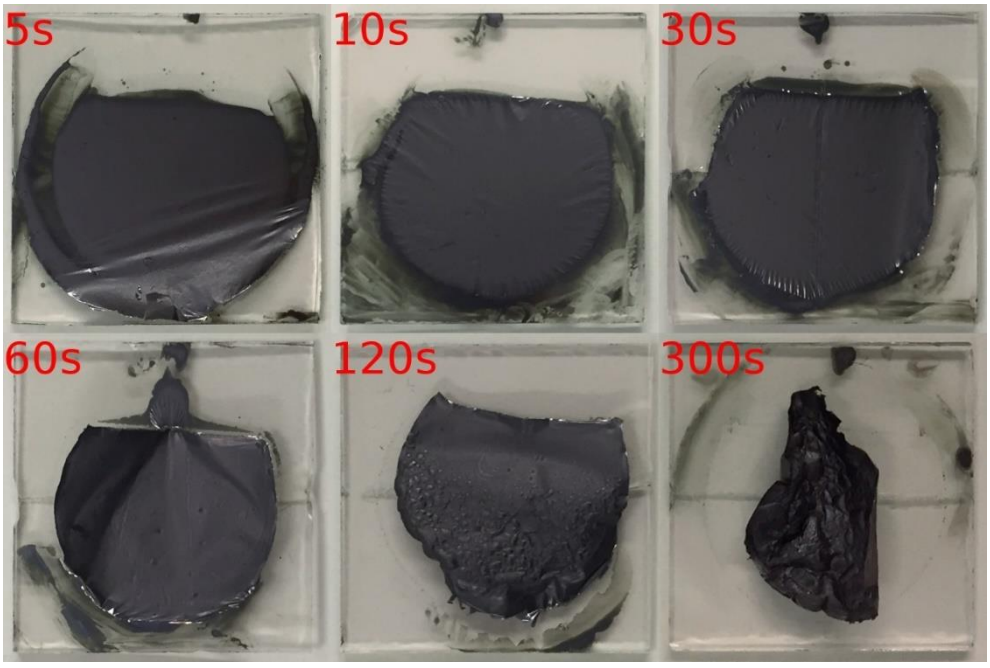

Figure 5.2.3: *digital photo (after vacuum annealing at 160 °C for 12 h) of $Ti_3C_2T_x$ films fabricated from PC concentrated solution at a potential of 5 V applied for different deposition times as specified in the upper-left corner for every sample.*

Given the good stability provided by PC at voltage higher than 5 V a further systematic study was designed to investigate the solution behavior and resulting films quality sweeping the 5-25 V range with a step size of 5 V (i.e. 5, 10, 15, 20, 25 V). From the previous experiments at 5 V and different times, a deposition of 30 s was deemed a nice trade-off to produce a self-standing film even at the lowest voltages and to not deplete completely the solution at the upper boundary of the potential interval explored.
Figure 5.2.4 shows digital picture for such samples (considering a concentrated PC solution) both right after EPD and after a 12 h vacuum annealing treatment at 160 °C. All the considerations expressed regarding samples obtained for 5 V deposition at different times hold their validity, from the spontaneous delamination at all voltages, to the bubble formation and film crumpling observed at high voltages or, to say it in other words, beyond a particular thickness value.

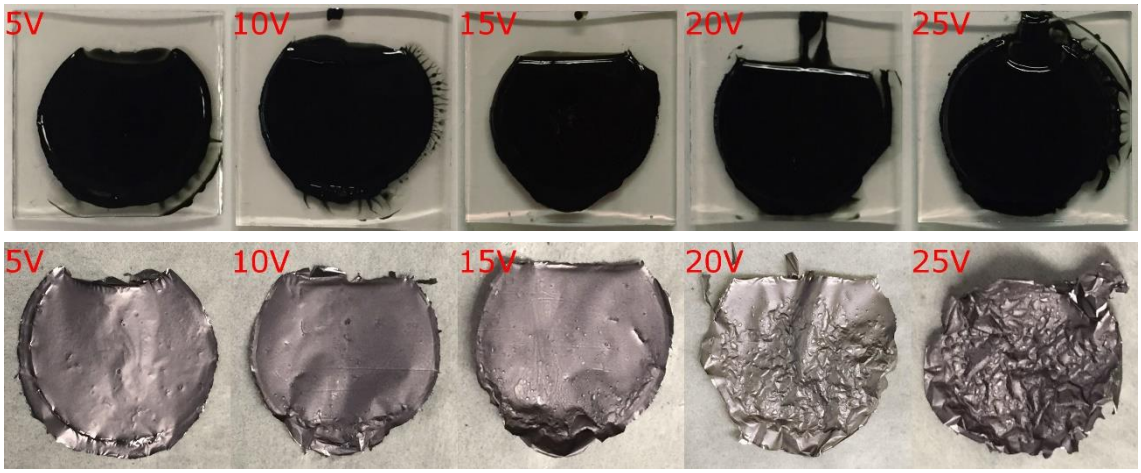

Figure 5.2.4: *digital photo depicting the annealing effect on $Ti_3C_2T_x$ films fabricated from PC concentrated solution for a fixed time of 30 s and 5 different applied potentials as specified in the upper-left corner for every sample. Top line shows samples right after deposition, whereas bottom line is relative to the same films after 12 h of vacuum annealing at 160 °C.*

Furthermore, the morphological characterization was extended with a series of depositions from a PC solution with 2 mg/mL particle loading at 5, 10, 20 and 30 V for a fixed time of 120 s. The goal was to inspect the influence of applied potential on the final film microstructure, particularly investigating flakes arrangement in terms of charge storage specific capacity potentialities.

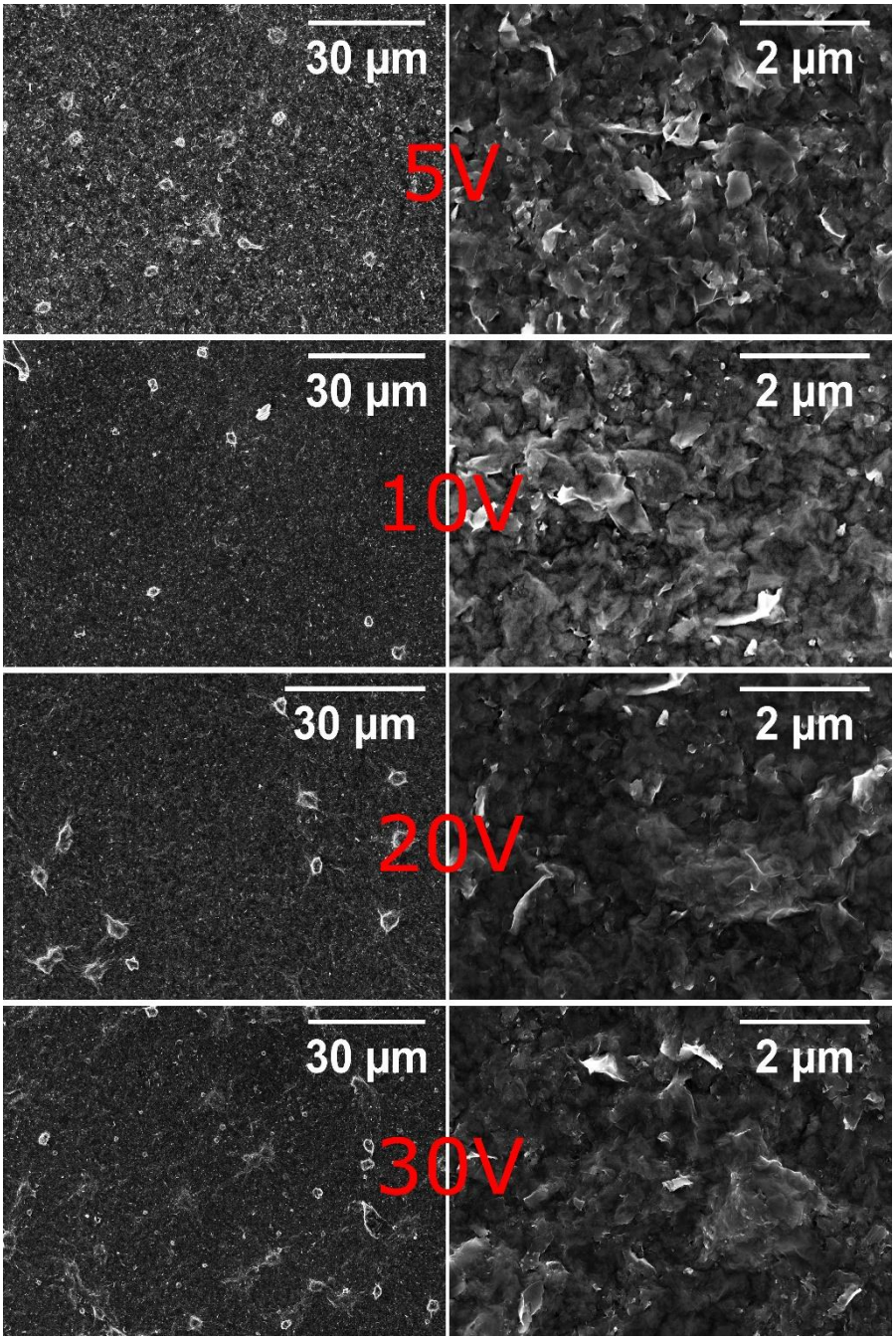

Figure 5.2.5: *surface morphology SEM images of $Ti_3C_2T_x$ films (after vacuum annealing at 35 °C for 30 min) deposited from PC solution (2 mg/mL) at different voltages for a constant time of 120 seconds. Single rows represent an individual film depicted at two levels of magnification (low on the left and high on the right) to understand macroscopic and microscopic features. Pictures were taken using the following instrument parameters: EHT 5 kV, working distance 3 mm and magnification 1K (left column) and, 17K (right column).*

In contrast to aqueous deposition, micrographs of the just introduced samples (see Figure 5.2.5) show the absence of macroscopic defects or voids that were present after the high-voltage aqueous depositions and little difference in morphology as a function of voltage. A thorough examination of the high magnification column (17K), however, demonstrates

that the highest voltages produced a slightly coarser and more compact structure, characterized by the presence of some aggregates surrounded by thinner particles. As briefly outlined in the section regarding aqueous solution, this might be due to the fact that at high deposition potentials, nanoparticles stability is hampered and they collapse in coarser coagulates even before or during electrophoresis. Moreover, the speed transmitted to particles by the high electric field causes more difficulties in the sitting phase and often the deposit shows a worsening in homogeneity. Nevertheless this interpretation looks here a bit stretched and maybe only the comments regarding the presence of a slightly coarser morphology holds true, being all the samples characterized by a substantial uniformity, independently of what potential is applied.

Finally, a few words have to be spent to describe the qualitative results produced by two preliminary studies carried out in order to explore both the possibility of producing transparent or semi-transparent coatings and the feasibility of EPD using a Pt coated glass slide in substitution for the generally used FTO substrates which were suspected to interfere electrochemically with MXene generating new species.
As for the first issue, **Figure 5.2.6** right panel shows how using a rather diluted solution of 2 mg/mL of MXene in PC at 5 V for a deposition time of 5 s allowed for semi-transparent coating fabrication, producing a slightly yellow film, so thin that it was possible to see through it. Although all the parameters should be optimized, this first trial is encouraging and (according to all the other observations resulted from more concentrated solutions) sensible guidelines to tune this kind of technology might be: working with low voltages and progressively decreasing the particle loading until the film would hopefully turn colorless (or at least less yellow). This part of the study allowed for one more observation regarding the solvent draining mechanism at the end of deposition and its effect on the deposit: thanks to the substrate transparency it was possible to notice the ongoing formation of the EPD coating in all the cases when the solution was enough diluted and, interestingly, a few times the act itself of evacuating the fluid from the cell caused the complete removal of the film (visually observable from outside the equipment). This has been ascribed to the surface tension of the liquid and the interaction of the latter with the deposit: given the poor adhesion of the particles to the substrate, the down-going movement of the fluid during the draining exerted a force high enough to wipe the glass surface and drag the deposited particles to the bottom. Therefore, it has been suggested that, independently from the film thickness, a small layer is removed every time during the solvent evacuation and, keeping this in mind, it can be understood that a transparent coating can be achieved only when the initial film thickness right after deposition is slightly greater than the one which will be removed due to the draining procedure. Furthermore, the moving free surface of the liquid was responsible for some

minor morphological features, as its position was able to deform the wet deposit and only a very uniform draining provided a flat film whereas a discontinuous extraction caused some irregularities and light undulations in the final material.

Regarding the FTO alternatives, on the other hand, some Corning (New York) microscope glass slides were cut into squared pieces 25x25 mm and sputter coated with platinum until the coating almost completely obscured the transparency of the material. Then normal EPD test were performed exactly as described above for FTO coated substrates. Not surprisingly, considering the well-known catalytic properties of that noble metal, water solutions exhibited immediately a vigorous electrolysis that made deposit fabrication unfeasible, foremost because the conductive coating was promptly peeled off the glass slide. At this point PC was tried in view of its non aqueous composition, but despite a slightly better behavior, in this case as well, platinum was progressively corroded and deposition halted after a short time compromising the process yield. **Figure 5.2.6** left panel shows a film produced on Pt coated substrate, proving that despite the non-optimal conditions some kind of deposition was anyway possible and opening new room for future explorations. At the end of the process, the sample has been vacuum annealed at 160 °C for 12 h and the resulting film was tightly bound to the substrate, not only introducing a significant difference with respect to what observed for FTO coated glass, but also providing a new method for those cases when delamination is an undesired result.

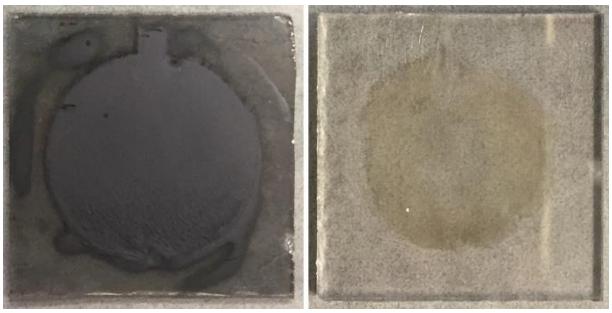

Figure 5.2.6: *digital photographs depicting samples fabricated in the preliminary stages of this work: on the left, example of deposition from PC solution on a platinum coated substrate, on the right example of semi-transparent coating.*

5.2.2 XRD

SEM imaging was matched with XRD analysis, performed on air dried films obtained from PC solution EPD at 5, 10, 20 and 30 V for a fixed time of 120 seconds using a particle loading of 2 mg/mL (see Figure 5.2.7). As already noted, for these samples a soft annealing treatment was applied, heating at 35 °C for only 30 minutes the material in an attempt to preserve a possible flake disorientation before particle collapsed in a tightly packed layered structure due to strong solvent evaporation. The four diffractograms show strong basal peak reflections (highlighted by vertical lines for (002) and (008)) at all voltages, with only a slight decrease in the (002) intensity at 30 V. At 29.0-29.2 Å for all applied potentials, dried PC-deposited films have c-LP much higher than water-deposited ones. Moreover, these values match well with the 29.6 Å value of vacuum-filtered and annealed film from the same PC suspension, but are much lower than the c-LP of 37.2 Å measured for reference a PC-intercalated multi-layer Ti3C2Tx. Therefore it is possible to conclude that PC does not seem to be intercalated in the interlayer space after vacuum annealing of PC-deposited films.

Finally, it is worth noting that some peaks related to the substrate and detected for the lowest voltages are alive even at 20 V, very likely due to the film thickness which grew very slowly with voltage because of the low PC solution concentration.

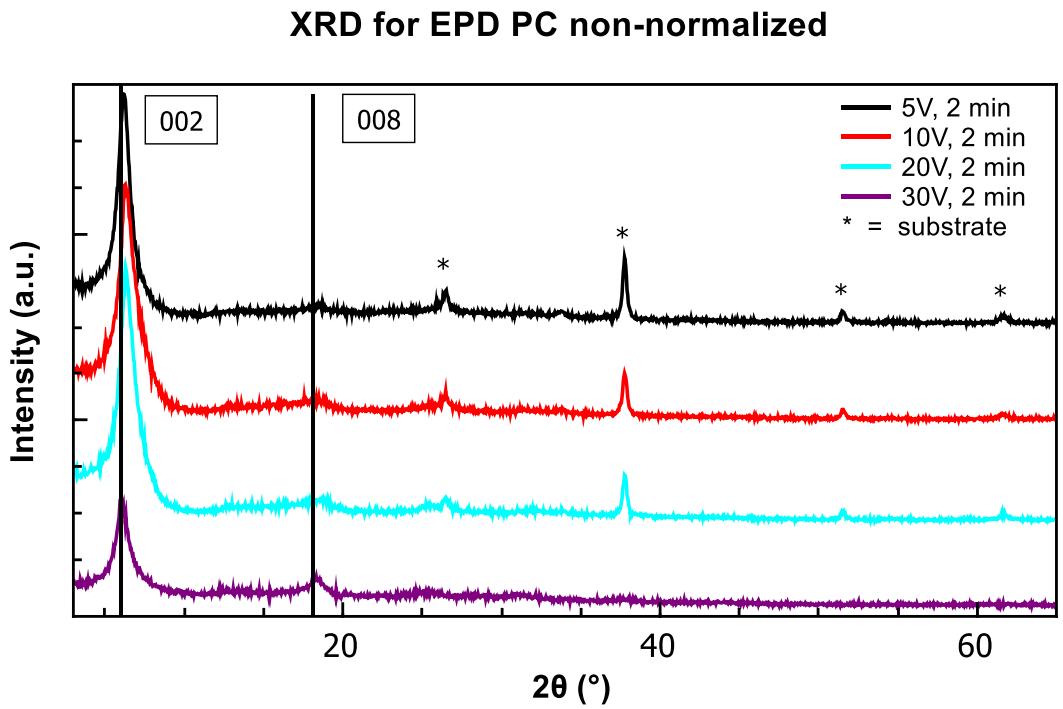

Figure 5.2.7: *X-ray diffraction of $Ti_3C_2T_x$ films on FTO substrate after EPD from PC suspension (2 mg/mL) for 2 min at 5, 10, 20, and 30 V. Asterisk are placed above peaks related to substrate coating and black vertical lines represent (00l) basal peaks.*

5.2.3 EPD Kinetics

In this section, kinetic of EPD for PC solutions is introduced, although only some major hints will be provided, as a detailed discussion is put off to § 6.1, where the reader will find a general description of the mechanisms on which the process is grounded.
Briefly, concentrated and diluted PC suspensions underwent EPD at an applied potential of 5 V for a set of 7 different times, 5, 10, 30, 60, 120, 300 and 600 s in order to plot the deposited mass vs deposition time graph depicted in **Figure 5.2.8**.
The qualitative observations are completely analogous to what highlighted in the aqueous system: after vacuum annealing at 160 °C for 12 h to get rid of all the solvent and prevent it from affecting excessively the weighed values the plot shows that independently from the specific concentration, the experimental points lay following an approximately exponential trend. The observation is reasonable considering that during deposition the particle loading in the suspension was progressively depleted and therefore less particles were available to increase the deposit mass. This resulted in an asymptotic behavior approaching for long times the theoretical maximum, given by the total mass suspended in the colloidal solution.

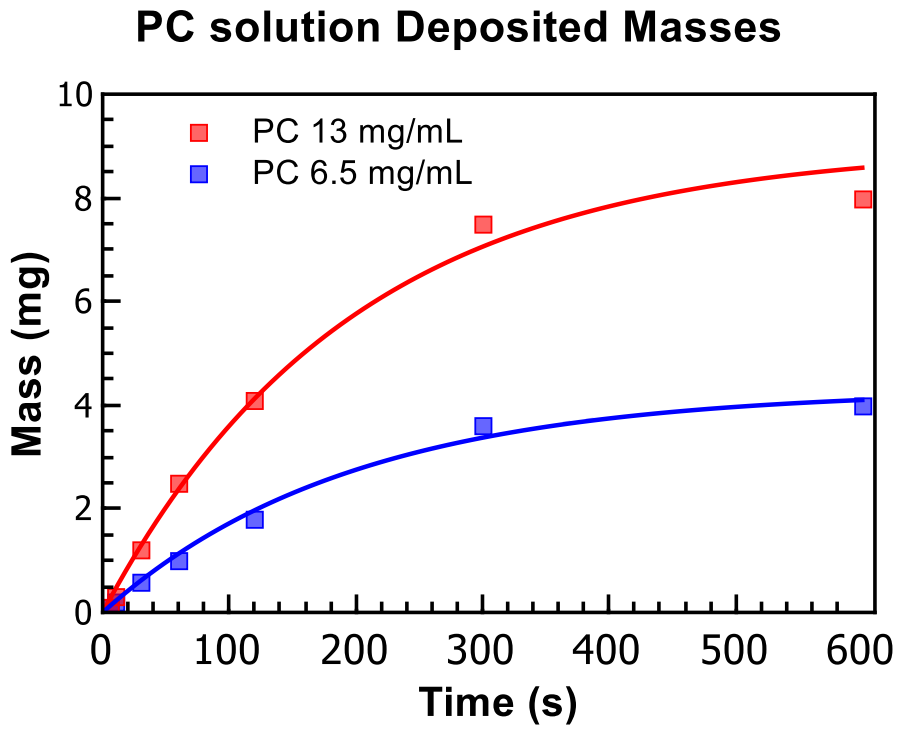

Figure 5.2.8: *kinetics of the EPD process under an applied potential of 5 V for both concentrated and diluted suspensions of $Ti_3C_2T_x$ in PC. Mass deposited after vacuum annealing at 160 °C for 12 h is plotted against the time allowed for deposition, along with the suggested fitting model.*

Hence, while the general PC solution behavior was similar to what experienced in the aqueous environment, things are different when it comes to process modelling: red line and blue line in **Figure 5.2.8** represent the fitting calculated for concentrated and diluted PC solutions, respectively. Sarkar *et al.* [56] studies were adopted to describe the process kinetics following the same discussion proposed for EPD from water suspensions: the curves were therefore shaped with an exponential model tending towards the maximum possible value of mass deposition, but when the adjustment necessary to account for the effect of constant voltage conditions (see § 5.1.3) was introduced the curves systematically underestimated the experimental points. Going back to the original model suggested for constant current depositions, however, produced an excellent agreement between theory and practice, introducing an issue in the quality of the theory that will be addressed and apparently solved in § 6.1, where a more deep scientific interpretation of these phenomena is provided.

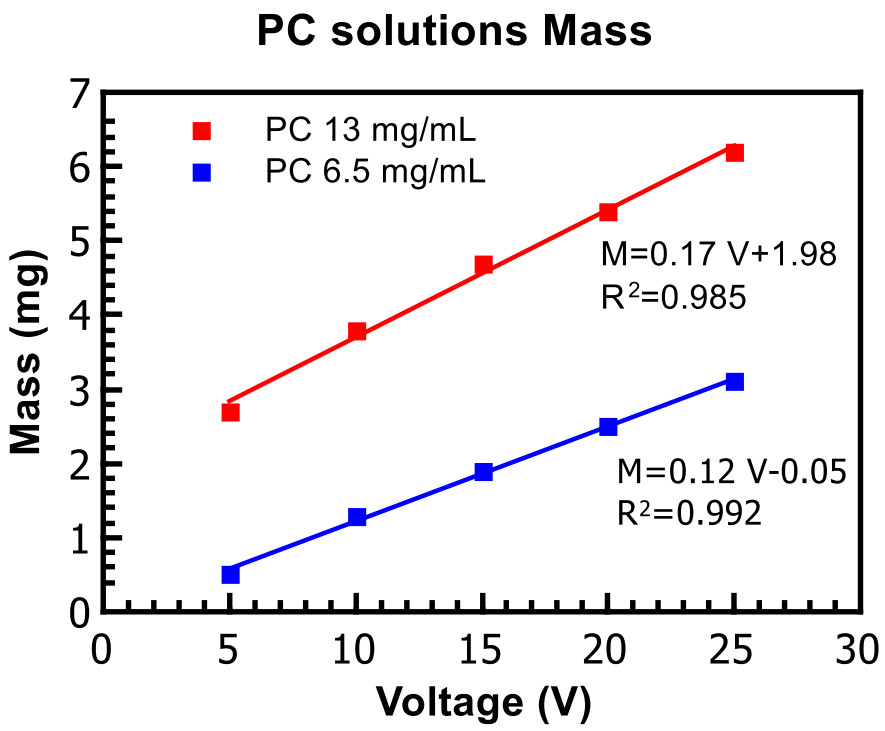

Figure 5.2.9: *Deposited mass (after vacuum annealing at 160 °C for 12 h) as a function of voltage, obtained setting a fixed process time of 30 s and exploring the 5-25 V range for both concentrated and diluted suspensions of $Ti_3C_2T_x$ in PC.*

As discussed above, PC solution permitted the investigation of film production for a constant time and different voltages, studying the process behavior in terms of applied potential and not of increasing time. **Figure 5.2.9** shows the masses after 12 h of vacuum annealing at 160 °C of films fabricated via EPD for 30 s sweeping the 5-25 V range with a step size of 5 V (i.e. 5, 10, 15, 20, 25 V) from concentrated and diluted PC solutions.

According to Hamaker's law [82] experimental points were expected to vary linearly with potential and this prediction remarkably matches to the collected results. Data relative to the concentrated and diluted solutions are represented in red and blue, respectively, along with two interpolating lines. Note that those lines are not a fitting obtained from the Hamaker equations but simply a fitting obtained by linear regression; nonetheless this kind of analysis is still very informative and allows to estimate values of deposited mass at voltages different from what tested (at least as long as they fall in the 5-25 V range) with a certain confidence, providing an interesting tool to tune the film fabrication. Two considerations are worth reporting, one of processing and applicative interest and the other highlighting an unexplained aspect. As for the first, it has to be noted that the R squared value is so close to one that the points are approximately placed along a line. As for the second, instead, the slopes of the two curves are very close, producing two parallel lines, where the red one is clearly intercepting the y axis at some point different than zero; considering that experimental points are supposed to follow Hamaker's law this result is unreasonable and so it is from a qualitative point of view, since, given a null potential, deposited mass it supposed to be negligible as well; nevertheless, to date this behavior is unexplained and more work is required to clarify what observed.

5.2.4 Film thickness

Following the same discussion structure offered to describe EPD results from water solution the present PC section ends with a review of the main observations regarding film thickness. Thickness of a deposit represents a fundamental PED parameter, not only because in can provide kinetics insight but also because often times it can be even more meaningful than deposited mass in terms of process control. Nevertheless, as already noted, this variable is highly sensitive to external factor such as gravity and inhomogeneity in the electric field, among others. The first cited cause of variability produced in the vertical cross-section of the samples a gradient, with thicknesses clearly lower on top and progressively increasing until a maximum value towards the bottom. It is hence evident that an incontrovertible thickness characterization was impossible and, despite all the efforts made, some error was introduced from the beginning by the measurement practice. As with what discussed for aqueous solutions two different techniques were adopted to carry out the measurements, choosing the one more appropriate for the specific sample, namely optical profilometry when films were still adhering to the substrate and SEM cross-section imaging whenever deposits were freestanding after drying. In order to minimize the effect of the aforementioned thickness gradient all the samples were analyzed at half of their height.

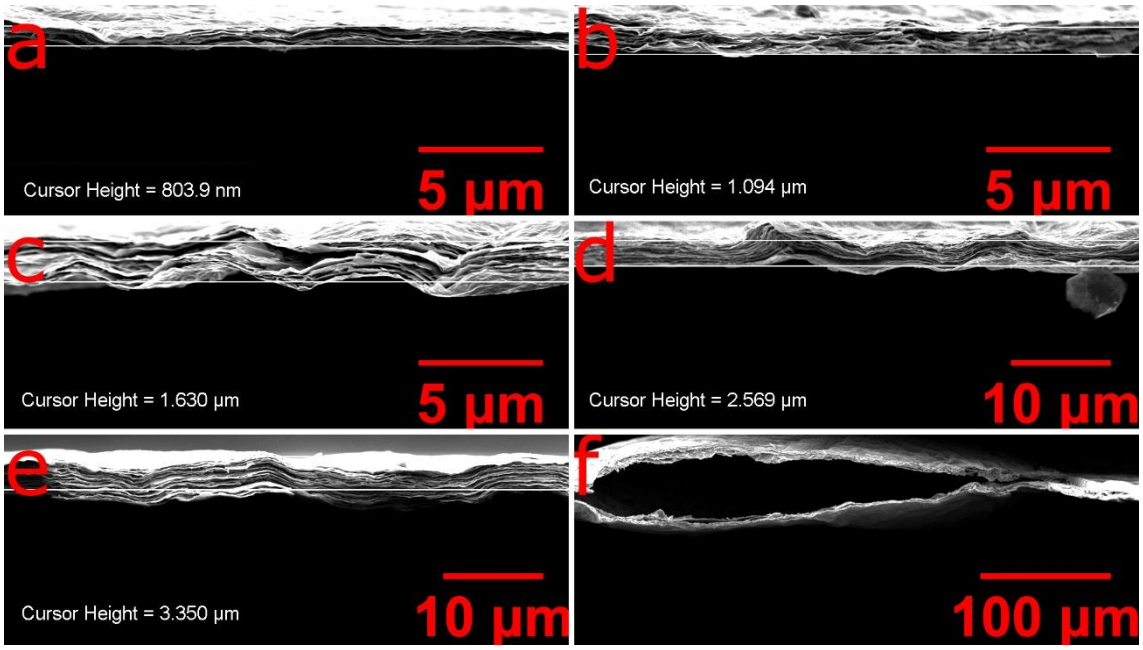

Figure 5.2.10: *example of thickness measurements conducted on deposited films produced from concentrated suspension of $Ti_3C_2T_x$ in PC at 5 V for 5, 10, 30 60, 120 and 300 s showed in a, b, c, d, e, and f respectively. Images where obtained via SEM, with the following instrument parameters: EHT 5 kV, working distance 3 mm and magnification 5K for a, b and c, decreased at 2K for d, e and at 0.2K in f.*

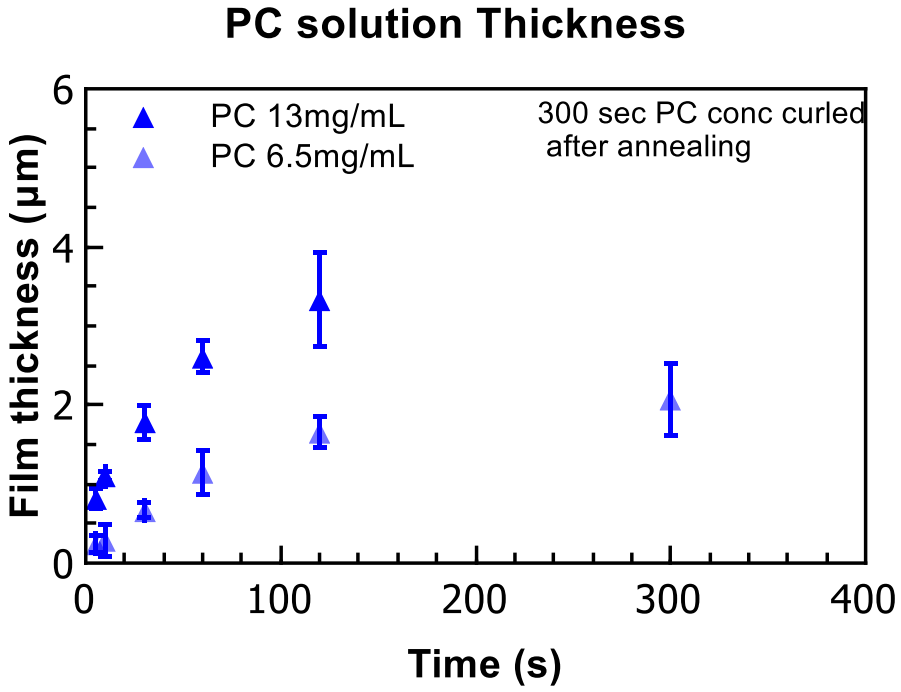

Figure 5.2.11: *film thickness after vacuum annealing at 160 °C for 12 h as a function of deposition time under an applied potential of 5 V for both concentrated and diluted suspensions of $Ti_3C_2T_x$ in PC.*

Figure 5.2.10 provides an example of thicknesses measured via SEM cross-section analysis on films fabricated from the concentrated PC solution in the systematic study with an applied potential of 5 V and different time intervals. Confirming what shown by SEM top views in **Figure 5.2.5**, $Ti_3C_2T_x$ flakes appear tightly stacked with their planes parallel to each other, forming structure comparable with the MXene paper produced by vacuum filtration. Interestingly, all but the 300 s samples exhibit a non-fully flat structure, with some waves and bulges interrupting their linearity: at this point it is not clear whether this is due to the EPD process or to the subsequent annealing step, yet it is not a major concern as film characteristics did not seem to be significantly negatively affected. Certainly caused by the heating treatments post-deposition, however, is the cavity cross-section shown in **Figure 5.2.10**f: after collecting in from the vacuum furnace, the film appeared curled and sprinkled of small bubbles trapped in the material; clearly such a morphology fully compromised the film quality impeding further studies. Therefore, from what discussed it could be inferred that PC solutions set a limitation in maximum thickness achievable, this representing a significant technological setback.

Nevertheless, such disadvantage wasn't confirmed by the thickness analysis carried out on samples obtained from concentrated and diluted PC solutions via EPD for 30 s at 5, 10, 15, 20 and 25 V and subsequent vacuum annealing at 160 °C for 12 h (namely the same films discussed in the previous kinetics dissertation). Analogously to what observed in **Figure 5.2.9** for the deposited mass, such films showed a linear trend in measured thicknesses with changing voltages, supporting the kinetics discussion, based on Hamsker's law introduced above. In red and blue the linear regression for concentrated and diluted PC solutions are shown, respectively: in this case the interpolation results more logical with respect to the corresponding analysis regarding mass, as both the line projections seems to intercept the thickness vs voltage plot origin, according to Hamaker's prediction and common sense.
Before moving to the SEM images regarding these samples, a last comment might be of interest: increasing the voltage, thickness grows and this is perfectly understandable since, as discussed in the present work as well, there should be a linear correlation between deposited mass and obtained thickness, being the areal density the link between the two variables. Nonetheless, a second factor might deeply influence this aspect because higher potential difference between the electrodes speeds up particle motion and allows for a shorter time to achieve an optimally arranged structure, resulting in a lower packing density of as-deposited film. Two different equations were suggested to describe the particle velocity when they collide with the electrode, the first by Stokes [83] and the second by Chen *et al.*:[84]

$$v_t = \frac{\varepsilon \xi E}{4\pi\eta} \quad (21)$$

$$v_t = \frac{zeE}{6\pi\eta r} \quad (22)$$

Where v_t is the particles terminal velocity, ε is the dielectric constant of the liquid, ξ is the surface charge density of the particle in the solvent, E is the electric field, η is the solvent viscosity, z is the charge of the particle, e is the elementary charge and r is the particle radius. In any case it is evident that keeping the system parameters constant (and this happens given that one is working with the same solution) as well as the deposition time, the particle speed, and hence the morphology and thickness can be controlled by the applied potential through the electric field.

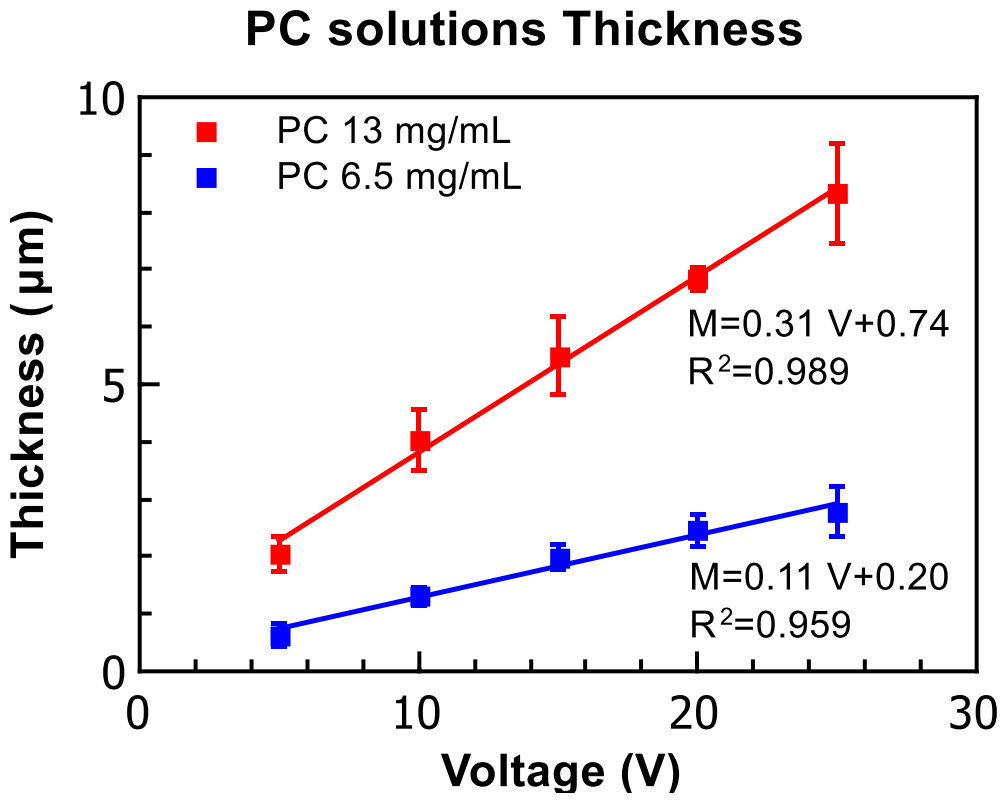

Figure 5.2.12: *film thickness (after vacuum annealing at 160 °C for 12 h) as a function of voltage, obtained setting a fixed process time of 30 s and exploring the 5-25 V range for both concentrated and diluted suspensions of $Ti_3C_2T_x$ in PC.*

Figure 5.2.13 provides an example of thicknesses measured via SEM cross-section analysis on films fabricated from the concentrated PC solution in the systematic study with changing applied potentials and 30 s of deposition time. Following the highlighted trend throughout all this work, the flakes appear tightly stacked with their planes parallel

to each other. Such feature is shared with samples produced at 5 V from PC solutions and in this case as well films exhibit a non-fully flat structure, with some waves and bulges interrupting the linearity: again, to date the origin of such inhomogeneity is unclear and the only hypothesis refers to the annealing step, which might release some vapors from the film inner and cause its kinking. However, the good news is, that the material characteristics don't seem to be significantly negatively affected as shown in the following chapter.

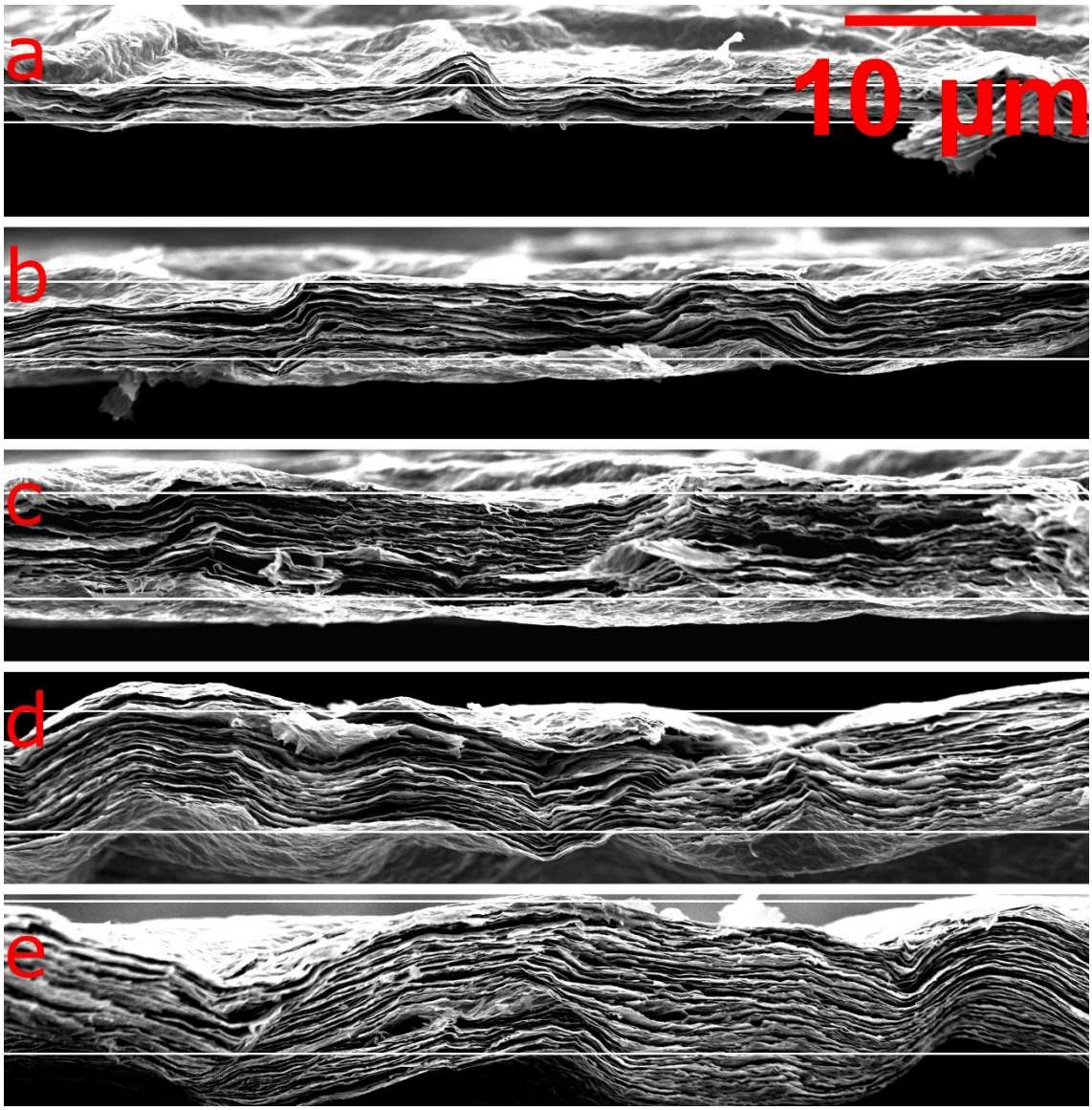

Figure 5.2.13: *example of thickness measurements conducted on deposited films produced from concentrated suspension of $Ti_3C_2T_x$ in PC applying for a fixed time of 30 s 5, 10, 15, 20 and 25 V showed in a, b, c, d, and e respectively. Images where obtained via SEM, with the following instrument parameters: EHT 5 kV, working distance 3 mm and magnification 2K for all the 5 films.*

Chapter 6

Overall film comparison

This chapter is devoted to illustrate a detailed analysis for EPD kinetics relative to both water and PC solution as well as a more comprehensive films thicknesses comparison and discussion. Afterwards, film characterization carried out via EDS and some insight into the material composition and possible effect of applied voltages are provided. Finally, given the wide range of functional applications in which MXene can find room, a couple of material performances are tested and results regarding specific capacity as working electrode in a supercapacitive cell and film resistivity are presented, paving the way for further and deeper investigations.

6.1 EPD from water and PC: kinetics comparison

Considering the diverse benefits shown by MXene EPD, understanding the kinetics phenomena in terms of deposition rate (and subsequently thickness) is theoretically and technologically a crucial requirement for films manipulation from the processing point of view.

Here some topics regarding kinetics of EDP will be recalled and many more details about the physical fundamentals of the mechanism are discussed. To summarize, the kinetics of constant-voltage deposition at 5 V were studied for both aqueous and PC suspensions by measuring the mass of dried films after annealing (see Chapter 5 for more information) as a function of deposition time and suspension concentration. For aqueous solutions, sufficiently long depositions caused the process to come asymptotically to a halt, as shown in **Figure 6.1.1** with red squares. The same figure also demonstrates deposition yield for concentrated suspensions compared to half-diluted suspensions, under nominally identical deposition conditions. Interestingly, even after the longest deposition times, the suspension was not fully depleted of $Ti_3C_2T_x$. An identical study was performed on two PC suspensions (see **Figure 6.1.1**, blue triangles) produced in order to achieve the same concentrations discussed above for the water ones: keeping the deposition conditions constant, the mass yield with time showed a similar behavior to what observed

for the aqueous system, even though, the key difference was that the MXene was visibly depleted from the PC suspension by the end of 600 s and even earlier.

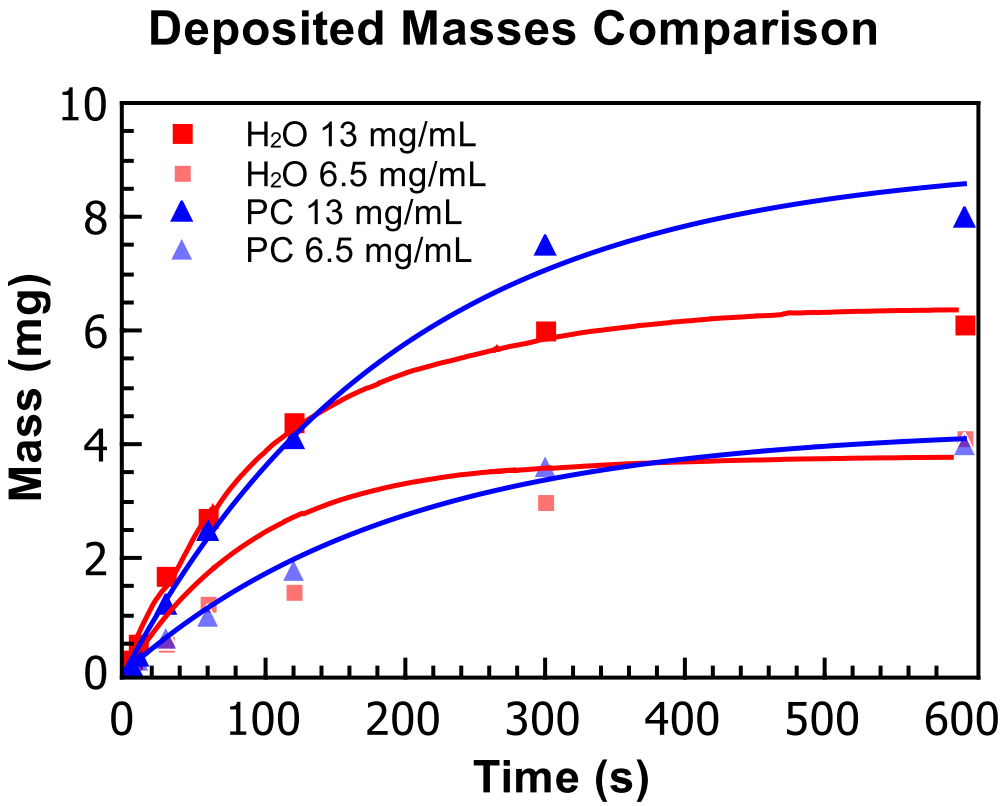

Figure 6.1.1: *kinetics overview of the EPD process under an applied potential of 5 V for both concentrated and diluted suspensions of $Ti_3C_2T_x$ in water and PC.*

As anticipated in the respective sections of Chapter 5 both for water and PC, deposition kinetics are often modelled using Hamaker's equation, *viz.*:[85]

$$w(t) = f\mu CAEt \qquad (23)$$

where w is the mass in mg, f is the efficiency of the process ($f \leq 1$), μ is the electrophoretic mobility, E is the electric field, A is the electrode surface area, C is the particle mass concentration, and t is the deposition time.[37,86] In the limit of short deposition times, C and E are approximately constant, which leads to a linear dependence of w on t. however, for longer deposition times, under constant-current conditions, systems deviate from this linearity due to the rapid decay in suspended particles concentration. Thus, the following equations were suggested to describe the kinetics:[37]

$$w(t) = w_o(1 - e^{-kt}) \qquad \textbf{(24)}$$

$$k = Afu/V \qquad \textbf{(25)}$$

where w_0 is the total available dispersed mass in suspension, u is the average velocity of the particles and V is the used volume of suspension.

Nonetheless, in a constant-voltage deposition process it is necessary to find a value of k which accounts for the current decrease due to the resistance of the forming deposit when the solution resistance is remarkably lower than the deposit is one, as usually happens if rather resistive ceramic nanoparticles are used. Accordingly to previous studies,[37] Equation **(24)** was adjusted by multiplying the exponential argument by a factor I_N which is a normalized value of the current – defined as $I(t)/I_{max}$ and determined from Figure 5.1.1 and Figure 5.2.1- measured throughout the process. Thanks to this correction and assuming $f = 1$, it was possible to fit with good approximation all the experimental weights collected from diluted and concentrated water suspensions, as shown by the solid curves in **Figure 5.1.6**.

This model was checked against the alternative conditions of constant current, as shown in **Figure 5.1.7**. Using a 6.5 mg/mL water suspension, the constant current experiment corroborated the selected model since Equation **(24)** gave good agreement with the measured masses as a function of time. Therefore, for a water solution such a simple theory was consistent with the experimental observations, providing an exponential trend for deposited mass under constant current conditions, which could be modulated through measured current in case of constant voltage set-up to take into account the electric field shielding caused by the growing deposit.

Nonetheless, what just discussed for water did not succeed in fitting the kinetics of deposition from PC suspensions under constant voltage conditions. As a matter of fact, the model obtained introducing the I_N factor to account for the growing film resistance produced curves that extremely underestimated the deposit weight for all times. This forced to try a new route capable of increasing the predicted values and a first alternative was easily explored by neglecting the electric field decrease across the film thickness and assuming constant current conditions, i.e. employing Equation **(24)** without further corrections. Despite the apparently poor physical foundation of this initial assumption, this second trial worked well and the agreement between predicted behavior and real measurements was quite good (**Figure 5.2.8**). Here, a possible explanation to this unexpected behavior is suggested thanks to the equations proposed by O. Van der Biest *et al.*,[87] where a description of the EPD process resistance was discussed in terms of an equivalent electric circuit generated by different contributions. When a deposit is growing

from particles suspended in a colloidal solution, the overall resistance can be described dividing the system in two regions, suspension and film, ideally connected in series, each one characterized by a parallel combinations of resistances generated by the mutual effect of solid particles and liquid solvent. For the suspension, they supposed the current is due to the flows of both individual ions present in the liquid and powder particles surrounded by their ion cloud, so that the resistance characterizing these two phenomena can be described as follows:

$$R_{l,sus} = \rho_{l,sus}\left(\frac{L-d}{A}\right) \qquad (26)$$

$$R_{p,sus} = \left(\frac{L-d}{\mu A C Q_{eff}}\right) \qquad (27)$$

Where $R_{l,sus}$ and $R_{p,sus}$ are the resistance of the liquid phase in the suspension and of the charged particles in the suspension, respectively, L and A are the electrode distance and surface area, d is the deposit thickness $\rho_{l,sus}$ is the resistivity of the liquid phase in the suspension, μ is the electrophoretic mobility of charged particles and Q_{eff} is the effective charge on the particle surface.

Similarly, the same study explored the growing film resistance behavior, pinpointing that a deposit is constituted by a powder matrix, with a packing fraction p, completely soaked in an interconnected liquid phase, where the individual resistance behavior can be calculated as follows:

$$R_{l,dep} = \frac{d}{\sigma_{l,dep} \cdot (1-p) \cdot A} \qquad (28)$$

$$R_{p,dep} = \frac{d}{\sigma_{p,dep} \cdot p \cdot A} \qquad (29)$$

Where $R_{l,dep}$ and $R_{p,dep}$ are the resistance of the interparticle liquid and of the powder bed, respectively, $\sigma_{l,dep}$ is the specific conductivity of the liquid phase (likely lower than the one measured for the suspension, since the particles are supposed to release their clouds of counterions when approaching the electrode) and $\sigma_{p,dep}$ is the specific conductivity of the powder forming the deposit.

These equations (from **(26)** to **(29)**), combined with the well-known result for the equivalent resistance of several resistances summed in parallel (namely the inverse of the individual reciprocal resistances summation) provided a tool to inspect what happens when water and PC solutions are compared in terms of EPD kinetics. As said before, Equation **(24)** is only valid if suspension and deposit resistances are comparable, while a correction is needed when the former shows to be significantly more conductive than the latter. Assuming that in the part of the EPD equivalent circuit relative to the deposit the resistance is essentially due to the powder characteristics and the liquid phase is negligible, given its relatively small amount and higher resistance, it is fair to speculate that here the resistances are comparable both in the water and PC systems.

However, things are different in the suspension component of the equivalent circuit, where not only water is more likely to be more conductive than PC, thanks to the relative ease with which electrolytes dissociates in aqueous environment, but also for the particle contribution, since mobility in water is approximately three times higher than what observed for PC. Combining these two observations it is evident that water suspension should have a lower resistance with respect to the PC one. Therefore, from a comparison of the two possible systems, it is now clear that the deposit growth influences more the total resistance during EDP of water rather than of PC, as in the latter case solution and film resistances are closer and the electric field drop across the deposit might be considered negligible. In light of that, the modeling of PC solution behavior using directly Equation **(24)** even under constant voltage conditions is explained, as well as the need to introduce the I_N factor for water, due to the heavier contribution of the film resistance on the overall system electrical characteristics for the latter.

To shed even more light on what described so far, it is meaningful to take into account the electrolysis effects occurring in the aqueous solution: outgassing observed during the deposition proved how part of the current was drained by a parasitic process and concomitantly suggested that the continuous outgassing (increasing with the amount of material) in the deposit contributed to local erosion of the film, pushing particles back to the suspension and requiring a further current depletion. Under constant voltage conditions the back flow of material, might have worked as a growing-with-time-resistance which provoked a time-drop in potential available for effective EPD, whereas the total absence of any turbulence for PC suspension made unnecessary to account for a growing in the resistance of the system from this point of view as well**.** Furthermore, what discussed in the present paragraph is considered to be the reason why even for the longest deposition times, the suspension was not fully depleted of $Ti_3C_2T_x$ in aqueous solution, in contrast to what observed for PC. Bubbles movements did not allow all the material to build the deposit and after a first stage when the particles where effectively migrating and growing the film despite the turbulences introduced by electrolysis, a time must have

come when the solid motion due to electrophoresis was compensate by powder sent backwards by outgassing, hence establishing a dynamic equilibrium condition which couldn't be overcome.
All what discussed is in good agreement with the kinetic comparison between water and PC suspensions provided in **Figure 6.1.1**: in both concentrated and diluted cases, water shows in the first stage a higher deposited mass than what observed for PC solution, and, for concentrated suspensions only after a given time the latter provides higher yields proving to be the best choice when looking for total depletion of solution's particles and maximum thickness. This behavior can be well explained considering the above discussion, since, in water, particles have a greater electrophoretic mobility than in PC and it is understood that, once a potential is applied, the deposition rate is higher. Nonetheless, with growing of the deposit, active sites for water electrolysis multiply and gas evolution increases generating a parasitic process that works against EPD and slows down its rate. Not surprisingly, therefore, the phenomenon is evident only for concentrated solutions, whereas working in diluted conditions produced a smaller deposit and hence the outgassing was less influent, so that total deposited mass for water and PC are comparable- as it should be, given that the particle loads of the two suspensions were comparable.

As stated in Chapter 5, often times the most critical EPD parameter is thickness produced on the substrate and the possibility of fabricating either self-standing films or well-adherent coatings. Being all the considerations proposed previously still valid (especially the ones about non-stirred EPD), it is worth adding here a few details and a comparison regarding samples obtained from water and PC-based suspensions.
Figure 6.1.2 is the "thickness counterpart" of **Figure 6.1.1** and therefore experimental points collected halfway between the top end the bottom of all samples are depicted for water and PC solutions considered in their two concentrations levels. As with mass, thickness appear to grow more quickly for water suspensions in the initial stage, but this does not surprise, all the more so considering the worst packing efficiency induced by a higher particle speed (that occurs for water owing to the higher particle mobility).

Finally, some quantitative insight into thickness increase can be found recalling Sarkar's equation and adjusting it in order to switch from mass to *h*, i.e, the deposit cross-section even for the case of non-stirred systems, as described by Maca *et al.*:[88]

$$h = \frac{100 w_0}{A \rho_{theo} \rho_{rel}} \left(1 - e^{-(\mu E/L)(H - x/v_s)}\right) \qquad (30)$$

Where w_0 is the total available dispersed mass in suspension, A the electrode surface area, ρ_{theo} the theoretical ceramics density, ρ_{rel} the relative deposit density after deposition, μ the particle mobility, E the electric field, L the distance between the electrodes, H the initial height of suspension level, x the vertical distance from the bottom of the electrophoretic cell and $v_s$sedimentation velocity.

Nevertheless, the model hasn't been tested on the collected data because of the aforementioned variability in the measurements carried out and the equation is given only for the sake of completeness.

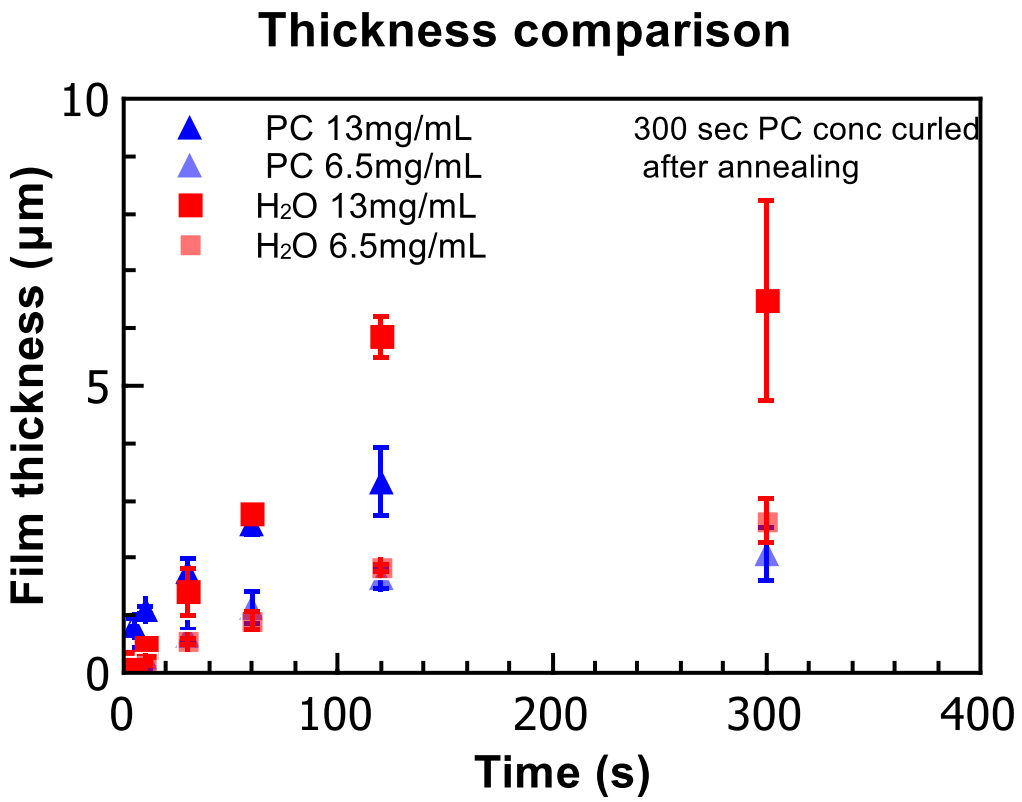

Figure 6.1.2: *film thickness overview as a function of deposition time under an applied potential of 5 V for both concentrated and diluted suspensions of $Ti_3C_2T_x$ in water and PC.*

6.2 EDS Analysis

To shed more light on the relative chemical compositions of films made by different methods, EDS was conducted on air-dried Ti_3C_2 films made by EPD and vacuum filtration from both suspensions. As illustrated in **Table 6.2.1**, water-based films showed a 3.0:2.2 molar ratio of Ti:C, which is close to the ideal ratio of 3:2, and very similar values of O, F, and Cl. These results suggest that the EPD process largely did not influence the chemical composition of the water-EPD films. On the other hand, the relative C content in the PC-based films after vacuum annealing at 160 °C is well above

that of the water-processed films. The O content also is highest for PC-based films produced at 20 and 25 V. While the higher C and O contents in PC-based films is consistent with residual PC in the films, it is unlikely that much PC would remain after vacuum annealing at 160 °C, given that 35-45 % wt. loss typically occurred. Moreover, ATR measurements on the films (not shown) gave no signs of absorption peaks associated with PC. On the other hand, the high voltages used for PC depositions could have led to electrochemical decomposition of PC, which has been reported to occur starting at 3 V in Li-containing PC solutions and above 5.6 V in pure PC.[81,89] The broad plateau in the current vs. time plot for 20 V PC deposition discussed in § 5.2.1 and the higher O content for this film also seem to support this reasoning. Finally, it should be noted that Cl is probably present as a surface termination.[90] More work is required to understand the reasons for the unexpected Ti/C ratio in the PC films.

Sample	Ti	C	O	F	Cl
VF (water)	3.0	2.2	0.7	1.2	0.4
EPD (5 V water)	3.0	2.2	0.7	1.0	0.2
VF (PC)	3.0	3.3	0.8	1.4	0.4
EPD (5 V, PC)	3.0	3.1	0.8	1.0	0.4
EPD (10 V, PC)	3.0	2.9	0.8	1.4	0.4
EPD (15 V, PC)	3.0	2.8	0.7	0.8	0.4
EPD (20 V, PC)	3.0	3.4	1.0	1.3	0.4
EPD (25 V, PC)	3.0	3.7	1.4	1.3	0.4

Table 6.2.1: *EDS results of relative elemental compositions, normalized per 3 Ti, of air-dried H_2O films and PC films vacuum annealed at 160 °C.*

6.3 Film resistivity and Electrochemical tests

Two examples of technological applications were investigated testing the performances of free-standing films measuring either their conductivity or their performances as electrode active material for electrochemical capacitors (Supercapacitors).

Electrical resistivity of the $Ti_3C_2T_x$ films made by EPD were investigated by four-point DC measurements and the results were compared to values reported for vacuum-filtered films. Films made by EPD at 5 V from aqueous suspensions had an electrical resistivity of 135 ± 10 μΩ-cm, or a conductivity of 7400 S/cm, whereas those made by EPD from PC suspensions at 5 V and 25 V showed resistivities of 128 ± 23 μΩ-cm and 176 ± 19 μΩ-cm, respectively. These resistivities are among the lowest reported for $Ti_3C_2T_x$ and slightly lower than those reported for highly-oriented spin-coated films,[23] epitaxial thin

films,[22] single-flake,[91] and other types of $Ti_3C_2T_x$ films,[92] as summarized in **Table 6.3.1**. This proves that EPD is a high-throughput and efficient method to make highly conductive $Ti_3C_2T_x$ films.

$Ti_3C_2T_x$ Sample Type	**Electrical Resistivity (μΩ·cm)**	**Reference**
EPD film (5 V, water)	135 ± 10	This work
EPD (5 V, PC)	128 ± 23	This work
EPD (25 V, PC)	176 ± 19	This work
Spin-coated film	154 ± 7 323	[23] [32]
Epitaxial thin film	176 ± 2	[22]
Single $Ti_3C_2T_x$ flake	204 ± 44	[91]
Electrosprayed film	340	[34]
Vacuum Filtered	220 ± 10	[92]

Table 6.3.1: *summary of electrical resistivities obtained for $Ti_3C_2T_x$ films in this work compared to the best values reported in literature for this material.*

As well-recognized, $Ti_3C_2T_x$ MXene stands out for its high capacitance (up to 246 F/g, or 910 F/cm^3) in sulfuric acid electrolyte[19,93] due to a pseudocapacitive charge storage mechanism.[94,95] Considering this, the electrochemical properties of the fabricated $Ti_3C_2T_x$ films were investigated by using the films directly as electrodes for electrochemical capacitors tested in 1 M H_2SO_4. **Figure 6.3.1**a-c show the electrode mass-normalized cyclic voltammograms of 2-3 μm-thick (0.8 - 1.2 mg/cm^2) electrodes produced by vacuum filtration, EPD from aqueous suspension, and EPD from a PC suspension. The most notable feature in all sets of CVs are the strong dependence of the anodic peak potentials on scan rate. The peak anodic potential increases from -0.80 to -0.61 V vs. Hg/Hg_2SO_4 for both water-based films, but shifts to more positive range of -0.80 to -0.52 V vs. Hg/Hg_2SO_4 for the PC EPD film. **Figure 6.3.1**d shows that the gravimetric capacitance values of vacuum-filtered water films, EPD water films, and EPD PC films are quite similar at all scan rates. Interestingly, the EPD PC film has the highest capacitance at 2 mV/s but declines the most quickly with increasing scan rates, whereas the two water-based films show nearly identical trends with scan rate. At 241 and 254 F/g, respectively, the capacitance values of water EPD and PC EPD films at 2 mV/s is nearly identical to that of a 5 um-thick roll-cast $Ti_3C_2T_x$ electrode (i.e. 246 F/g).[19] **Table 6.3.2** summarizes the volumetric capacitances of all three films tested herein.

Galvanostatic charge-discharge testing at a current density of 10 A/g was also conducted on the water and PC-based EPD films. The non-triangular shapes of the voltage vs. time

profiles, shown in the insets of **Figure 6.3.1**e-f, are consistent with the pseudocapacitive nature of the charge storage mechanism suggested by the corresponding CV's and previous work on $Ti_3C_2T_x$. At least 100 % capacitance retention is observed after 10,000 charge-discharge cycles for both EPD films (**Figure 6.3.1**e-f). We speculate that the PC EPD films' larger c-LPs, surface structure differences, and chemical composition differences compared to aqueous films could each contribute differently in the charge storage of the two EPD films, and future studies will help to clarify their relative roles.

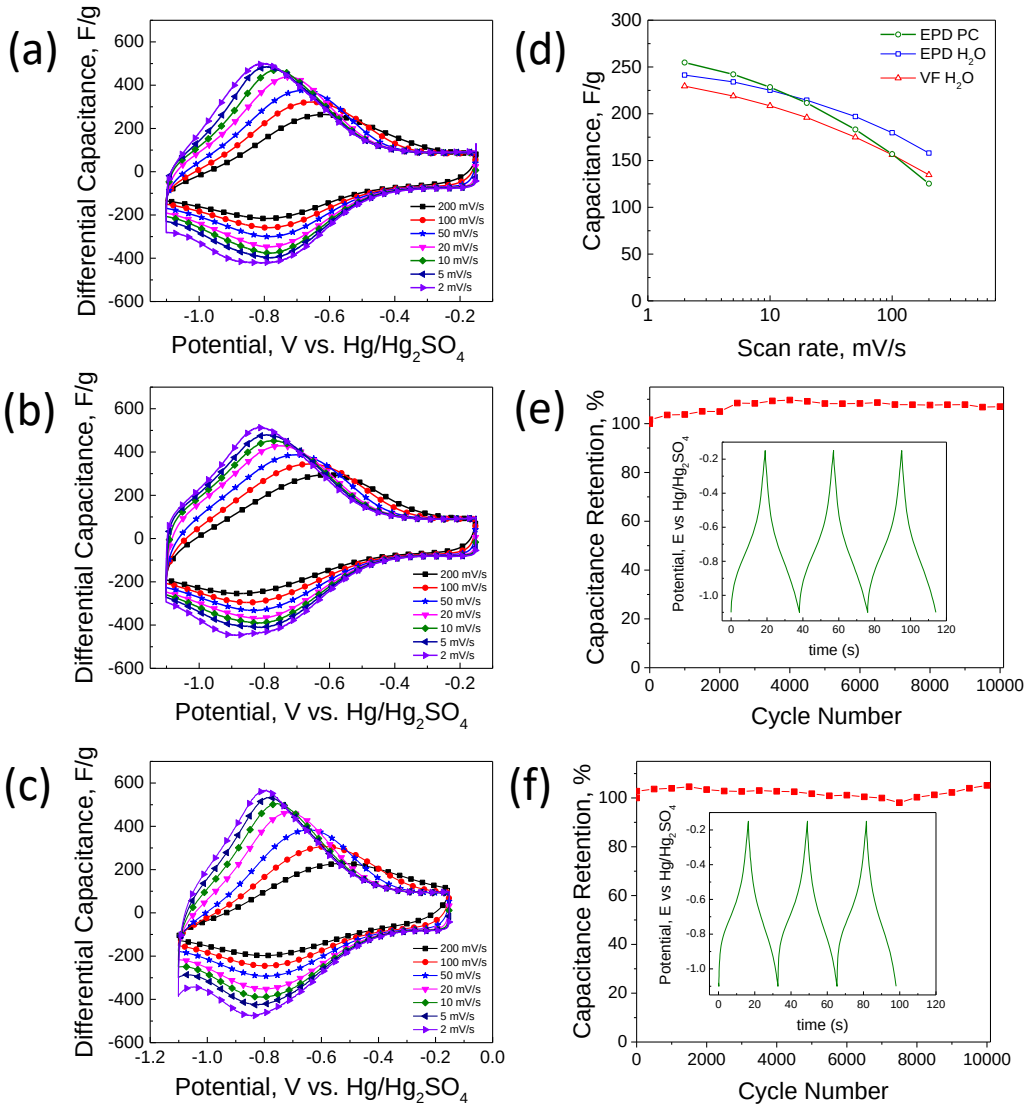

Figure 6.3.1: *performance of 3-um thick $Ti_3C_2T_x$ films as supercapacitor electrodes in 1 M H_2SO_4 (a-c) Cyclic voltammograms of VF H_2O, EPD H_2O, and EPD PC, respectively, (d) scan rate dependent capacitance, (e-f) galvanostatic charge-discharge tests conducted at 10 A/g for EPD H_2O and EPD PC films, respectively.*

	VF-H_2O (3.5 ± 0.2 g/cm^3)		**EPD-H_2O (3.7 ± 0.1 g/cm^3)**		**EPD-PC (4.1 ± 0.5 g/cm^3)**	
Scan Rate (mV/s)	**F/g**	**F/cm^3**	**F/g**	**F/cm^3**	**F/g**	F/cm^3
200	134	471 ± 26	158	584 ± 15	125	513 ± 62
100	156	546 ± 31	179	664 ± 17	156	643 ± 78
50	174	612 ± 34	197	729 ± 19	183	750 ± 91
20	196	686 ± 39	214	793 ± 21	211	867 ± 105
10	208	729 ± 41	225	833 ± 22	228	936 ± 114
5	218	766 ± 43	234	865 ± 23	242	992 ± 121
2	229	803 ± 45	241	893 ± 24	254	1044 ± 127

Table 6.3.2: *gravimetric and volumetric capacitances of $Ti_3C_2T_x$ samples tested as electrodes in 1 M H_2SO_4 in three-electrode configuration. Errors in the volumetric capacitance values are associated with electrodes' thickness variation.*

Chapter 7

Summary and outlook

Currently, 2D materials are meeting increasing enthusiasm thanks to their outstanding and peculiar properties which renders them promising in several technologically advanced applications. Nonetheless their processability is currently an issue and despite many publications with this respect, more efforts are needed to improve final product quality and scale the production up to cost-effective processes.

The studies conducted in this work focused mainly on synthesis and optimization of 2D Ti3C2Tx (MXene) colloidal suspensions both in water and propylene carbonate and in their processing via electrophoretic deposition (EPD).

Initially the aim was to select the optimal working conditions to achieve the highest MXene concentration in both the solvents, since, as highlighted by the following EPD studies, achieving a high particle load proved to be critical for the process. The goal was accomplished trying different etching time and exploring several levels of retained humidity in the MXene sediment before starting the sonication treatment necessary to delaminate the exfoliated structure. As for water, concentrations up to 15 mg/mL were obtained by sonicating the material in distilled water right after the end of the washing process. On the other hand the most concentrated PC-based suspensions (up to 13 mg/mL) were obtained when the powders were poured in PC according to a ratio of 1 g of $Ti_3C_2T_x$ per 30 mL of solvent after retained water in the sediment was around 25 wt% of the MXene powder, assuming, grossly, an approximate mass conversion of 1:1 between Ti_3AlC_2 and $Ti_3C_2T_x$.

Both suspensions, including diluted versions, were tested for EPD and deposited films from 3 to 10 μm thick were produced successfully. The study mainly focused on constant voltage EPD in the range of 3 to 30 V and the relationships between applied voltage, deposition time and solvents' nature on morphology, orientation of flakes, and chemical compositions were discussed. The results differed depending on whether water or PC was used as suspending media: in the first case, not surprisingly, voltages higher than 5 V produced gas evolution, ascribable to water electrolysis, that lead to the formation of pores and less oriented structures; in PC, on the other hand, the overall film morphology appeared to be rather independent of the applied voltage. Such a distinct behavior could

be harnessed targeting different applications, as water solutions could be of use when high macroscopic surface area is required, whereas PC is to be preferred in those cases where homogeneity of the deposit and enhancing the deposition rate using higher voltages are more valuable features. The characterization was performed by SEM, EDS, and XRD. At the optimal voltage of 5 V the EPD kinetics was successfully modelled for both aqueous and non-aqueous solutions with concentrations of 13 and 6.5 mg/mL: this result was achieved thanks to the relationships suggested by Sarkar and Nicholson,[56] introducing a small adjustment to account for the distinct behavior shown by the two solvents.

Finally some of the as-synthesized films were tested to inspect their performances in two different possibilities of functional applications: film conductivity and gravimetric capacity. At 7400 S/cm, the free-standing $Ti_3C_2T_x$ deposited from aqueous suspensions delivered a remarkable electrical conductivity, matching the highest reported values for highly oriented $Ti_3C_2T_x$ made by spin coating. Furthermore, free-standing films showed gravimetric capacitances comparable to values already reported in literature when tested in 1 M H_2SO_4 as electrodes for electrochemical capacitors.

The present work has been a preliminary – albeit detailed – study for feasibility of MXene EPD ($Ti_3C_2T_x$ specifically, and further work is required to asses the method effectiveness on other MXenes), so it is not surprising that many possibilities of future developments are easy to be suggested and quite simple to explore. First, the experimental equipment could be modified in order to analyze the effect of different electrodes' spacings or to accommodate more solution and allow thicker deposits and kinetics inspection for longer times. Furthermore, as for PC solutions, higher voltages should be explored to test the solvent stability and a detailed constant current deposition study might be of interest. Also water solutions are rich of development hints, as the opened structure obtained at "high" voltages has to be tested in a supercapacitor yet and might disclose remarkable performances. Moreover, the possibility of working in a pressurized or de-pressurized EPD environment to control the electrolysis might be considered, given that the parasitic phenomenon provided an unexpected tool to tune the material microstructure. In addition, the film morphology could be tuned using a stirred system to get rid of the vertical thickness gradient and the understanding of transparent and semi-transparent coatings formation should be deepened as well. Finally, for both suspensions different depositing substrates have to be tested and especially grating – like a metallic mesh - might provide a way to open the interparticle spaces and boost the gravimetric capacitance.

Even without further developments, however, the EPD film production showed that the method is promising as an alternative and much more cost- and time-efficient way to process MXenes, due to the ease of scaling it up and to the shorter time required compared to the traditional vacuum filtering approach.

Chapter 8

List of references

1. Novoselov KS, Geim1 AK, Morozov S V., et al. Electric Field Effect in Atomically Thin Carbon Films. *Science (80-).* 2004;306:666-669.
2. Pacilé D, Meyer JC, Girit ÇÖ, Zettl A. The two-dimensional phase of boron nitride: Few-atomic-layer sheets and suspended membranes. *Appl Phys Lett*. 2008;92.
3. Coleman onathan N, Lotya M, O'Neill A, et al. Two-Dimensional Nanosheets Produced by Liquid Exfoliation of Layered Materials. *Science (80-).* 2011;331:568-571.
4. Jariwala D, Sangwan VK, Lauhon LJ, Marks TJ, Hersam MC. Emerging device applications for semiconducting two-dimensional transition metal dichalcogenides. *ACS Nano*. 2014;8.
5. Peng X, Peng L, Wu C, Xiea Y. Two dimensional nanomaterials for flexible supercapacitors. *Chem Soc Rev*. 2014;43:3303-3323.
6. Kim H, Abdala AA, Macosko CW. Graphene/Polymer Nanocomposites. *Macromolecules*. 2010;43:6515–30.
7. Scherson DA, Palencsár A. Batteries and Electrochemical Capacitors. 1827.
8. Naguib M, Kurtoglu M, Presser V, et al. Two-Dimensional Nanocrystals Produced by Exfoliation of Ti_3AlC_2. *Adv Mater*. 2011;23:4248–53.
9. Sun ZM. Progress in research and development on MAX phases: a family of layered ternary compounds. *Int Mater Rev*. 2011;56:143-166.
10. Naguib M, Mochalin VN, Barsoum MW, Gogotsi Y. 25th Anniversary Article: MXenes: A New Family of Two-Dimensional Materials. *Adv Mater*. 2014;26:992-1005.
11. Naguib M, Kurtoglu M, Presser V, et al. Two-dimensional nanocrystals produced by exfoliation of Ti3AlC2. *Adv Mater*. 2011;23(37):4248-4253. doi:10.1002/adma.201102306.
12. Naguib M, Mashtalir O, Carle J, et al. Two-dimensional transition metal carbides. *ACS Nano*. 2012;6(2):1322-1331. doi:10.1021/nn204153h.
13. Naguib M, Halim J, Lu J, et al. New Two-Dimensional Niobium and Vanadium Carbides as Promising Materials for Li-Ion Batteries. *J Am Chem Soc*. 2013;135(43):15966-15969. doi:10.1021/ja405735d.
14. Ghidiu M, Naguib M, Shi C, et al. Synthesis and characterization of two-dimensional Nb4C3 (MXene). *Chem Commun (Camb)*. 2014;50(67):9517-9520. doi:10.1039/c4cc03366c.
15. Anasori B, Xie Y, Beidaghi M, et al. Two-Dimensional, Ordered, Double Transition Metals Carbides (MXenes) SI. *ACS Nano*. 2015;9(10):9507-9516. doi:10.1021/acsnano.5b03591.
16. Yang J, Naguib M, Ghidiu M, et al. Two-Dimensional Nb-Based M4C3 Solid Solutions (MXenes). Zhou Y, ed. *J Am Ceram Soc*. 2016;99(2):660-666. doi:10.1111/jace.13922.
17. Zhou J, Zha X, Chen FY, et al. A Two-Dimensional Zirconium Carbide by Selective Etching of Al3C3 from Nanolaminated Zr3Al3C5. *Angew Chemie*. 2016;128(16):5092-5097. doi:10.1002/ange.201510432.
18. Naguib M, Halim J, Lu J, et al. New two-dimensional niobium and vanadium

carbides as promising materials for Li-ion batteries. *J Am Chem Soc*. 2013;135(43):15966-15969. doi:10.1021/ja405735d.
19. Ghidiu M, Lukatskaya MR, Zhao M-Q, Gogotsi Y, Barsoum MW. Conductive two-dimensional titanium carbide "clay" with high volumetric capacitance. *Nature*. 2014;4(7529):1716. doi:10.1038/nature13970.
20. Wang X, Kajiyama S, Iinuma H, et al. Pseudocapacitance of MXene nanosheets for high-power sodium-ion hybrid capacitors. *Nat Commun*. 2015;6:6544. doi:10.1038/ncomms7544.
21. Liang X, Garsuch A, Nazar LF. Sulfur Cathodes Based on Conductive MXene Nanosheets for High- Performance Lithium – Sulfur Batteries. *Angew Chem Int Ed Engl*. 2015;54:1-6. doi:10.1002/anie.201410174.
22. Halim J, Lukatskaya MR, Cook KM, et al. Transparent Conductive Two-Dimensional Titanium Carbide Epitaxial Thin Films. *Chem Mater*. 2014;26(7):2374-2381.
23. Dillon AD, Ghidiu MJ, Krick AL, et al. Highly Conductive Optical Quality Solution-Processed Films of 2D Titanium Carbide. *Adv Funct Mater*. 2016;26(23):4162-4168. doi:10.1002/adfm.201600357.
24. Hantanasirisakul K, Zhao M-Q, Urbankowski P, et al. Fabrication of Ti3C2Tx MXene Transparent Thin Films with Tunable Optoelectronic Properties. *Adv Electron Mater*. 2016;2(6):1600050. doi:10.1002/aelm.201600050.
25. Ying Y, Liu Y, Wang X, et al. Two-dimensional titanium carbide for efficiently reductive removal of highly toxic chromium(VI) from water. *ACS Appl Mater Interfaces*. 2015;7(3):1795-1803. doi:10.1021/am5074722.
26. Wang L, Yuan L, Chen K, et al. Loading Actinides in Multilayered Structures for Nuclear Waste Treatment: The First Case Study of Uranium Capture with Vanadium Carbide MXene. *ACS Appl Mater Interfaces*. 2016;8(25):16396-16403. doi:10.1021/acsami.6b02989.
27. Ren CE, Hatzell KB, Alhabeb M, Ling Z, Mahmoud KA, Gogotsi Y. Charge- and Size-Selective Ion Sieving Through Ti3C2Tx MXene Membranes. *J Phys Chem Lett*. 2015;6(20):4026-4031. doi:10.1021/acs.jpclett.5b01895.
28. Han M, Yin X, Wu H, et al. Ti3C2 Mxenes with Modified Surface for High-performance Electromagnetic Absorption and Shielding in the X-Band. *ACS Appl Mater Interfaces*. 2016:acsami.6b06455. doi:10.1021/acsami.6b06455.
29. Yuchang Q, Wancheng Z, Fa L, Dongmei Z. Titanium carbide (MXene) nanosheets as promising microwave absorbers. *Ceram Int*. 2016. doi:10.1016/j.ceramint.2016.07.150.
30. Hong Ng VM, Huang H, Zhou K, et al. Recent progress in layered transition metal carbides and/or nitrides (MXenes) and their composites: synthesis and applications. *J Mater Chem A*. 2017;5(7):3039-3068. doi:10.1039/C6TA06772G.
31. Mashtalir O, Naguib M, Mochalin VN, et al. Intercalation and delamination of layered carbides and carbonitrides. *Nat Commun*. 2013;4:1716. doi:10.1038/ncomms2664.
32. Mariano M, Mashtalir olha, Antonio F, et al. Solution-processed Titanium Carbide MXene films examined as highly transparent conductors. *Nanoscale*. 2016:16371-16378. doi:10.1039/C6NR03682A.
33. Shah S, Habib T, Gao H, et al. Template-free 3D titanium carbide (Ti3C2Tx) MXene particles crumpled by capillary forces. *Chem Commun*. 2016. doi:10.1039/C6CC07733A.
34. Ali A, Belaidi A, Ali S, Helal MI. Transparent and conductive Ti3C2Tx (MXene) thin film fabrication by electrohydrodynamic atomization technique. *J Mater Sci Mater Electron*. 2016;27(5):5440-5445. doi:10.1007/s10854-016-4447-z.
35. Xu S, Wei G, Li J, et al. *Binder-Free Ti3C2Tx MXene Electrode Film for Supercapacitor Produced by Electrophoretic Deposition Method*.; 2017. doi:10.1016/j.cej.2017.02.144.
36. Pickard WF. Remarks on the Theory of Electrophoretic Deposition. *J Electrochem Soc*. 1968;115:105C-108C (1968).
37. Sarkar P, Nicholson PS. Electrophoretic Deposition (EPD): Mechanisms, Kinetics

and Application to Ceramics. *J Am Ceram Soc*. 1996;79(8):1987-2002. doi:10.1111/j.1151-2916.1996.tb08929.x.
38. Zhang Z, Huang Y, Jiang Z. Electrophoretic Deposition Forming of SiC-TZP Composites in a Nonaqueous Sol Media. *J Am Ceram Soc*. 1994;77:1946–1949. doi:10.1111/j.1151-2916.1994.tb07075.x.
39. Ferrari B, Moreno R. Zirconia Thick Films Deposited on Nickel by Aqueous Electrophoretic Deposition. *J Electrochem Soc*. 2000;147(8):2987. doi:10.1149/1.1393636.
40. Oakes L, Zulkifli D, Azmi H, et al. One Batch Exfoliation and Assembly of Two-Dimensional Transition Metal Dichalcogenide Nanosheets Using Electrophoretic Deposition. *J Electrochem Soc*. 2015;162(11):D3063-D3070. doi:10.1149/2.0181511jes.
41. Sugimoto W, Yokoshima K, Ohuchi K, Murakami Y, Takasu Y. Fabrication of Thin-Film, Flexible, and Transparent Electrodes Composed of Ruthenic Acid Nanosheets by Electrophoretic Deposition and Application to Electrochemical Capacitors. *J Electrochem Soc*. 2006;153(2):A255. doi:10.1149/1.2138570.
42. Sugimoto W, Terabayashi O, Murakami Y, Takasu Y. Electrophoretic deposition of negatively charged tetratitanate nanosheets and transformation into preferentially oriented TiO2(B) film. *J Mater Chem*. 2002;12(12):3814-3818. doi:10.1039/b204185e.
43. Diba M, Fam DWH, Boccaccini AR, Shaffer MSP. Electrophoretic deposition of graphene-related materials: A review of the fundamentals. *Prog Mater Sci*. 2016;82:83-117. doi:10.1016/j.pmatsci.2016.03.002.
44. Nam MS, Patil UM, Park B, Sim HB, Jun SC. A binder free synthesis of 1D PANI and 2D MoS2 nanostructured hybrid composite electrodes by Electrophoretic deposition (EPD) method for supercapacitor application. *RSC Adv*. 2016;6:101592-101601. doi:10.1039/C6RA16078F.
45. An SJ, Zhu Y, Lee SH, et al. Thin Film Fabrication and Simultaneous Anodic Reduction of Deposited Graphene Oxide Platelets by Electrophoretic Deposition. 2010:1259-1263. doi:10.1021/jz100080c.
46. Nowotny H. Strukturchemie Einiger Verbindungen der Ubergangsmetalle mit den elementen C, Si, Ge, Sn. *Prog Solid State Chem*. 1970;2:27–70.
47. Barsoum MW. *MAX Phases*. Wiley-VCH; 2013.
48. El-Raghy T, Barsoum MW, Sika M. Reaction of Al with Ti_3SiC_2 in the 800–1000°C temperature range. *Mater Sci Eng*. 2001;298:174–78.
49. Zhang HB, Zhou YC, Bao YW, Li MS, Wang JY. Intermediate phases in synthesis of Ti_3SiC_2 and $Ti_3Si(Al)C_2$ solid solutions from elemental powders. *J Eur Ceram Soc*. 2006;26:2373-2380.
50. Zhang X, Xu J, Wang H, et al. Ultrathin Nanosheets of MAX Phases with Enhanced Thermal and Mechanical Properties in Polymeric Compositions: $Ti_3Si_{0.75}Al_{0.25}C_2$. *Angew Chemie Int Ed*. 2013;52:4361–65.
51. Ghidiu M, Lukatskaya MR, Zhao M-Q, Gogotsi Y, Barsoum MW. Conductive two-dimensional titanium carbide /`clay/' with high volumetric capacitance. *Nature*. 2014;516(7529):78-81. doi:10.1038/nature13970.
52. Ghidiu M, Halim J, Kota S, Bish D, Gogotsi Y, Barsoum MW. Ion-Exchange and Cation Solvation Reactions in Ti3C2 MXene. *Chem Mater*. 2016;28(10):3507-3514. doi:10.1021/acs.chemmater.6b01275.
53. Lyklema J. Principles of the Stability of Lyophobic Colloidals in Non-aqueous Media. *Adv Colloid Interface Sci*. 1968;2:65-114.
54. Remo LA. Effect of C_3, C4 and C5 Alcohols and Water on Stability of Dispersions with Alumina and Alumina Hydroxide. *Discuss Faraday Soc*. 1966;42:232.
55. Wang G, Sarkar P, Nicholson PS. The influence of pH on the Electrostatic Stability of Alumina Suspensions in Ethanol. *J Am Ceram Soc*. 1996.
56. Sarkar' P, Nicholson PS. Electrophoretic Deposition (EPD): Mechanisms, Kinetics, and Application to Ceramics. *J Am Ceram Soc*. 1996;(79):1987-2002.
57. Chan DYC, Pashley RM, White LR. A Simple Algorithm for Calculation of Electrostatic Repulsion between Identical Charged Surfaces in Electrolyte. *J*

Colloid Interface Sci. 1980;77:283-285.
58. Derjaguin B V., Landau L. Theory of Stability of Highly Charged Lyophobic Sols and Adhesion of Highly Charged Particles in Solutions of Electrolytes. *Acta Physicochim URSS*. 1941;14:633-652.
59. Verwey EJW, Overbeek JTG. *Theory of Stability of Lyophobic Colloid*. Amsterdam: Elsvier; 1948.
60. Hamaker HC, Verwey EJW. The Role of the Forces between the Particles in Electrodeposition and Other Phenomena. *Trans Faraday Soc*. 1940;36:180-185.
61. Koelmans H, Overbeek JTG. Stability and Electrophoretic Deposition of Suspensions in Non-Aqueous Media. *Discuss Faraday Soc*. 1954;18:52-63.
62. Brown DR, Salt FW. The Mechanism of Electrophoretic Deposition. *J Appl Chem*. 1963;15:40-48.
63. Giersig M, Mulvaney P. Formation of Ordered Two-Dimensional Gold Colloid Lattices by Electrophoretic Deposition. *J Phys Chem*. 1993;97:6334-6336.
64. Zhang Z, Huang Y, Jiang Z. Reply to "Comment on 'Electrophoretic Deposition Forming of SiC-TZP Composites in Nonaqueous Sol Media.'" *J Am Ceram Soc*. 1995;78:3167-3168.
65. Boccaccini AR, Roether JA, Thomas BJ. C, et al. The Electrophoretic Deposition of Inorganic Nanoscaled Materials. *J Ceram Soc Japan*. 2006;114:1-14.
66. Matthews D, Altus A, Hope A. Photochemical Electron Transfer in the System Polypyrrole-Methylene Blue. *Aust J Chem*. 1994;47:1163-1170.
67. McNally EA, Zhitomirsky I, Wilkinson DS. McNally, E. A., Zhitomirsky, I. andWilkinson. *Mater Chem Phys*. 2005;91:391–398.
68. Teranishi T, Hosoe M, Tanaka T, Miyake M. Size Control of Monodispersed Pt Nanoparticles and Their 2D Organization by Electrophoretic Deposition. *J Phys Chem*. 1999;103:3818-3827.
69. Ogata N, Van Tassel J, Randall CA. Electrode formation by electrophoretic deposition of nanopowders. *Mater Lett*. 2001;49:7-14.
70. Miller JR, Burke AF. Electrochemical capacitors: Challenges and opportunities for real-world applications. *Electrochem Soc*. 2008;17(1):53-57. doi:10.1201/9781420069709.
71. Chmiola J, Yushin G, Gogotsi Y, Portet C, Simon P, Taberna PL. Anomalous increase in carbon capacitance at pore sizes less than 1 nanometer. *Science (80-)*. 2006;313:1760-1763.
72. Abruña HD, Kiya Y, Henderson JC. Batteries and electrochemical capacitors. *Phys Today*. 2008;61(12):43-47. doi:10.1063/1.3047681.
73. Smith FM. Measurement of sheet resistivity with four-point probe. *Bell Labs Tech*. 1957;37:711-718.
74. Gardolinski JEFC, Lagaly G. Grafted organic derivatives of kaolinite. *Clay Miner 2005*. 2005;40:547.
75. Abdelmalak MN. MXenes: A New Family of Two-Dimensional Materials and its Application as Electrodes for Li-ion Batteries. 2014.
76. Ghidiu M, Lukatskaya MR, Zhao M-Q, Gogotsi Y, Barsoum MW. Conductive two-dimensional titanium carbide "clay" with high volumetric capacitance. *Nature*. 2014. doi:10.1038/nature13970.
77. Feng A, Yu Y, Jiang F, et al. Fabrication and thermal stability of NH4HF2 etched Ti3C2 MXene. *Ceram Int*. 2017;43(8):6322-6328. doi:10.1016/j.ceramint.2017.02.039.
78. Ghidiu MJ, Halim J, Kota S, Bish D, Gogotsi Y, Barsoum MW. Ion-Exchange and Cation Solvation Reactions in Ti3C2 MXene. *Chem Mater*. 2016;28(10):3507-3514. doi:10.1021/acs.chemmater.6b01275.
79. Diba M, Fam DWH, Boccaccini AR, Shaffer MSP. Progress in Materials Science Electrophoretic deposition of graphene-related materials : A review of the fundamentals. *Prog Mater Sci*. 2016;82:83-117. doi:10.1016/j.pmatsci.2016.03.002.
80. Ma J, Wang C, Peng KW. Electrophoretic deposition of porous hydroxyapatite scaffold. 2003;24:3505-3510. doi:10.1016/S0142-9612(03)00203-5.

81. Campbell SA, Bowes C, McMillan RS. The electrochemical behaviour of tetrahydrofuran and propylene carbonate without added electrolyte. *J Electroanal Chem*. 1990;284(1):195-204. doi:10.1016/0022-0728(90)87072-R.
82. Hamaker HC. Formation of a Deposit by Electrophoresis. *Trans Faraday Soc*. 1940;36.
83. Hiemenz PC, Rajagopalan R. *Principles of Colloid and Surface Chemistry, Third Edition*. New York: CRC Press; 1997.
84. Chen H-W, Huang K-C, Hsu C-Y, et al. Electrophoretic deposition of TiO2 film on titanium foil for a flexible dye-sensitized solar cell. *Electrochim Acta*. 2011;56(23):7991-7998. doi:10.1016/j.electacta.2010.10.099.
85. Hamaker HC. Formation of a deposit by electrophoresis. *Trans Faraday Soc*. 1940;35:279-287.
86. Ferrari B, Moreno R. EPD kinetics : A review. 2010;30:1069-1078. doi:10.1016/j.jeurceramsoc.2009.08.022.
87. van der Biest O, Put S, Anné G, Vleugels J. Electrophoretic deposition for coatings and free standing objects. *J Mater Sci*. 2004;39(3):779-785. doi:10.1023/B:JMSC.0000012905.62256.39.
88. Maca K, Hadraba H, Cihlar J. Electrophoretic deposition of alumina and zirconia I . Single-component systems. 2004;30:843-852. doi:10.1016/j.ceramint.2003.09.021.
89. Novak P, Christensen PA, Iwasita T, Vielstich W. Anodic oxidation of propylene carbonate on platinum, glassy carbon and polypyrrole. An “in-situ” FTIR study. *J Electroanal Chem*. 1989;263(1):37-48. doi:10.1016/0022-0728(89)80122-6.
90. Kajiyama S, Szabova L, Iinuma H, et al. Enhanced Li-Ion Accessibility in MXene Titanium Carbide by Steric Chloride Termination. *Adv Energy Mater*. 2017:1601873. doi:10.1002/aenm.201601873.
91. Lipatov A, Alhabeb M, Boson A, Gogotsi Y. Effect of Synthesis on Quality, Electronic Properties and Environmental Stability of Individual Monolayer Ti3C2 MXene Flakes. *Adv Electron Mater*. 2016;in press:1-8. doi:10.1002/aelm.201600255.
92. Li C, Kota S, Hu C, Barsoum MW. On the Synthesis of Low-Cost, Titanium-Based MXenes. *J Ceram Sci Technol*. 2016;7(3):301-306. doi:10.4416/JCST2016-00042.
93. Fu Q, Wen J, Zhang N, et al. Free-standing Ti3C2Tx electrode with ultrahigh volumetric capacitance. *RSC Adv*. 2017;7:11998-12005. doi:10.1039/C7RA00126F.
94. Lukatskaya MR, Bak S, Yu X, Yang X, Barsoum MW, Gogotsi Y. Probing the Mechanism of High Capacitance in 2D Titanium Carbide Using In Situ X-Ray Absorption Spectroscopy. *Adv Energy Mater*. 2015;5(15):n/a-n/a. doi:10.1002/aenm.201500589.
95. Hu M, Li Z, Hu T, Zhu S, Zhang C, Wang X. High-Capacitance Mechanism for Ti3C2Tx MXene by in Situ Electrochemical Raman Spectroscopy Investigation. *ACS Nano*. 2016:acsnano.6b06597. doi:10.1021/acsnano.6b06597.
96. Miller JR, Simon P. Fundamentals of Electrochemical Capacitor Design and Operation. *Electrochem Soc Interface*. 2008;c:31-32. http://www.electrochem.org/dl/interface/spr/spr08/if_spr08.htm.